NTNU
Norwegian University of
Science and Technology

The Effect of LiFSI Salt Concentration and Electrolyte Additives on the Performance of Silicon Anodes for Lithium-Ion Batteries

Nils Runar Mulder

Nanotechnology
Submission date: June 2018
Supervisor: Ann Mari Svensson, IMA

Norwegian University of Science and Technology
Department of Materials Science and Engineering

Preface

This thesis partly builds on the project thesis delivered by the author in the fall of 2017 with the title "The effect of LiFSI and $LiPF_6$ lithium salts and anion receptors on the performance of Si anodes for Li-ion batteries". Parts of the project thesis were used as a starting point for the theory and experimental sections in this report, but have been extensively rewritten. The project thesis and this master thesis are part of the ongoing research project "Silicon anodes for Li-ion batteries, optimized binder, electrolyte and cathode" (SiBEC). The project has several partners, including Institute for Energy Technology (IFE), Elkem, Dupont, CerPoTech and SINTEF, as well as Norwegian University of Science and Technology (NTNU). This project was carried out at the Department of Materials Science and Engineering at NTNU. I would like to thank my supervisor Ann Mari Svensson for excellent guidance, quick feedback and informative discussions. I would further like to thank a range of people in the battery group at NTNU, especially Henning Kaland for training, help, discussions and tips on both experimental and analytical work, Karina Asheim for discussions, tips, tricks and training in electrolyte preparation and cell testing, and Andreas Norberg for assistance with the glovebox. Additionally, I send my thanks to Sverre Vegard Pettersen, for his excellent help with the XPS experimental and analytical work. Lastly, I would like to thank Miriam R. From for always supporting me throughout this last semester, as well as my parents for helping me organize and proofread this thesis.
In the summer of 2017, I had an internship at IFE, where I got training from experienced and knowledgeable people. During my time at IFE, I was introduced to key challenges with silicon anodes for use in Li-ion batteries, as well as their fabrication and characterization. This knowledge has been invaluable, and I would like to thank Jan Petter Mæhlen as well as lab-engineer Marius Uv Nagell and researcher Asbjørn Ulvestad for training, discussions and experiences. During this project they have assisted me by producing and sending electrodes of high quality that have been vital for this thesis.

Abstract

Lithium-ion batteries (LIBs) are currently the dominant battery technology. However, the increasing technological demands in areas like energy storage, transportation and consumer electronics, require significant upgrades of the LIB with regard to energy density, power density, cost and safety. Commercial LIBs use a graphite anode, which despite having a long cycle life and low cost, is not energy dense, cheap or safe enough to meet future requirements. A part of the solution may be to utilize silicon as the anode material instead of graphite. Silicon has a ten times higher theoretical capacity, is cheaper and is considered safer. However, silicon struggles with large volumetric changes during lithiation and delithiation, leading to a thick solid electrolyte interface (SEI) layer and high irreversible capacity loss. In order to avoid these detrimental effects, different electrolyte compositions and additives can be used to try to tailor the SEI layer. In addition, additives can interact with the Li-salt, increasing the Li^+ conductivity and controlling Li-salt decomposition.

In this project, the effect of electrolyte concentration on cell performance and SEI characteristics of Si anodes for LIBs has been investigated. The effect of various concentrations of the Li-salt lithium bis(fluorosulfonyl)imide (LiFSI) in 1:1 wt% ethylene carbonate:diethyl carbonate (EC:DEC) solvents on cell capacity was studied, resulting in an optimal concentration of 3 M. The positive effects of high salt concentration may be attributed to a reduction of the Li^+ desolvation energy and possibly lower resistance in the SEI layer for concentrated electrolytes. The capacity obtained with 3 M LiFSI at a discharge rate of 1 C, was 1050 $mA\,h\,g^{-1}$ after about 30 cycles, before it gradually dropped to 120 $mA\,h\,g^{-1}$ after 200 cycles. The additives fluoroethylene carbonate (FEC) and the anion receptor (AR) additive tris(hexafluoroisopropyl) borate (THFIPB) were combined (separately and together) with 3 M LiFSI to determine their effect on cell performance and SEI composition. An optimal electrolyte composition of 3 M LiFSI with 10 wt% FEC and 2 wt% THFIPB in EC:DEC was found, constantly yielding between 200-300 $mA\,h\,g^{-1}$ higher capacity than only 3 M LiFSI throughout the entirety of the 200 cycles.

Post-mortem studies including Fourier Transform Infrared Spectroscopy (FTIR), X-ray Photoelectron Spectroscopy (XPS), Energy-Dispersive X-ray Spectroscopy (EDX), Focused Ion Beam (FIB) and Scanning Electron Micrscopy (SEM) were performed on the cycled anodes in order to investigate the SEI composition. The post-mortem investigations concluded that increasing the Li-salt concentration lead to a change in the SEI formation mechanism. At dilute salt concentration, the SEI formation was mainly dominated by EC-reduction, while it was dominated by Li-salt degradation at high salt concentrations. The latter mechanism lead to a less carbonaceous SEI, with more lithium fluoride (LiF) and LiFSI-degradation products. Furthermore, the post-mortem studies indicated that FEC promoted an even higher amount of LiF, while at the same time forming a protective initial SEI layer, leading to less salt decomposition and higher cell performance. It is suggested that THFIPB did not take part in SEI reactions, but rather coordinated to the FSI^- anion, promoting Li^+ conductivity in the electrolyte.

Even though increased salt concentration leads to higher performing half cells, achieving a high capacity retention is still a challenging issue. It seems that an SEI dominated by inorganic components is not sufficiently stable. In future work, concentrated electrolytes should be combined with other additives, like vinylene carbonate (VC) and small amounts of lithium hexaluorophosphate ($LiPF_6$), in order to obtain high-performing, stable half cells that can work well in full-cell configurations too.

Sammendrag

Litium-ion (Li-ion) batterier er dagens dominerende batteriteknologi. Likevel stiller batteriavhengig teknologi som energilagring, transport og forbrukselektronikk stadig strengere krav til parametre som energitetthet, effekttetthet, kostnader og sikkerhet. Kommersielle Li-ion batterier bruker en grafittanode som, tross lang levetid og relativt lav kostnad, ikke er energitett, billig eller trygg nok til å imøtekomme disse kravene. En del av løsningen kan være å bruke silisium som anodemateriale i stedet for grafitt, da silisium har ti ganger høyere teoretisk kapasitet, er billigere, og er ansett som tryggere. Ulempen er at silisium sliter med store volumetriske endringer under litiering og de-litiering, noe som fører til et tykt "solid electrolyte interface" (SEI)-lag, samt høyt irreversibelt tap av kapasitet. For å unngå disse ulempene, kan man undersøke bruken av ulike elektrolytter og additiver til å skreddersy SEI-laget. I tillegg kan additivene interagere med Li-saltet, slik at ionekonduktiviteten øker, og nedbrytning av Li-salter kontrolleres.

I dette prosjektet har batteri-ytelsen og sammensetningen av SEI-laget på bakgrunn av elektrolyttkomposisjon, blitt undersøkt i Li-ion batterier med silisium-anode. Mer spesifikt er virkningen av Li-saltkonsentrasjonen av saltet litium bis (fluorosulfonyl)imide (LiFSI) i 1:1 vektprosent etylenkarbonat:dietylkarbonat (EC:DEC) på kapasiteten blitt undersøkt, noe som førte til en optimal konsentrasjon på 3 M. Den positive innvirkningen av økt saltkonsentrasjon kan tilskrives senkingen av aktiveringsenergien forbundet med oppløsningen av Li^+, samt mulig lavere resistans i SEI-laget for konsentrete elektrolytter. Kapasiteten ved en utladningsrate på 1 C var 1050 $mA\,h\,g^{-1}$ etter rundt 30 sykluser, før den gradvis falt og stabiliserte seg på omtrent 120 $mA\,h\,g^{-1}$ etter 200 sykluser.

Additivene fluoroetylenkarbonat (FEC) og den anioniske reseptoren (AR) tris-(heksafluoroisopropyl) borate (THFIPB) ble forsøkt kombinert (både separat og sammen) med 3 M LiFSI for å undersøke effekten på batteriets ytelse og SEI-komposisjon. En optimal elektrolyttkomposisjon bestående av 3 M LiFSI med 10 wt% FEC og 2 wt% THFIPB i EC:DEC ble funnet, og ga jevnt over mellom 200-300 $mA\,h\,g^{-1}$ høyere kapasitet enn det 3 M LiFSI klarte gjennom 200 sykler.

Post-mortem studiene Fourier Transform Infrared Spectroscopy (FTIR), X-ray Photoelectron Spectroscopy (XPS), Energy-Dispersive X-ray Spectroscopy (EDX), Focused Ion Beam (FIB) og Scanning Electron Micrscopy (SEM) ble brukt på de syklede anodene for å undersøke komposisjonen av SEI-lagene. Post-mortem undersøkelsene konkluderte at økt Li-saltkonsentrasjon førte til en endring i mekanismen bak SEI-dannelsen. Mekanismen gikk fra å være dominert av EC-reduksjon ved lave saltkonsentrasjoner, til å bli dominert av salt-dekomponering ved høye saltkonsentrasjoner. Sistnevnte mekanisme førte til en mindre karbon-rik SEI, med mer litium fluorid (LiF) og LiFSI-degraderingsprodukter. FEC fremmet dannelse av enda mer LiF, samt et beskyttende initielt SEI-lag som hindret salt fra dekomponering, slik at halvcellene ga høyere ytelse. Det blir foreslått at THFIPB ikke deltok i SEI-reaksjonene, men heller bandt seg til FSI^--anionet, slik at konduktiviteten av Li^+-ionene i elektrolytten økte.

Selv om økt saltkonsentrasjon førte til høyere ytelse i halvcellene, er det fremdeles utfordrende å oppnå vedvarende høy kapasitet over mange sykluser. Det virker

nemlig som om et SEI-lag dominert av uorganiske komponenter ikke er stabilt nok. I fremtidig arbeid foreslås det å kombinere høykonsentrerte elektrolytter med andre additiver, som vinylkarbonat (VC) og litium heksafluorofosfat ($LiPF_6$) for å virkeliggjøre høyt ytende, stabile halvceller som også fungerer godt i fullcellekonfigurasjon.

Table of contents

Chapter 1

Introduction

As the end of the fossil fuel age is drawing ever closer, and the green shift is gradually taking over, the interest for environmentally friendly solutions is at an all-time high. The future energy demand is ever-increasing due to a growing population with better living standards, and ways of acquiring, and equally important, storing energy, is of significant importance. Lithium-ion batteries (LIBs) are the current market leader when it comes to consumer electronics, electrical cars and energy storage systems, owing to their high energy density, high power density, long life and environmental friendliness.[1] However, in order to meet future demands of being an integral part of storing renewable energy, and further improve areas like transportation and hand-held devices, the LIB must improve aspects like energy density, power density, cost and safety.[2,3] One of the promising alternatives to meet these new criteria is to replace graphite with silicon in the anode of the LIB.[4,5] This may theoretically increase the anode capacity tenfold[6] and also drive down costs, as silicon is an abundant and inexpensive material.[5] Silicon-based anode materials do, however, have three major challenges that need to be successfully addressed before they may be commercialized, namely 1) great volume expansion upon lithiation followed by an equally large volumetric decrease upon delithiation, leading to cracks and collapse of the silicon structure,[7] 2) the formation of an unstable, continuously growing solid electrolyte interface (SEI) layer due to the cracks promoting electrolyte decomposition on the anode, leading to capacity fade,[8] and 3) poor intrinsic electric conductivity.[9]

In order to combat these issues, the large research field of silicon anodes has emerged. To overcome the problems with an unstable and thick SEI, changes in electrolyte salt and inclusion of electrolyte additives have been investigated. For instance, lithium bis(fluorosulfonyl)imide (LiFSI) has reportedly outperformed the more conventional lithium hexafluorophosphate ($LiPF_6$).[10]

Lately, the effect of increasing Li-salt concentration in battery electrolytes in order to improve power rate capability, capacity retention and SEI characteristics, has also been investigated. Increased Li-salt concentration typically reduces ionic conductivity due to increased viscosity and decreased salt dissociation, but enhances the amount of Li^+ cations in a given volume, reducing their transport path. In

addition, increased Li-salt concentration may reduce undesired reactions between the solvents and the anode material, thereby reducing the amount of SEI formed. By finding a balance between these counteracting properties, the electrolyte concentration may therefore be optimized in terms of battery performance.
Although promising additive candidates like fluoroethylene carbonate (FEC) and vinylene carbonate (VC) have been reported to increase cycling performance and reversibility,[11,12] problems related to these candidates still exist. FEC does, for instance, not form a sufficiently flexible SEI layer to accommodate the large volumetric changes of silicon. VC, on the other hand, forms a dense and flexible SEI layer, but with low ionic conductivity,[12] leading to low rate performance. Another approach that has not yet received as much attention, is the use of anion receptor (AR) additives, like tris(hexafluoroisopropyl) borate (THFIPB). This group of additives may increase ion conduction by increasing the Li^+ transport number, which is of great importance with regard to charge and discharge rate, practical capacity and cycling stability.[13,14] AR addition may furthermore protect the anions in the lithium salt, preventing them from dissolution into products that catalytically decompose the electrolyte.[15] This way, ARs can prevent thick SEI layers. Lastly, some ARs may be strong enough to break the interaction between the Li^+ cation and F^- anion.[13] AR addition might therefore tailor the SEI, by dissolving inorganic components like LiF, Li_2O and Li_2O_2.[13] Although AR additives have reportedly enhanced properties like capacity retention, Coulombic efficiency, thermal stability and ionic conductivity in graphite,[16–18] a detailed elaboration of the effect on cell performance and SEI formation in the presence of these additives is yet to be reported for silicon anodes.

Aim of this work

This thesis aims at investigating the effect of LiFSI salt concentration and selected additives on the performance and SEI characteristics of Si anodes for LIBs. Specifically, the changes in solution structure with respect to Li-salt concentration will be investigated, and related to the electrochemical performance of Si in the various electrolytes. The SEI composition will be examined by using post-mortem spectroscopic techniques on the cycled anodes. The post-mortem techniques include Fourier transform infrared spectroscopy (FTIR), X-ray photoelectron spectroscopy (XPS) and energy dispersive X-ray spectroscopy (EDX). Additionally, the influence of FEC and the anion receptor additive THFIPB are studied, with the aim of determining their role in the performance and SEI composition of the half cells. Highly uniform silicon anodes prepared at the Institute for Energy Technology (IFE) are used in order to obtain a reproducible result. Our hypothesis is that concentrated electrolytes increase half cell capacity, by promoting thinner and more stable SEI layers. The additives will provide an additional increase in performance due to their effect on both the electrolyte and the SEI layers. The answers obtained will contribute to finding solutions regarding the current challenges related to silicon anodes in Li-ion batteries.

Chapter 2

Theory

2.1 Fundamentals of Li-ion batteries

2.1.1 Working principle

In the following section, Li-ion batteries (LIBs) will be explained based on the book *"Lithium Batteries"* by Julien, Mauger, Vijh and Zaghib.,[19] as well as the article *"The Li-Ion Rechargeable Battery: A Perspective"* by Goodenough and Park.[3]
Like every battery, a LIB consists of two electrodes (anode and cathode) that are separated by an electrolyte and a separator, as seen in figure 2.1.1. The electrodes may be connected by an external circuit to initiate electrochemical reactions. In order for the LIB to be rechargeable, the solid electrodes need to be able to intercalate Li-ions in a reversible manner, such that both reduction and oxidation (redox) reactions can take place at both electrodes, depending on whether the LIB is charged or discharged. In a conventional LIB, the anode consists of graphite, while the cathode consists of a transition metal oxide, like Li_xCoO_2. The liquid electrolyte consists of a salt, like $LiPF_6$, dissolved in alkyl carbonate solvents like ethylene carbonate (EC) and diethyl carbonate (DEC).
Upon charging the battery, an external voltage is applied, which in turn initiates oxidation of the $LiCoO_2$ cathode, according to

$$\mathrm{LiCoO_2} \rightleftarrows \mathrm{Li_{1-x}CoO_2} + x\mathrm{Li^+} + xe^-. \tag{2.1}$$

This reaction yields an electric current of electrons through the external circuit towards the anode. The top arrow corresponds to discharging and the bottom arrow to charging of the LIB. Analogously, a reduction reaction occurs at the anode, according to

$$x\mathrm{Li^+} + xe^- + 6\mathrm{C} \rightleftarrows \mathrm{Li}_x\mathrm{C}_6. \tag{2.2}$$

The build-up of negative charge in the anode leads to migration of the positive Li-ions that intercalate into the graphite structure, causing a change in the electrochemical potential. The intercalation of Li-ions during charging is often referred to as lithiation. Upon discharge, oxidation of the anode occurs, and the difference in

electrochemical potential of electrons can be utilized to perform work on a source on the way. Like before, the electric field makes the Li^+-ions migrate back from the anode (in a process known as delithiation) to the cathode, intercalating into the Li_xCoO_2 structure.

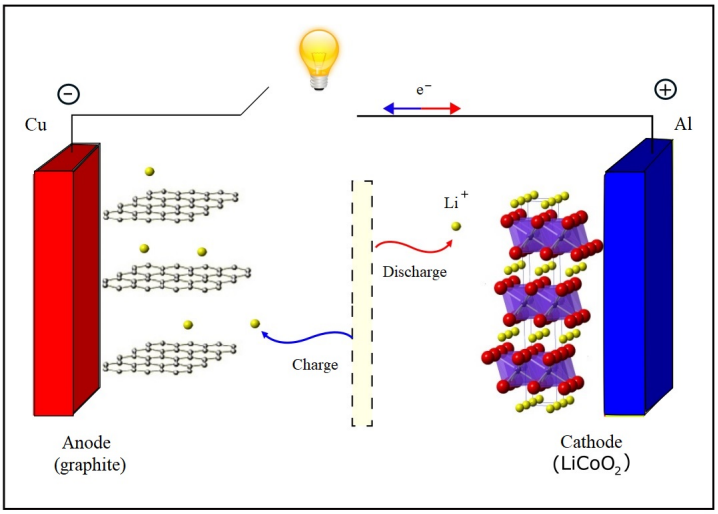

Figure 2.1.1: Schematic of the working principle of the LIB. Two electrodes are separated by an electrolyte, with a separator in between, preventing short circuit. Aluminum (Al) and Copper (Cu) current collectors improve the current distribution from/to the active materials. Inspired by Goodenough and Park.[3]

2.1.2 Terms and parameters of importance

In rechargeable batteries like the LIB, the words "cathode" and "anode" only make sense half of the time, as oxidation and reduction reactions occur at alternating electrodes depending on whether the battery undergoes charge or discharge. Often, the terms "negative electrode" and "positive electrode" are preferred to anode and cathode, where the negative electrode is defined as the electrode with the lowest potential versus the other electrode. In galvanic cells, the convention is that the electrode undergoing oxidation upon discharge is termed anode, while the electrode undergoing reduction upon discharge is termed cathode, and this terminology is also adopted for secondary (rechargeable) batteries. This report will therefore stick to the latter terminology.
When discussing LIBs, there are many different parameters of importance. The most important in this report are the following ones:

1. **Energy:** The total amount of energy stored in a LIB can be expressed as:[3]

$$\text{Energy (Wh)} = \int_0^Q V(q)dq, \tag{2.3}$$

where $V(q)$ is the potential when a charge q is moved from one electrode to another. The energy is generally expressed per unit weight (specific energy, Wh/kg) or per unit volume (energy density, Wh/L).

2. **Power density:** The maximum available power per unit volume (in liters), W/L. It determines the battery size required to achieve a given performance target.

3. **Capacity:** The capacity is a measure of the total amount of charge that can be stored in the battery, typically measured in Ah or mAh. The total capacity of a LIB depends on both anode and cathode capacity, so in order to get high-capacity LIBs, *both* anode *and* cathode materials must be optimized with regard to specific capacities.

4. **Specific capacity:** Unlike the more general term "capacity", the specific capacity describes the capacity explicitly for the anode or the cathode, and is measured in $\mathrm{mA\,h\,g^{-1}}$. The theoretical specific capacity for the anode and cathode often deviate, as it can be defined as[19]

$$\text{Specific capacity } (\mathrm{mA\,h\,g^{-1}}) = \frac{nF}{M_w}, \tag{2.4}$$

where n is the number of electrons in the reaction, F is the Faraday constant rewritten to $\mathrm{mA\,h\,g^{-1}}$-equivalent (26 801.5) and M_w is the atomic or molecular weight of the compound.

5. **Coulombic efficiency:** Shows how large percentage of the Li-ions the LIB is able to exploit from the previous charge, meaning that it is a term correlated to the capacity fade of the LIB. It is defined as

$$\text{CE } (\%) = 100 \times \frac{Q_{dis}}{Q_{ch}}, \tag{2.5}$$

where Q_{dis} and Q_{ch} are the discharge and charge capacities, respectively. A deviation from CE = 100% means that some capacity is irreversibly lost, referred to as irreversible capacity loss (ICL):

$$\text{ICL } (\%) = \frac{Q_{ch} - Q_{dis}}{Q_{ch}}. \tag{2.6}$$

The ICL is typically higher at early cycles, as some of the lithium is incorporated in the solid electrolyte interface (SEI) layer, and therefore becomes irreversibly lost.

6. **Self discharge (calendar life)**: The time an inactive battery can be stored before it is considered unusable, usually considered as having only 80% of its initial capacity.

2.2 Electrode materials

2.2.1 Overview

Since the commercialization of the LIB by Sony in 1991,[8] there has been a constant drive to seek improved solutions for more powerful batteries with cheap materials. Several materials are being investigated as potential replacements of the cathode and anode in next generation LIBs (summarized in figure 2.2.1). However, before any of these new materials can be adapted and commercialized, a more thorough understanding of all the factors affecting battery performance (chemistry, up-scaling, packaging, etc.) needs to be developed.[20] In order to increase the energy density of LIBs, two main approaches may be used:[21] The development and implementation of either 1) high voltage cathode active materials as electrodes, or 2) high capacity anode and cathode electrode materials. As electrolytes tend do decompose at voltages above 4.2 V (vs. Li/Li^+), the first approach requires development of electrolytes with wider electrochemical window stability. Approach 2 clarifies an important point with regard to developing next-generation LIBs with improved energy density, namely that the total specific battery capacity is dependent on *both* specific capacity of the anode *and* the cathode, according to[22]

$$\text{Specific battery capacity } (\text{mA h g}^{-1}) = \frac{C_A C_C}{C_A + C_C}, \tag{2.7}$$

where C_A and C_C are the specific capacities for the anode and cathode, respectively. This thesis only aims at investigating C_A for silicon anodes, but there is much research being done to improve C_C as well. Sulphur, for instance, is an element of major interest, reportedly with a theoretical specific capacity of 1675 mA h g^{-1}.[19] For current LIBs, the anode consists of graphite with C_A being 372 mA h g^{-1} and a cathode with C_C typically set to 150 mA h g^{-1}. From equation (2.7), this results in a battery capacity of 107 mA h g^{-1}. If silicon can be realized as an anode material, the battery capacity may increase with about 25% (using $C_A = 1200$ mA h g^{-1}), as illustrated in figure 2.2.2.

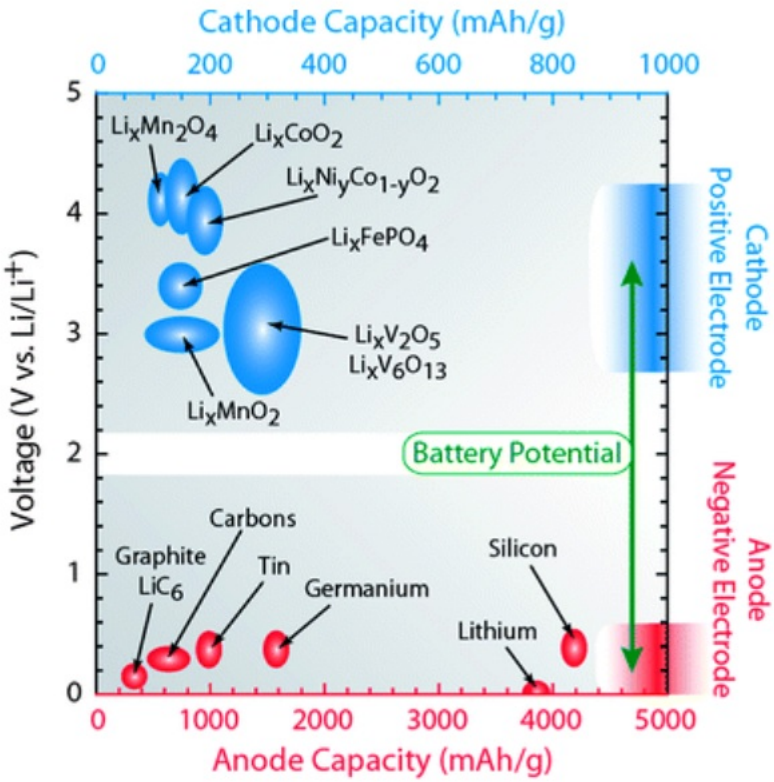

Figure 2.2.1: Diagram illustrating the Li-ion capacity and electrochemical reduction potentials with respect to Li-metal for a range of cathode and anode materials. Adapted from Osiak et al.[20] Reprinted under the following licence.[23, 24]

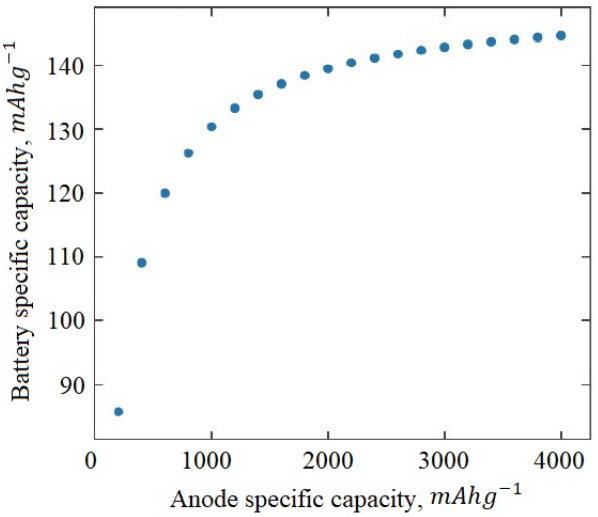

Figure 2.2.2: Plot of total specific battery capacity versus specific anode capacity, according to equation (2.7), setting $C_c = 150$ mA h g^{-1}.

In the following section, a brief overview of current commercial and researched electrode materials, as discussed by Osiak et al.,[20] will be presented.

2.2.2 Cathode materials

The cathode is the source of the Li-ions in a LIB, and is most commonly made of layered or spinel lithiated metal oxides, like $LiCoO_2$ (LCO), $LiNi_{1/3}Mn_{1/3}Co_{1/3}O_2$ (NMC), $LiFePO_4$ (LFP) and $LiMn_2O_4$ (LMO).[19,20] As it is easy to prepare a layered structure of extremely high quality using $LiCoO_2$, it is currently one of the most popular layered metal oxide cathode structures. In recent years, NMC has grown increasingly popular, as nickel-based systems have higher energy density, lower cost, and longer cycle life than the cobalt-based cells. In spinel cathodes, like $LiMn_2O_4$, the atomic structure of manganese and lithium ions results in a three-dimensional network of channels for lithiation and delithiation, allowing fast insertion/removal of Li-ions during discharge/charge processes. LFP is a popular choice due to its desired characteristics in terms of fast charge, cycling and safety. Cathode materials have relatively low theoretical specific capacities when compared to anode materials (typically one order of magnitude lower).
In half cell configurations, lithium metal is often used as a cathode material, as it serves as a pseudo-reference electrode, providing data for the individual electrode voltage versus lithium.[25]

2.2.3 Anode materials

The anode in the LIB is typically chosen with the following criteria in mind:[21]

1. Reversible capacity, i.e. intercalation and deintercalation
2. Good ionic and electrical conductivity
3. Long cycle life
4. High rate of lithium diffusion into the active material
5. Low cost
6. Low toxicity and high eco-compatibility.

Currently, graphite is the material that best meets these criteria, and is therefore the preferred anode material. As graphite is not the ultimate anode material, since it has too low energy density and safety, and too high cost, conciderable research has, and is, being done to find anode materials with improved properties. Anode materials are typically divided into three main categories, according to their (de)lithiation mechanism:

1. **Intercalation anodes:** The currently commercialized LIBs use graphite anodes. These anodes work by the principle of intercalation. Here, lithium ions intercalate/deintercalate in and out of the gaps between the graphite layers (graphene). Graphite is by far the most studied and used anode material in LIBs, owing to its low working potential vs. lithium, relatively low cost and good cycle life.[21] However, as graphite only can intercalate one Li-ion for every six carbon atoms, its reversible capacity is limited to 372 $\mathrm{mA\,h\,g^{-1}}$. Furthermore, the lithium diffusion rate in graphite is low, resulting in low power density. Because of these undesired properties, other intercalation type anodes that reportedly have higher specific capacity, power density, cyclability and safety, like titanium based oxides, are being investigated.

2. **Conversion anodes:** Lithium can react reversibly with a range of transition metal oxides through a reaction refered to as conversion. The transition metal compounds are typically oxides, phosphides, sulphides or nitrides, indicated as $\mathrm{M_xN_y}$, where M = Fe, Co, Cu, Mn or Ni, while N = O, P, S or N.[21] The reversible reaction unfolds according to the general reaction[21]

$$\mathrm{M_xN_y} + z\mathrm{Li^+} + z\mathrm{e^-} \rightleftarrows \mathrm{Li}_z\mathrm{N_y} + x\mathrm{M}.$$

   These anodes exhibit high reversible capacities (500-1000 $\mathrm{mA\,h\,g^{-1}}$), but are still far away from commercialization, due to poor capacity retention and large potential hysteresis,[21] as well as a wide voltage window.

3. **Alloying anodes:** The reversible alloying of metals and semi-metals with lithium is used to achieve significant improvement of theoretical specific capacity. The reason for this is the large lithium storage capacity these materials

offer. Typical alloying materials are silicon, tin, tin oxides, germanium, antimony, phosphorus, magnesium and silver. A severe drawback to this group of anode materials is that they suffer greatly from large volumetric expansion and contraction during lithiation and delithiation. The repeated volume changes cause severe mechanical stresses and strains, leading to irreversible structural changes, formation of cracks in the active material causing loss of structural and electrical integrity of the electrode, pulverization and irreversible capacity fading.[20] Recently, considerable effort is put into research concerning these challenges. Solutions like down-sizing of active material, developing flexible binders, coating the active material to accommodate the volume changes, and making more mechanically robust composites, are currently being investigated. Despite its challenges, silicon ticks all the aforementioned points for anode materials, especially with regard to costs, and is therefore considered one of the most promising candidates for commercialization.

2.3 Electrolyte mixtures

2.3.1 Electrolyte

The following section is largely based on the work of Xu, who published an excellent overview of electrolytes.[26]
The main purpose of the electrolyte in a LIB is to conduct ions between the electrodes, so that the electron exchanges occurring at the electrodes produce a directional flow of current. It is therefore crucial for the electrolyte to be ionically conductive and electrically insulating. In addition, the energy gap between the electrolyte's lowest unoccupied molecular orbital (LUMO) and highest occupied molecular orbital (HOMO) needs to be higher than the difference between the energy levels of the cathode and anode; otherwise the electrolyte will be reduced instead of the anode.[20]
Liquid electrolytes consist of an ionic compound (salt) dissolved in solvents. As the operating potentials of LIBs are so high that aqueous solutions would electrolyze if used as electrolyte, aprotic, non-aqueous solvents are used.[20] An ideal electrolyte solvent should, in addition to the characteristics mentioned, have the following properties:[27]

1. Be able to dissolve salts to sufficient concentration, i.e. have a high dielectric constant (ϵ).

2. Have a low viscosity (be fluid) so that it can facilitate ion transport.

3. Form a stable solid electrolyte interface on the anode (extensively described in the upcoming section), passivating the anode from further electrolyte decomposition.

4. Remain inert to all cell components, especially the charged electrode surfacecs during cell operation.

5. Remain liquid in a wide temperature range, i.e. have a low melting point and a high boiling point.

6. Be safe, nontoxic and economical.

Finding an ideal electrolyte mixture is a highly complex task, and a lot of research is currently being done in this field. Considerations of transport properties, electrochemical stability, temperature range, wetting properties, safety, toxicity, cost and compatibility with both anode and cathode materials are necessary and, in reality, always require a compromise. For instance, ionic conductivity of the electrolyte is both dependent on low viscosity for high ionic mobility, while also requiring a high dielectric constant (to dissolve salt) synonymous with high viscosity. This seemingly impossible compromise leads to the use of mixtures consisting of solvents with different properties, forming a solution with the desired properties. In LIBs, a mixture of ethylene carbonate (EC) and diethyl carbonate (DEC) is an example of such a co-solvent mixture.
EC (figure 2.3.1 a) is regarded as the most vital co-solvent in an electrolyte. The reason for this is that EC, in addition to having a high dielectric constant with a reasonably low viscosity (as seen in table 2.3.1), promotes superior surface chemistry on graphitic anodes.[27] EC forms a very good protective SEI film on graphite, which is required to protect the fragile graphene layer structure. EC does, however, have a high melting point, which causes it to be used in cooperation with other solvents. DEC (figure 2.3.1 b), for instance, has a very low melting point, and can keep EC in liquid form when mixed together. Additionally, DEC has a much lower viscosity than EC, promoting ion mobility.

Table 2.3.1: Physiochemical properties of EC and DEC. The table is based on data presented in the work by Xu.[27]

Solvent	$\mathbf{M_w}$	$\mathbf{T_m/°C}$	$\mathbf{T_b/°C}$	**Viscosity/cP**	ϵ **25°C**
EC	88	36.4	248	1.90 (40°C)	89.78
DEC	118	−74.3	126	0.75 (25°C)	2.81

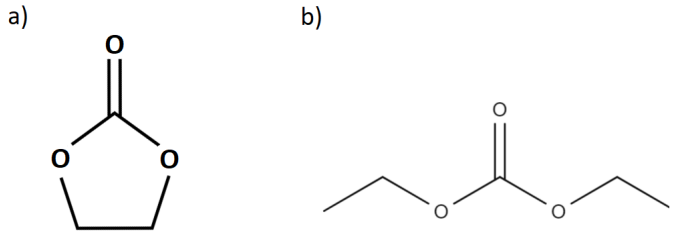

Figure 2.3.1: Chemical structures of EC (a) and DEC (b).

2.3.2 The solid electrolyte interface (SEI)

At voltages under about 0.8 V (versus Li/Li^+), EC-containing electrolytes start to decompose onto the anode material.[28] This decomposition generates a collection of solid products, usually consisting of lithium salts and carbonaceous polymeric by-products, known as the solid electrolyte interface (SEI). This interface layer will immediately passivate the electrode surface, preventing it from decomposing the electrolyte further. On the other hand, it impedes Li^+-transport, which in turn makes the LIB less efficient.[26] Ideally, the SEI layer would remain conductive to Li-ions while still being electronically insulating. According to Gauthier et al.,[29] this is critical to ensure high Coulombic efficiency, voltage efficiency, cycle life and safety. Understanding the electrochemical and chemical reactions between the electrode and the electrolyte is therefore of vital importance, as they influence the composition, microstructure, and properties of the SEI.
A multitude of techniques exist to examine the chemical composition of the SEI. Still, it is not an easy task to interpret the obtained data due to the numerous possibilities of reaction pathways (including side reactions) that may occur during the lithiation processes. The literature is not in unison when reporting their findings on the components of the SEI. The most commonly reported compounds are presented in table 2.3.2.

Table 2.3.2: Contents of the SEI as reported in the literature. Most relevant entries are included; the full table, including references, is found in the work of Verma, Maire and Novák.[30] "R" represents an alkyl group.

Component	Note
$(CH_2OCO_2Li)_2$	Also known as lithium ethylene dicarbonate (LEDC). Being a two electron reduction product of ethylene carbonate (EC), it is found mostly in the SEI of the EC based electrolytes.
$ROCO_2Li$	Present in the outermost layer of the SEI. They occur in most propylene carbonate (PC) containing electrolytes, especially when the concentration of PC in the electrolyte is high.
Li_2CO_3	Not always present. Normally present in the SEI formed in EC or PC based electrolytes. It may also appear as a reaction product of semicarbonates with HF, water or CO_2.
ROLi	Most commonly found in the SEI formed in ether electrolytes like tetrahydrofuran (THF), but may also appear as a dimethyl carbonate (DMC) or ethyl methyl carbonate (EMC) reduction product. It is soluble and may thus undergo further reactions.
LiF	Mostly found in electrolytes comprising of fluorinated salts like $LiAsF_6$, $LiPF_6$, $LiBF_4$. Is a major salt reduction product. HF also reacts with semi carbonates to form LiF byproducts. The amount of LiF increases during storage.
Polycarbonates	Present in the outermost layer of the SEI, close to the electrolyte phase. Imparts flexibility to the SEI.
LiOH	Mainly formed due to water contamination. It may also result from reaction of Li_2O with water or with ageing.

2.3.3 Salts and additives

An ideal electrolyte salt should meet the following criteria:[27]

1. It should be completely dissolved and dissociate in the electrolyte, such that the solvated ions can move with high mobility.

2. The anion should resist oxidative decomposition at the cathode.
3. The anion should be inert to the electrolyte solvents.
4. The anion and cation should be inert to the other cell components.
5. The anion should be nontoxic and thermally stable.

The lithium salts typically used in LIBs are given in table 2.3.3.

Table 2.3.3: Typical lithium salts used in non-aqueous liquid electrolytes, and their characteristic parameters: molecular weight (M_w), melting point (T_m), decomposition point in solution (T_{dec}), reported aluminum (Al) corrosion and conductivity (σ) in EC:DEC or PC (separated by / in the table). The table is an adaption from the one presented in the work by Xu.[27]
[a] conductivity of 1 M in EC:EMC (3:7 v/v) electrolyte, found by Han et al.[10]

Salt	**M_w ($g \cdot mol^{-1}$)**	**T_m (°C)**	**T_{dec} (°C)**	**Al corrosion**	**σ ($mScm^{-1}$) (1.0M at 25°C)**
Li tetrafluoroborate $LiBF_4$	93.9	293	>100	No	3.4 / 4.9
Li hexafluorophosphate $LiPF_6$	151.9	200	∼80	No	5.8 / 10.7
Li hexafluoroarsenate $LiAsF_6$	195.9	340	>100	No	5.7 / 11.1
Li perchlorate $LiClO_4$	106.4	236	>100	No	5.6 / 8.4
Li trifluoromethanesulfonate LiTF	155.9	>300	>100	Yes	1.7 / −−
Li bis(trifluoromethanesulfonyl) imide LiTFSI	286.9	234	>100	Yes	5.1 / 9.0
Li bis(fluorosulfonyl) imide LiFSI	187.1	145	>100	Yes	9.73[a]

Among lithium salts, the fluorinated inorganic anions, like PF_6^- (in the lithium salt $LiPF_6$), are especially favored due to their superior dissolution and dissociation properties in non-aqueous media, and their excellent ability to passivate positive electrode surfaces and substrates.[26] However, the PF_6^- anions are moisture sensitive, and tend to be increasingly reactive at elevated temperatures. These properties lead to the decomposition of $LiPF_6$ to the gaseous PF_5, which may react with trace amounts of H_2O or alcohols to produce HF.[10] In addition, Sloop et al.[15] found that PF_5 catalyzes EC decomposition on the electrode, causing a thick SEI. As SEI thickness impedes battery performance, and HF may reduce calendar life and cycle life time,[31] in addition to being a safety problem in the case of thermal runaway in the battery,[32] the search for alternative salts continues. One of the alternatives is LiFSI.

LiFSI has exhibited higher thermal stability at a wide temperature range, higher ionic conductivity and higher stability towards hydrolysis and subsequent decomposition to HF than $LiPF_6$. Furthermore, the performances of both graphite- and silicon-based lithium ion cells have been reported as better for LiFSI than for $LiPF_6$.[10,32] In spite of its positive attributes, the reported effects of LiFSI are still under debate, with reports of also poor thermal stability and corrosion of the aluminum current collector often used in LIBs,[33] due to the presence of chlorine impurities in the salt. It is therefore vital that the salt is of high purity and of high quality. Lastly, the SEI formed in graphitic LIBs upon addition of LiFSI is reportedly comparably smooth to that of $LiPF_6$,[34] and it is essential to investigate whether this positive effect also holds true for silicon based LIBs.

In order to maintain the protective role of the SEI, but at the same time ensure high transport of Li^+ through the layer, scientists have tried to tailor the SEI by adding additives to the electrolyte. The purpose of these additives is to "sacrifice" themselves in the formation of the SEI, so that they, with their desired properties, become part of it. A more detailed description of salts and additives and their effect on the SEI is found in sections 2.5.4 and 2.5.5, respectively.

2.4 Silicon as an anode material

2.4.1 Background

As conventional LIB technology does not fulfill future demands with regard to energy density, cost and safety, a large variety of proposed solutions have emerged. One of the most promising solutions is the substitution of the graphite anode with a silicon anode. In addition to being abundant, cheap and non-toxic, silicon can be alloyed with up to 4.4 lithium atoms per silicon atom, creating an alloy with high electrochemical capacity. The theoretical capacity of the fully lithiated alloy $Li_{4.4}Si$ is 4212 $mA\,h\,g^{-1}$, an order of magnitude higher than graphite (372 $mA\,h\,g^{-1}$).[7] However, the biggest challenge for commercializing silicon anodes is the enormous volumetric expansion it undergoes during lithiation (up to more than 400%[19]), resulting in high internal stress, electrode pulverization and subsequent loss of electrical contact between the active material and current collector, leading

to poor reversibility and capacity fade.[7] Figure 2.4.1 shows the evolution of the number of publications related to Si anode LIBs during the last years, revealing a sharp growth that has stabilized during the last years.

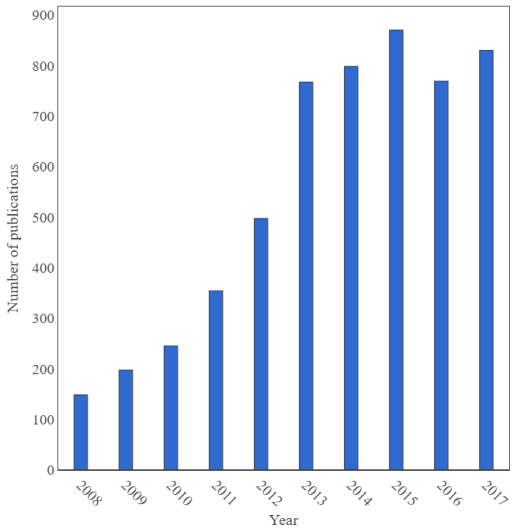

Figure 2.4.1: Number of publications related to Si anode LIBs during the last decade. The terms "silicon" "anode" and "lithium-ion battery" were used in the SciFinder database.

2.4.2 Lithiation mechanism

Lithiation of silicon follows an alloying mechanism, as described in section 2.2.3. For crystalline silicon at room temperature, the first lithiation will change the crystalline silicon phase to an amorphous phase (Li_xSi).[35] According to Key et al.,[36] the amorphous phase is highly lithiated, with 3.4 ± 0.2 Li-atoms per Si-atom. Theoretically, the most Li-rich equilibrium phase in the Li-Si system is $Li_{22}Si_5$, which results in a theoretical specific capacity of 4212 $mA\,h\,g^{-1}$.[37] However, several studies, including the one by Obrovac et al.,[35] have shown that the final phase of lithiated Si at room temperature is not the equilibrium $Li_{22}Si_5$ phase. By using ex situ X-ray powder diffraction, Obrovac et al. studied structural changes during the Li-Si alloying process, and found that the amorphous $Li_{22}Si_5$ phase crystallizes to a metastable $Li_{15}Si_4$ phase at room temperature when the potential of the electrode falls below about 50 mV vs Li/Li^+. According to Ogata et al.,[38] this metastable crystalline phase is associated with an unfavorable overvoltage, resulting in a lower operating voltage for the battery. If the metastable Li-Si phase is not avoided, the degree of lithiation will be lower, and thus the capacity drops. On the other hand, if the battery is charged to high voltages for maximum lithiation, the volumetric expansion is more severe, and cyclability of the battery is reduced. Thus, by controlling the voltage operating window of the battery, a compromise between

capacity and cyclability is introduced. It appears that cycling silicon anodes above 50 mV avoids the formation of crystallized phases completely, and results in better cycling performance.[35]
Silicon anodes typically include a native SiO_2 layer, which also takes part in the initial lithiation of the battery. It is commonly understood that SiO_2 is a conversion type anode, but the exact lithiation mechanism and final products obtained through the conversion reaction are still debated. The general findings point to the formation of electrochemically active Li_xSi, as well as Li_2O, $Li_2Si_2O_5$ and/or Li_4SiO_4 side products.[39]

2.4.3 Solid electrolyte interface on silicon anodes

For commercial LIBs with graphitic anodes, the SEI formed is both thin and stable, ensuring high safety and long cycle life.[40] On the other hand, the currently researched LIBs utilizing silicon anodes, suffer from an unstable and continuously growing SEI, due to silicon's enormous volumetric changes during lithiation and delithiation. These volumetric changes lead to cracking of the silicon structure, exposing new surfaces that host subsequent growth of new SEI, as depicted in figure 2.4.2. SEI formation is a highly complex process, as it depends on the chemical composition of the electrolyte, additives and binder material, morphology, type and pre-treatment of anode material, cycling method, etc.[7] Because of the complexity of the SEI, a lot of research is currently being conducted to determine the chemical composition of the SEI, especially when certain additives are present in various concentrations.

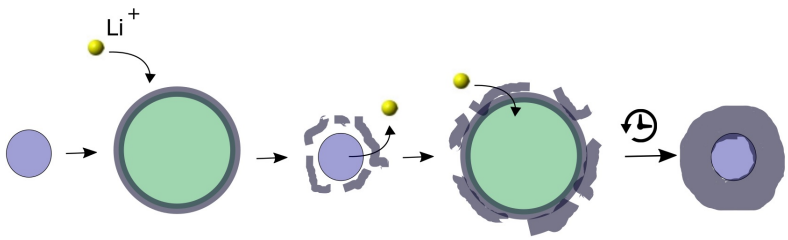

Figure 2.4.2: SEI formation (grey) on silicon particle (blue). The lithiated silicon (green) undergoes a large volumetric change. Upon delithiation, the SEI decomposes, and becomes part of a thicker SEI upon the next lithiation. Over time a thick SEI is formed. Inspired by Wu et al.[41]

The components given in table 2.3.2 are typical for standard LIBs with graphitic anodes. For silicon anodes, a range of other components are found, due to the presence of silicon. The most common ones are siloxanes, Li_xSiO_y, Li_xSiF_y and SiO_xF_y,[11,29] as well as other inorganic compounds specific to the lithium salt used.[30] An in-depth analysis of the SEI formation mechanism, as well as the effect of electrolytes, salts and additives on the SEI formation and composition, is presented in sections 2.5.3 - 2.5.5.

2.4.4 Challenges of silicon anodes and approaches so far

The large volumetric changes of silicon during cycling lead to several challenges. As the silicon expands and contracts, the electrode material may pulverize and fracture, causing lithium to be trapped within the active material and/or SEI. In addition, the active material is gradually consumed due to continuous electrolyte exposure during cycling, which may lead to loss of electrical contact.[7] All of these issues contribute to low Coulombic efficiency and poor capacity retention. Furthermore, the ever-growing SEI will seriously reduce ionic diffusion to/from the anode.[7] In order to overcome the aforementioned challenges, researchers are currently investigating all aspects of the LIB to find solutions. A short summary, inspired by Szczech and Jin[7] of some of the main research directions are given below.

1. **Size reduction of active material**: For the last decade, major effort has been put into solving the challenges of LIBs using nanoscale active materials. Nanoscale dimensions allow quick relaxation of stress, making nanoparticles more resistant to fracture than bulk particles, resulting in increased reversibility. In addition, the Li^+-diffusion path will be shorter and enhanced along grain boundaries and surfaces. However, the large surface-to-volume ratio in the nanoscale results in more SEI, which may be harmful for cell performance. Furthermore, Li et al. found that their silicon nanoparticle (SiNP) anode material suffered greatly from agglomeration (also known as sintering) of the SiNPs.[42] The SiNPs agglomerated into dense microsized blocks that did not take further part in the electrochemical reactions. In addition, nanoscale materials are often synonymous with increased costs, and challenging handling.

2. **Cycling parameters**: As described in section 2.4.2, silicon undergoes a phase transition from crystalline to amorphous alloy during the first cycle. The amorphous phase is more stress-resilient than the crystalline phase, and by limiting the voltage cut-offs, the active material may continue being amorphous, resulting in higher reversibility and cycle life of the electrode. An added effect of a smaller voltage-window is that the volumetric changes are not as large, reducing the electrode pulverization. The drawback of this is that the capacity of the battery will be impaired. However, the overall cell capacity does not depend too much on the anode capacity after the latter reaches 1500-2000 $\mathrm{mA\,h\,g^{-1}}$, as seen in figure 2.2.2. Therefore, sacrifice of anode capacity may still give high-capacity cells.

3. **Coating of the active material**: In order to avoid issues with sintering, low intrinsic conductivity, volumetric changes and electrochemical instability, inactive matrices can be used. The most popular coating material for silicon anodes is carbon. Carbon has excellent electrical conductivity, which is vital for the electron conductivity of the anode material. In addition, the internal resistance of the battery is lowered when carbon is added to the silicon. Furthermore, carbon can reduce the probability of sintering occurring between i.e. nanoparticles.[43] Liu et al. reported a simple fabrication

process resulting in carbon yolk-shell structures that capped the volumetric changes of the silicon nanoparticles that constituted the inside of the structures.[44] This novel anode material showed high capacity (~2800 $mAh/g_{Si/C}$ at C/10 for the first cycle, while stabilizing at ~1500 $mAh/g_{Si/C}$ for later cycles at 1 C) and long cycle life (74% capacity retention after 1000 cycles). The results were attributed to the carbon yolk-shell, allowing the silicon to expand and shrink freely without producing a thick SEI layer. Other designs have also showed great promise, like in another study of Liu et al.,[45] where a pomegranate anode design was developed. Here, single silicon nanoparticles were encapsulated by a spacious carbon layer (so that the silicon could expand/contract), that were encapsulated in large ensembles inside a thicker carbon layer in micrometre-size pouches. This anode design achieved a high capacity of 1160 $mAh/g_{Si/C}$ after 1000 cycles at a rate of C/2. In addition, the capacity retention was 97% from the 2nd to 1000th cycle. Even though carbon coating is promising, it may decrease the energy density of the anode as well as being challenging to fabricate on a uniform, industrial scale.

4. **Binder material**: To address the issue concerning disconnection of the active material due to the large volumetric changes of silicon, flexible binders are desired. The type of binder used is critical, as it can greatly influence the cycling lifetime and stability of the LIB. For graphite, the most common binder used is poly(vinylidene fluoride) (PVDF), due to its good electrochemical stability.[46] Despite these positive attributes, PVDF does not possess the mechanical tensile strength nor adequate adhesion properties to cope with the large volumetric changes of the (de)lithiation of silicon.[46,47] Therefore, much effort is being put into developing binders that can accommodate the (de)lithiation processes in silicon. Carboxymethylcellulose (CMC) is arguably the most popular choice for silicon-based anodes, as it is more flexible and has higher mechanical strength than PVDF, resulting in higher battery performance.[47] Additionally, CMC has excellent solubility in water, which is advantageous for the environment. However, water may cause surface oxidation of silicon, which may cause negative effects on both Coulombic efficiency and long term cycling.[47] In addition, water traces are undesired when using $LiPF_6$ salt, as they lead to undesired HF formation.[8] Recently, poly(acrylic acid) (PAA) has been explored as a binder option, as it has similar mechanical properties as CMC, but an increased number of carboxylic groups that promote anode performance and allow for better tuning of binder properties.[47]

5. **Electrolyte and additives**: Composition of both electrolyte and additives is arguably the most important factor with regard to achieving a stable SEI layer. As this thesis aims at determining the effect of electrolytes and additives on cycling performance and SEI properties, the role of electrolytes and additives are elaborated in greater detail in the following sections.

2.5 The Role of the solution structure

2.5.1 Overview

During the last decades, significant effort has been put into developing both anode and cathode materials. Advances in electrolyte research, on the other hand, have progressed at a slower pace.[48] This is often attributed to the complexity of the interactions between the electrolyte and the electrode materials, making it challenging to draw any firm conclusions and finding optimal solutions. Yet, the electrolyte is crucial for optimization of LIB technology, as the bulk electrolyte dictates vital properties for battery operation, like ionic conductivity, viscosity and stability. Only recently, significant efforts have been put into understanding the effect of the solution structure of electrolytes on both electrolyte properties and SEI formation. The electrolyte solution structure is primarily determined by two different interactions of the electrolyte components: the interaction between the Li-cation and the salt anion, and the interaction between the cation and the polar aprotic organic solvent.[49] Herein, the concentration, and type, of the lithium salt used is paramount. In the following section, the effect of the solution structure on electrolyte properties and SEI formation will be presented, as based on the reviews of Zheng et al.[50] and Yamada and Yamada.[51]

2.5.2 Effect of solution structure on electrolyte properties

At common concentrations of Li-salt (∼1 M), the solution structure is typically dominated by solvent-separated ion pairs (SSIPs) and free solvent molecules (as seen in figure 2.5.1 a and b). Here, the lithium cation is typically coordinated to 3 or 4 solvent molecules. This solution structure promotes ion mobility, resulting in a high ion conductivity and low viscosity. In addition, salt dissolution is high. The commonly used electrolyte is within the range of 1-1.2 M based on prior optimization, as well as the fact that the ionic conductivity of a range of aprotic solvents and Li-salts tends to peak at this concentration (as seen in figure 2.5.2).[51,52] This practice assumes that maximizing the electrolyte conductivity results in an optimal battery rate capability. However, several studies have shown that highly concentrated electrolytes (of Li-salt) may lead to far superior rate performance than for instance the commercialized 1 M $LiPF_6$ in EC:DMC electrolyte.[53,54]

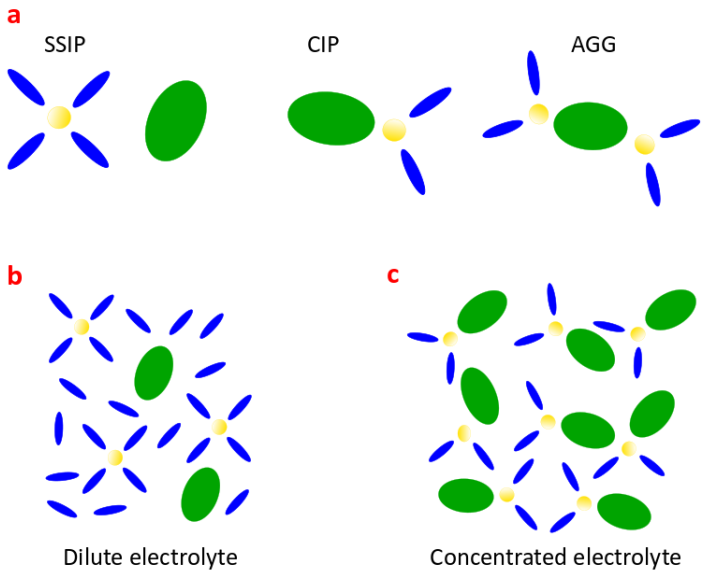

Figure 2.5.1: Illustration of solvent separated ion pair (SSIP), contact ion pair (CIP) and aggregates (AGG), as well as the solution structure in dilute and concentrated electrolytes. The yellow sphere represents the lithium cation, the blue ellipse represents a solvent molecule, and the green ellipse represents the lithium salt anion. Inspired by Zheng et al.[50]

Lately, significant effort has been put into research regarding highly concentrated electrolytes due to reports of various unusual functionalities that seem beneficial for battery applications. In highly concentrated electrolytes, a shift from SSIP to contact ion pairs (CIPs) and aggregates (AGGs) (figure 2.5.1 a) occurs. Here, the lithium cation is typically coordinated to only 1-2 solvent molecules, resulting in an electrolyte with low ionic conductivity and high viscosity (2.5.1 c). The high viscosity will in turn lead to relatively poor wettability of the electrodes and separator. These effects have long been regarded as undesired, as these characteristics are associated with low battery rate performance. However, as the Li-salt concentration increases, the number of Li^+ cations within a given volume also does so. Concentrated electrolytes may be beneficial for to two reasons. Firstly, the increased Li-salt concentration improves the electrolyte's reductive stability due to reduced availability of reactive solvent and sacrificial anion reduction.[52] Secondly, the increased Li^+ cation density leads to a higher Li^+ transfer number.[52]
In addition to both increased thermal, oxidative and reductive stability,[50,51] the increase of Li-salt concentration promotes battery safety, as the flammability of the electrolyte is reduced.[55]
Seo et al. investigated the solution structure of various concentrations of $LiPF_6$ in different carbonate solvents.[56] By analyzing the changes in the FTIR spectra of the carbonyl group of the carbonate solvents, they determined the solvation num-

ber as a function of salt concentration. The solvation number indicates how many solvent molecules coordinate to a Li^+ cation in solution. A low solvation number implies that the ions in the solution form aggregates and CIPs, and can therefore indicate a change in solution structure. In order to calculate the solvation number for the different electrolytes, Seo et. al deconvoluted the carbonyl peaks of the FTIR-spectra. Then, they determined the relative amount of coordinated solvent with the assumption that each band had equivalent IR sensitivity and that the area of the absorption was proportional to the amount of coordinated and uncoordinated solvent. The relative areas of coordinated and uncoordinated carbonate were then used to estimate the concentration of solvent molecules coordinated to the Li^+ cation using equation (2.8). Here, C^o, and C_{Li} are the concentrations of coordinated carbonate, total carbonate solvent, and lithium salt, respectively, N is the average solvation number, and A_{CO} and A_{UC} are relative areas of the IR bands for coordinated carbonate and uncoordinated carbonate, respectively.

$$N = \frac{A_{CO}}{(A_{CO} + A_{UC})} \frac{C^o}{C_{Li}}. \tag{2.8}$$

For DEC, the value of C^o is 8.25.[56]

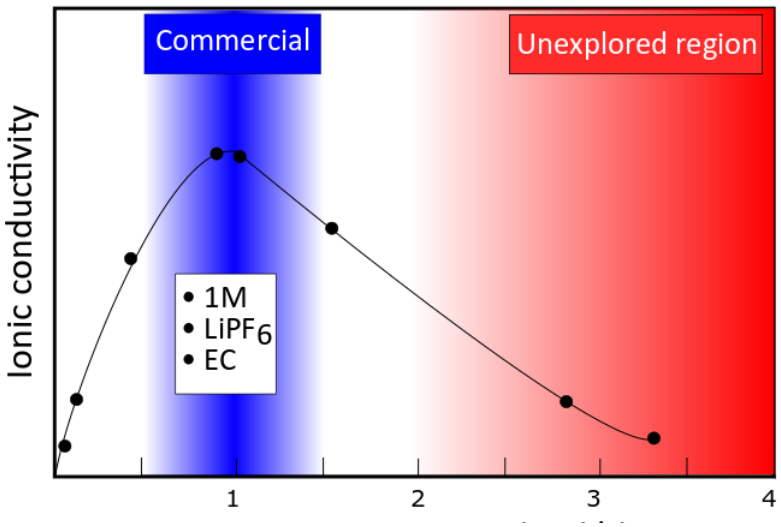

Figure 2.5.2: Typical ionic conductivity curve of Li salt in an aprotic solvent mixture. Inspired by Yamada and Yamada.[51]

Elsewhere, Xu, von Cresce and Lee[57] investigated the desolvation process of Li^+ in EC-based electrolytes. In order for a Li^+ cation to escape from the bulk electrolyte into the active anode material, an activation energy, which can be translated to internal resistance,[58] is required to disrupt the Li^+ ion from its solvation sheath. The

findings suggest that concentrated electrolytes effectively reduce this energy, as the solvation number of these electrolytes is lower, indicating that Li^+ is coordinated to fewer solvent molecules. Therefore, concentrated electrolytes will yield higher overall performance as the energy-loss concerning Li^+ desolvation is reduced.
The influence of the solution structure on the SEI formation mechanism is also of significant interest in this project, and is therefore discussed in detail in the following section.

2.5.3 Effect of solution structure on SEI and the SEI formation mechanism

Studies regarding battery interfaces have arguably been the part of battery research that has progressed the slowest, due to the complexity of electrolyte decomposition in dynamic conditions and on various substrates with different surface and material properties.[50] Still, interfaces do play a vital role in determining the mass flow and electrochemical kinetics, and thus the power, stability, and safety, of LIBs. For dilute electrolytes of ∼1 M, the SEI formation is extensively studied and is generally understood, but for concentrated electrolytes, the formation, evolution, and the nature of the SEI are not conclusively understood yet.[50] For concentrated electrolytes, the interfacial reaction pathways and properties of the SEI layer are altered. The explanation for this is often ascribed to a fundamental difference in the SEI formation mechanism, due to the significant difference in solution structure. In dilute electrolytes, the solution structure is dominated by SSIPs and free solvent molecules. This promotes reductive reactions of solvent molecules onto the anode, leading to an SEI layer dominated by organic solvent species, with some inorganic components originating from Li-salt as well. However, as the concentration increases, the solution structure changes from being dominated by SSIPs to being dominated by CIPs and AGGs, effectively reducing the amount of free solvent molecules. This changes the SEI formation mechanism from being dominated by solvent reduction to being dominated by inorganic salt decomposition. For fluorinated salts, like $LiPF_6$ and LiFSI, this promotes the formation of a LiF rich, more stable, thin and compact SEI layer, which effectively suppresses further reactions between the active electrode and the electrolyte.[50]
Correspondingly, Zheng et al. related the change in the SEI formation mechanism to the electrical double layer arising between the anode and the surrounding electrolyte.[50] In dilute electrolytes, the inner Helmholtz layer, depicted in figure 2.5.3 a), is dominated by free solvent molecules that dictate the electrode-electrolyte reactions once an electric field is applied (i.e. during battery operation). This promotes SEI formation consisting of solvent decomposition. As salt concentration is increased, the availability of free solvent molecules decreases, such that the salt anions enter the inner Helmholtz layer, as depicted in figure 2.5.3 b). This will in turn promote decomposition of salt anions onto the anode material, leading to an SEI dominated by inorganic components, like LiF.

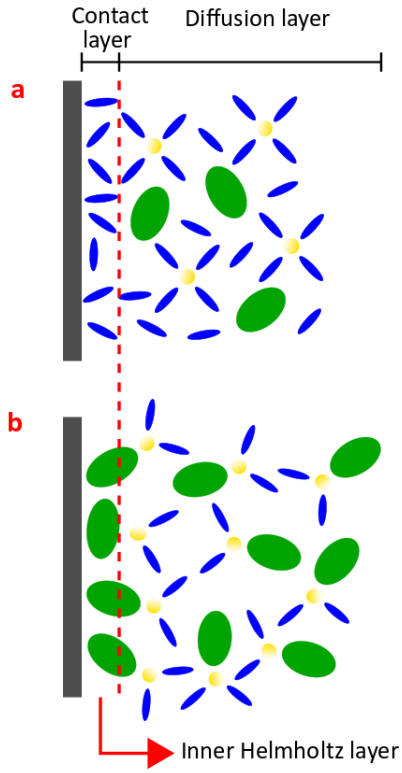

Figure 2.5.3: SEI layer formation mechanisms, explained by the electrical double layer, for dilute (a) and concentrated (b) electrolytes. Inspired by Zheng et al.[50]

Interestingly, this mechanism seems to be widely applicable for a range of different battery chemistries. For example, Nie et al.[48] investigated the effect of increasing the concentration of $LiPF_6$ on electrochemical properties, SEI formation and SEI composition in binder-free graphitic half cells with PC electrolyte. Using a combination of cyclic voltammetry and galvanostatic cycling, Nie et al. revealed that low concentration of $LiPF_6$ (1.2 M) in propylene carbonate (PC) lead to a continuous electrolyte reduction onto the anode material, with no (de)intercalation of the binder-free graphite. By Fourier transform infrared spectroscopy (FTIR) and nuclear magnetic resonance (NMR) measurements, they further discovered that the electrolyte was dominated by solvent separated ion pairs ($Li^+(PC)_4//PF_6^-$) which resulted in the continuous formation of lithium propylene dicarbonate (LPDC) on the anode material, as confirmed by transmission electron microscopy (TEM) and energy dispersive X-ray spectroscopy (EDX). The LPDC did not adhere well to the graphite structure, failing to passivate the anode, thereby promoting further electrolyte decomposition. By increasing the $LiPF_6$ concentration to 3 M, the electrolyte reduction decreased significantly, which further manifested in a thinner SEI

layer, consisting mostly of LiF. Nie et al. hypothesized that this behaviour arose due to a shift from solvent-separated ion pairs at low $LiPF_6$ concentration, to contact ion pairs ($Li^+(PC)_3PF_6$) at high $LiPF_6$ concentration, as observed with NMR. Elsewhere, highly concentrated LiTFSI and LiFSI electrolytes have reportedly been successful in suppressing the corrosive processes that normally occur with dilute LiFSI/LiTFSI based electrolytes on the aluminum current collector during charging to high (>3.8V) voltages. Yamada et al. suppressed aluminum corrosion to voltages up to 4.5 V (vs Li/Li^+) by using 5 M LiFSI in acetonitrile (AN).[59] The high concentration hinders the Al^{3+} formed at high voltages to be solvated by free AN solvent, preventing it from diffusing from the Al surface, continually corroding the Al. The high LiFSI concentration restricted the solvation of Al^{3+} due to lack of free solvent molecules and reduced diffusivity of the $Al(FSI)_3$ complex.
High concentrations of LiFSI have also successfully been utilized to hinder dendritic growth of Li-metal in Li-metal batteries. Qian et al. utilized a 4 M LiFSI/DME electrolyte in a Li//Li symmetric cell, achieving a cell that operated at 10 mA cm^{-2} for more than 6000 cycles, and a Li//Cu cell operated at 4 mA cm^{-2} for over 1000 cycles with an average CE of 98.4%.[52] According to Zheng et al.,[50] this achievement may be explained by the significant differences in solution structure between dilute and concentrated electrolytes. In dilute electrolytes, the free solvent molecules react with the Li-metal, creating undesired side products and low Coulombic efficiency. Conversely, at high concentrations, the free solvent molecules are coordinated to the Li^+ ions, which effectively stabilizes the solvent molecules and their undesired side reactions with the Li-metal. In addition, a compact and highly conductive SEI layer forms on the Li-metal surface, mitigating anion degradation during extended cycling.
Highly concentrated electrolytes have also shown great promise in more exotic battery technology, like lithium-sulfur (Li-S),[60,61] lithium-air (Li-O_2),[62] sodium-metal[63] and aqueous energy storage systems.[64,65]

2.5.4 Role of electrolyte and electrolyte salts on the SEI

Electrolyte composition greatly influences both the morphology and composition of the SEI layer. Today, electrolytes typically consist of carbonate solvents, like EC, DEC, PC and DMC, as they form stable SEI products and have suitable LUMO levels.[7,29,30] These solvents create organic degradation products, while the lithium salt leaves inorganic components in the SEI. Salts and solvents may also affect the SEI dissolution occurring at elevated temperatures.[30]
$LiPF_6$ (figure 2.5.4 a) is one of the most popular lithium salts used in silicon anode research today. It exhibits high ionic conductivity and electrochemical stability in solutions like EC:DEC, while avoiding toxicity, corrosion or violent reactions that are typically found in other candidates.[32] However, $LiPF_6$ is involved in chemical reactions that turn out to promote extensive SEI formation and impede battery performance. First of all, $LiPF_6$ dissolves to become[8]

$$LiPF_6\ (s) \rightarrow LiF\ (s) + PF_5\ (g). \tag{2.9}$$

Being highly water sensitive, PF_5 reacts with trace amounts of H_2O found in the electrolyte, according to

$$PF_5\,(g) + H_2O\,(aq) \rightarrow POF_3\,(g) + 2HF\,(g). \tag{2.10}$$

Sloop et al. found that PF_5 in high concentrations acts as a catalyst for the ring-opening polymerization of EC,[15] leading to increased SEI formation and thickness, which impedes capacity retention. By using depth-resolved photoelectron spectroscopy, Philippe et al.[8] observed that LiF, PF_6^- and $LiPF_6$ become integral parts of the SEI structure, especially with long term cycling. Furthermore, Philippe et al. found evidence supporting that the HF created upon cycling may react with Li_2O (formed during reactions between native SiO_2 and Li) according to

$$Li_2O\,(s) + 2HF\,(g) \rightarrow 2LiF\,(s) + H_2O\,(aq), \tag{2.11}$$

such that the water content self-replenishes and promotes further HF formation. Another reaction path towards LiF formation and subsequent promotion of PF_5 is[31]

$$Li^+\,(aq) + HF\,(g) \longleftrightarrow LiF\,(s) + H^+\,(aq) \tag{2.12}$$

$$H^+\,(aq) + PF_{6^-}\,(aq) \longleftrightarrow HF\,(g) + PF_5\,(g). \tag{2.13}$$

HF is a major concern, as it may lead to undesired modifications of the favorable interactions between the binder and the active material surface, and even act as an etchant on native SiO_2 found in the active material.[8,31] Philippe et al. also found that HF reacts with the surface SiO_2 to form partially fluorinated species, SiO_xF_y, that grow upon cycling. Furthermore, HF poses a major safety issue, especially at elevated temperatures.

As the $LiPF_6$ salt continuously decomposes (as seen from equation (2.9)) and promotes reactions that may be detrimental on battery performance, investigations on more stable salts is essential. LiFSI (figure 2.5.4 b) possesses some qualities that make it intriguing for further studies, and will be used as lithium salt in this project.

Using LiFSI, Philippe et al. reported an SEI layer consisting of the same carbonaceous species that are observed when $LiPF_6$ is used as salt.[32] Unlike $LiPF_6$, however, LiFSI did not degrade as much, and did not have a negative impact on the battery performance. In fact, Philippe et al. believe that LiFSI decomposes during the initial discharge to form a surface passivation layer that prevents further reduction of the salt. Furthermore, LiFSI is not prone to hydrolysis in the same way as $LiPF_6$, and is not involved in the dissolution of Li_2O observed in equation (2.11). This is mainly because LiFSI prevents the formation of HF[32] in equations (2.10) and (2.13). LiFSI neither takes part in the formation of SiO_xF_y. Instead, SiO_2 continuously reacts with lithium, increasing the levels of lithium silicate Li_4SiO_4 found at the surface of the electrode. Therefore, the favorable interactions between the binder and the active material surface are preserved.[32]

There is, however, some controversy surrounding the stability of the LiFSI salt. In a modelling study regarding the effect of the FSI^- anion on the SEI of $Li_{13}Si_4$ surfaces, Piper et al. found that FSI^- rapidly releases F^- by breakage of the S−F bond, which most likely contributes to the formation of LiF in the SEI.[66] In addition, the SO_2 group is released, suggesting that the SEI consists of small, inorganic compounds. These results were confirmed by Budi et al., who used ab inito molecular dynamics simulations and X-ray photoelectron spectroscopy (XPS) to show that the FSI^- anion indeed rapidly sheds both F and SO_2.[67] Nie and Lucht studied the role of the lithium salt on the formation and composition of the SEI in LIBs containing binder-free graphite anodes.[34] Their results reflect the findings of Piper et al. and Budi et al. Nie and Lucht used XPS to find that the ratio between O:F was 1:1 in the SEI of both the anodes cycled in $LiPF_6$ and those cycled in LiFSI, suggesting that LiFSI releases as much F as $LiPF_6$. This is surprising, as LiFSI is considered a more stable salt than $LiPF_6$. Therefore, LiFSI could also be prone to hydrolysis, as proposed by Xu.[27] As LiFSI performs better than $LiPF_6$,[10,32] it is unlikely that the de-fluorinated FSI^- anion acts as a catalyst for EC decomposition, like PF_5 does. Nie and Lucht also found that LiF was present in the SEI for LiFSI.

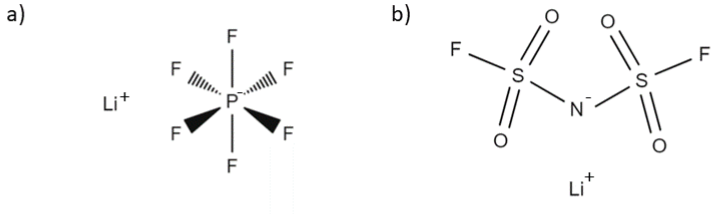

Figure 2.5.4: Structures of $LiPF_6$ (a) and LiFSI (b).

2.5.5 Role of additives on the SEI

The incorporation of additives in electrolytes has been considered for enhancing the stability of the SEI layer. Since additives alter the SEI composition, both SEI stability and its effect on ionic conductivity must be considered.[7] Today, two of the most common additives are fluoroethylene carbonate (FEC) and vinylene carbonate (VC), as they reportedly have increased cycling performance and reversibility. FEC is among the most widely used electrolyte additives with regard to silicon anodes.[12,68] FEC is preferred due to two reasons. Firstly, FEC has a reduction potential that is higher ($1.1 - 1.2$ V) than those of typical electrolyte solvents (like EC, $0.7 - 0.8$ V), such that FEC is reduced before the solvent.[28] This preferential reduction forms a preliminary SEI that prevents further solvent reduction, thus keeping the SEI thin.[28] Secondly, FEC addition promotes reversibility, but the reason for this is not exactly understood yet. Generally, the reversibility is attributed to FEC taking part in forming a flexible polymeric SEI layer. This is

caused by decomposition of FEC to VC-derived products,[69] according to reaction scheme 1, in figure 2.5.5. However, Nakai, Kubota, Kita and Kawashima[70] reported that FEC forms much LiF during decomposition, according to reaction scheme 2 in figure 2.5.5. Yet, the role of LiF in silicon is not clear, with reports deeming it both vital and unnecessary for reversibility. For instance, Etacheri et al.[69] and Jaumann et al.,[71] downplayed the role of LiF with regard to battery reversibility, and concluded that LiF is a mere by-product in the interface reactions. Schroder et al., on the other hand, suggested that LiF is crucial for SEI stability, and hence capacity retention during cell cycling.[72] These discrepancies not only show that SEI investigations are not arbitrary, but also suggest that the anode material design, as well as chemical composition of anode material and electrolyte, may affect the observed mismatches. Etacheri et al. used silicon nanowires with 1 M $LiPF_6$ in EC/DMC (1:1 wt%) with 10 wt% FEC, Jaumann et al. used silicon thin films (50 nm) with 1 M $LiPF_6$ in DMC:EC:FEC (2:1:1 volume%), while Schroder et al. used silicon nanoparticles (5 nm) in 1 M $LiPF_6$ in EC:DEC (1:1 wt%) with 10 wt% FEC.

There have not been conducted many studies on the effect of FEC with LiFSI, but Trask et al. studied the effect of FEC on electrolytes with different Li-salts in full cells containing 15 wt% nanosilicon-bearing graphite anodes.[73] They found no significant difference between the performance of 1.2 M LiFSI and 1.2 M $LiPF_6$ when mixed with EC/EMC/FEC (EMC = ethyl methyl carbonate), in 27/63/10 wt% ratio. This result indicates that the Li-salts play a smaller role in performance degradation than the electrolyte solvent.

LiF may also play an important role in ion conductivity through the SEI layer. In another publication, Jaumann et al.[12] found that the LiF materializes like nanocrystals in the SEI, forming grain boundaries for the Li^+ to diffuse along. In addition, they found that FEC addition promotes the formation of LiF. Recently, however, Veith et al. reported that FEC actually causes less LiF formation when compared to electrolytes ($LiPF_6$ EC/DMC) not consisting of the additive.[28] By using in situ spectroscopic methods, they found that their FEC-containing electrolytes produced SEI layers with $\sim 14\%$ LiF, versus $\sim 80\%$ for electrolytes without FEC. Therefore, the detailed impact of adding FEC is still up for discussion, but it seems indisputable that FEC causes a more stable, slightly flexible SEI layer including some LiF nanocrystals that may promote Li^+ diffusion.

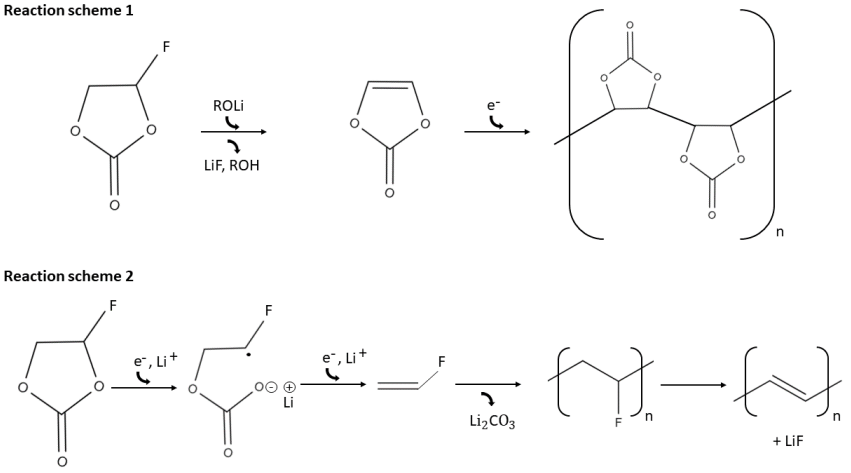

Figure 2.5.5: FEC reaction pathways, as suggested by Etacheri et al.[69] (scheme 1) and Nakai, Kubota, Kita and Kawashima[70] (scheme 2).

Despite their positive attributes, both FEC and VC have some drawbacks, and it is still ambiguous when FEC or VC is more beneficial in silicon anode cells.[12] In fact, the positive effects of FEC on silicon are not unanimous, as partially contrary results regarding the additive have been reported.[12] FEC does for instance not form a sufficiently flexible SEI-layer to accommodate the large volumetric changes of the silicon anode during (de)lithiation, and the capacity drops due to the presence of non-conducting LiF nanocrystals that insulate the silicon particles. On the other hand, these LiF nanocrystals may facilitate easier Li-diffusion by acting as promotors of grain boundaries that the Li^+ can diffuse along.[12] FEC may also have a negative effect on the cathode. Studies have shown that VC, on the other hand, forms a dense and flexible SEI layer, making it better suited for silicon anodes. However, the VC-derived SEI suffers from low ionic conductivity due to the absence of defects, leading to low rate performance.[12]
Another class of additives that have not yet received as much attention is the anion receptor (AR) additives, like tris(pentafluorophenyl) borane (TPFPB), and tris(hexafluoroisopropyl) borate (THFIPB) (figure 2.5.6). ARs can specifically complex with anions to reduce the attraction between Li^+ and the anions, enhancing the ionic conductivity of electrolytes.[74] Increasing ionic conductivity is of great importance with regard to charge and discharge rate, capacity and cycling stability.[13,14] In addition to an organic phase, the SEI consists of large amounts of insoluble inorganic materials like LiF, Li_2O_2 and Li_2CO_3. These inorganics lead to increased impedance, and by extension, capacity loss.[75] Anion receptors can solvate and remove the F^-, OH^-, O_2^- and O_2^{2-} anions that are present in the SEI.[75] Furthermore, Qin et al. have suggested that some ARs may be strong enough to break up the interaction between the Li^+ cation and F^- anion, thereby dissolving LiF.[13] AR addition might therefore tailor the SEI, by dissolving the inorganic

components like LiF, Li_2O and Li_2O_2.[13] In current research, the most represented boron-based AR is tris(pentafluorophenyl) borane (TPFPB).
The research done on silicon anodes with anion receptor addition to the electrolyte is scarce. Han et al.[16] studied the effect of TPFPB concentration in 1 M $LiClO_4$ in EC:DEC on Si thin films and found that increasing TPFPB concentration (up to 5 wt%) increased both capacity retention and Coulombic efficiency. Most noteworthy for this work, was the reported formation of a stable SEI layer upon addition of TPFPB. By using a combination of Electrochemical Impedance Spectroscopy (EIS), SEM and XPS, Han et al. suggested that the addition of TPFPB led to suppression of solvent decomposition as well as the formation of stable LiF compounds in the SEI. This latter suggestion contradicts the idea that TPFPB dissolves LiF, and rather leads to LiF nanocrystals that introduce grain boundaries that promote lithium diffusion. It is not given that these findings hold true for all silicon anode morphologies or varying lithium salts.
There has been done considerable research on TPFPB for graphitic anodes. Most importantly, TPFPB has been shown to have a positive effect on
interfacial impedance and capacity retention.[76] This is because TPFPB can bind to the lithium salt anion according to

$$PF_6{}^- + \text{TPFPB} \longrightarrow PF_6{}^- - \text{TPFPB}, \tag{2.14}$$

hindering subsequent dissolution to PF_5 (as in equations (2.9) and (2.13)) and HF formation. This also results in a higher Li^+ transport number, improving the kinetics. However, AR addition is a two-edged sword, as too large amounts (>3 wt% or >0.1 M[76]) may lead to

$$PF_6{}^- + \text{TPFPB} \longrightarrow PF_5 + \text{TPFPB} - F^-. \tag{2.15}$$

The exact amount of TPFPB added before a negative effect is observed, is debated. Von Wald Cresce et al. found that an addition of more than 0.1 mol% TPFPB may be too much,[77] as it leads to fragmentation of PF_6^- and the formation of TPFPB-F^-, according to equation (2.15). Therefore, TPFPB addition in too large amounts may lead to deterioration of battery performance as it promotes PF_5 formation, leading to a thicker SEI layer. The chance of this happening should be bigger for TPFPB, as it has a very high fluoride affinity, as calculated by Chen and Amine.[74] In fact, Chen and Amine propose to use weaker ARs that still can dissolve LiF, but simultaneously suppress the decomposition of $PF_6{}^-$. One solution may be to use ARs with electron-rich atoms like O. One of these ARs is THFIPB, which will be used as AR additive in this work.
There are currently* no results for the use of THFIPB as an additive in silicon anode half cells. Results on graphite are almost non-existing as well. However, results from Nilssen, Tezel and Svensson indicated that 1 wt% THFIPB improved the stability and reversibility of graphitic cathodes in 1 M $LiPF_6$ dissolved in 3:7 EC:DMC.[78] Fukutsuka, Nakagawa, Miyazaki and Abe found that THFIPB addition lead to a protective surface film on their $LiCoPO_4$ cathode, owing to the THFIPB-F complex formed in their 0.1 M LiF + 0.1 M THFIPB/PC electrolyte.[79] The

*According to Google Scholar, June 11th, 2018.

exact chemical composition of the surface layer was not determined. By using XPS and cyclic voltammetry, they found that THFIPB coordinated moderately to the free F^- anions, which lead to the desired passivating film characteristics. They also confirmed that TPFPB interacted too strongly with F^-, hindering the formation of a stable passivation layer.
As THFIPB is a similar AR as TPFPB, it is expected that the addition of THFIPB will lead to similar effects as observed upon TPFPB addition. As for TPFPB, too much THFIPB may tip the scales and lead to increased formation of PF_5 and HF, or otherwise decompose the Li-salt. A detailed elaboration of the SEI formed in the presence of these additives, and their effect on the performance of silicon anode LIBs (including LiFSI salt) is yet to be reported.

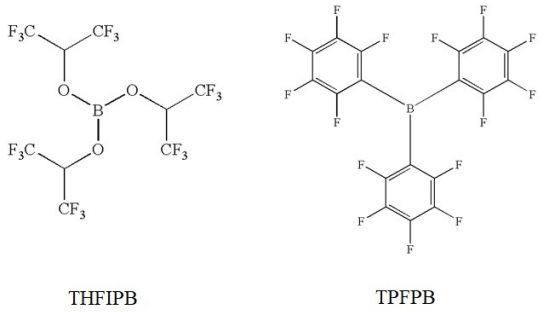

Figure 2.5.6: Structures of THFIPB and TPFPB.[75]

.

2.6 Characterization techniques

2.6.1 FTIR

Fourier Transform Infrared Spectroscopy (FTIR) is a fast and effective technique used to measure a sample's absorption of infrared radiation (IR). When IR is passed through a sample, the molecules within will absorb some of the energy and start to vibrate and/or rotate. The energy required to initiate these molecular motions is highly specific, and depends on both atomic mass and bond strength. As the characteristic energy, E, is related to the frequency, f (through the relation $E = hf$, where h is Planck's constant), the absorbed IR frequencies are also characteristic for different functional groups. Thus, by detecting the transmitted IR of the sample and analyzing the resulting IR absorbance spectrum, it is possible to determine the molecular composition of the sample in question. However, not all vibrational modes are IR active, as a change in dipole moment is necessary. LiF is therefore one of the components not visible in FTIR.
By performing a Fourier transform of the spectrum, the instrument can measure all frequencies at the same time, rather than incrementing over the entire frequency range. IR spectra are often reported as a function of wavenumber, which is the reciprocal of wavelength. Its relation to energy is thus $E = hc/\lambda$, where c is the speed of light in vacuum. The wavenumber is often given in cm^{-1}, and a typical IR range during measurement is the mid-IR; $4000 - 400\ \text{cm}^{-1}$.
Attenuated Total Reflectance FTIR (ATR-FTIR) is an accessory to the FTIR technique, allowing for faster and simpler measurements with less preparation and more versatility regarding materials. The ATR-FTIR uses total internal reflectance caused by a crystal in direct contact with the sample, leading to an evanescent surface wave that is subsequently analyzed. The typical penetration depth of an ATR-FTIR is in the range of $0.5 - 2.0$ µm, making it ideal to analyze the small amounts of material making up the silicon anodes.

2.6.2 XPS

X-ray Photoelectron Spectroscopy (XPS) is a spectroscopic technique that can determine the elemental composition of a sample, as well as empirical formula, chemical state and electronic state of the elements in the material. In XPS, a sample is irradiated with X-rays while the kinetic energy and amount of electrons escaping the surface of the material are measured simultaneously. The escaping electrons have characteristic energies due to their quantum states, making it possible to deduct which element or chemical bonds they originally belonged to. The XPS is equipped with a sample holder that may be introduced into a glovebox, making it possible to preserve the inert Ar atmosphere such that the chemical composition of the SEI does not change due to air contact.

2.6.3 FIB

Focused Ion Beam (FIB) microscopy is a technique in which ions are used to image and manipulate the surface of a sample. The manipulation is done by means of sputtering or material deposition, with the possibility of achieving structures smaller than 100 nm. In this work, the FIB will mostly be used to prepare highly reproducible cross sections in the anode samples, so that the bulk anode material and SEI layer can be investigated by electron microscopy and EDX. The NanoLab FIB is a DualBeam FIB, meaning that in addition to the Gallium (Ga) ion-beam, an electron beam can be used for imaging during operation. The challenge of using a FIB to manipulate matter, is that the interactions with the ion beam and sample might significantly change the morphology of the material. Thus, characterization of surfaces manipulated by an ion beam must be interpreted with great care.

2.6.4 SEM and EDX

Scanning electron microscopy (SEM) is a technique whereby electrons are used to create an image. When electrons are accelerated towards a material, they will interact with the material by penetrating into it. The geometry and depth of this penetration is termed the interaction volume, and is approximately pear shaped. The "stem" is at the surface of the material, and the volume balloons out below the surface. This interaction volume increases with acceleration voltage and decreases with atomic number. SEMs can be operated in two main ways: viewing backscattered electrons (BSE) or secondary electrons (SE). BSEs are incident electrons escaping from the sample, whereas SEs are electrons freed by the collision of the incident electrons within the material. Generally BSEs mainly contain information about atomic number contrast, because the number of electrons that escape from the material becomes higher with increasing atomic number. As the interaction volume becomes larger, the electrons penetrate deeper and are less likely to escape. SEs are used for topographical contrast, as they are only emitted from very close to the surface, and are therefore very sensitive to surface incline.
Most SEMs include an Energy Dispersive X-ray Spectroscopy (EDX) spectrometer. EDX is an analytical technique for obtaining elemental analysis and chemical composition of a sample. By bombarding a solid specimen with a highly focused electron beam, the electrons orbiting the atoms in the sample will get excited and subsequently decay, emitting characteristic X-rays, as seen in figure 2.6.1. These X-rays are analyzed by the EDX spectrometer, resulting in information about the localized elemental composition. By raster-scanning the sample, a chemical map of the entire elemental composition of the specimen may be obtained.

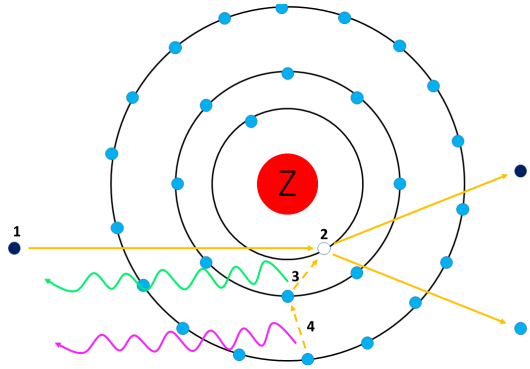

Figure 2.6.1: Principle of X-ray generation in EDX. According to the Rutherford-Bohr model, electrons orbit the positive nucleus at certain orbit states with specific corresponding energies. As electrons from the electron beam are fired at the specimen (1), they might knock electrons out of their orbit (2). This leads to the decay of electrons from higher to lower energy states ((3) and (4)), resulting in the release of characteristic X-rays corresponding to the energy difference between the orbitals.

Chapter 3

Experimental

3.1 Overview

Silicon electrodes fabricated by screen printing of Si powder were received from Institute for Energy Technology (IFE). The chemical composition of the silicon electrodes is 73.18%, with 10.97% carbon black. The rest is made up of CMC binder and buffer chemicals. Different compositions of electrolyte were mixed and subsequently used in the assembly of the coin cells. The cells were then cycled and disassembled before post-mortem investigations of the silicon electrodes using FTIR, XPS, FIB, SEM and EDX were performed. Furthermore, the solution structure of the varying LiFSI concentrations was investigated by FTIR.

3.2 Cell manufacture

3.2.1 Electrolyte mixing

Electrolyte solutions consisting of EC and DEC (1:1 in wt%) mixed with concentrations ranging from 1 M to 5 M LiFSI were prepared. After determining the optimal LiFSI concentration, new electrolytes containing both the optimal amount of LiFSI and different concentrations of the anion receptor THFIPB were prepared. For reference, a solution consisting of 3 M LiFSI in EC:DEC with 5 wt% FEC was made. Finally, a solution containing EC:DEC with 3 M LiFSI, 2 wt% THFIPB and 10 wt% FEC was prepared, to investigate whether the desired properties of the increased salt concentration as well as additives lead to a high-performing electrolyte solution. Figure A.1 in the appendix provides a graphical representation of the electrolyte creation process. The following list shows an overview of all electrolytes that were prepared and tested in a half-cell configuration for this project:

1. 1 M LiFSI in EC:DEC
2. 2 M LiFSI in EC:DEC
3. 3 M LiFSI in EC:DEC

4. 5 M LiFSI in EC:DEC

5. 3 M LiFSI + 6 wt% THFIPB in EC:DEC

6. 3 M LiFSI + 3 wt% THFIPB in EC:DEC

7. 3 M LiFSI + 2 wt% THFIPB in EC:DEC

8. 3 M LiFSI + 5 wt% FEC in EC:DEC

9. 3 M LiFSI + 2 wt% THFIPB + 10 wt% FEC in EC:DEC (termed as "mix" in this report).

The electrolytes were prepared inside an argon-filled glovebox (MBraun) with < 0.1 ppm O_2 and < 0.1 ppm H_2O, at about 2 mbar over-pressure. First, equal amounts of EC (Sigma Aldrich, anhydrous, 99%) and DEC (Sigma Aldrich, anhydrous $\geq$ 99%) were mixed, before LiFSI (TCI Euope, $>$ 98% purity) was added. The additives used were THFIPB (TCI Europe, >95% purity) and FEC (Sigma Aldrich, 99%).

3.2.2 Coin cell assembly

The received electrode sheets were punched out into 16 mm electrode disks using a specially designed hand-held anode cutter (Hohsen Corp.). The disks were subsequently weighed and subtracted of the mass of the Cu current collector, in order to determine the loading. The disks were then taken into the glovebox. In order to obtain the lithium counter-electrode, lithium metal was prepared inside the glovebox by gently brushing it to remove any potential oxide layers. 14 mm lithium disks were then punched out. The half cells were assembled according to figure 3.2.1, using Hohsen 2016 coin cells with a porous polypropylene separator (Celgard, K2400), silicon electrode, gasket, lithium disk as counter electrode and a 0.3 mm thick spacer. In order to avoid any short circuits and to get a uniform current distribution, care was taken when centering the electrodes, spacer and separator. 20 µL electrolyte was applied to the silicon electrode before placing the separator, and an additional 20 µL was applied before the lithium counter electrode was placed. The fact that 2×20 µL electrolyte was used, ensured complete wetting and promoted ionic contact between the two electrodes. The electrolytes used are as described in section 3.2.1, and 3-4 cells were made with each electrolyte solution, resulting in 30 cells. The cell assembly was finalized by crimping the coin cells using an automatic coin cell crimper (Hohsen Corp.).

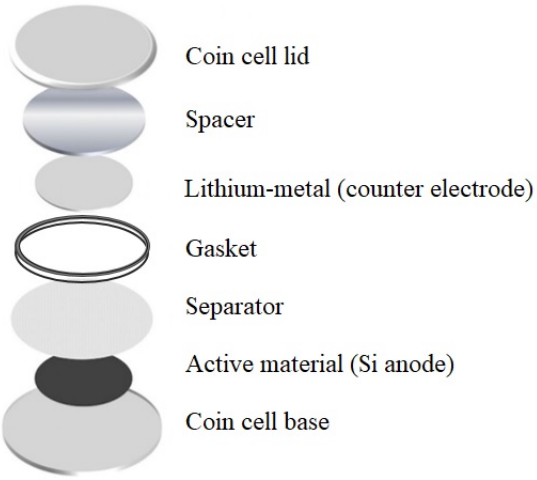

Figure 3.2.1: Coin cell components and configuration. Edited from Birkl et al.[80]

3.3 Electrochemical testing

The coin cells were electrochemically tested by the following protocol in a Lanhe CT2001A LAND battery testing system:

1. Discharge 500 mA h g^{-1} followed by charging up to 1.0 V.
2. Discharge 1000 mA h g^{-1} followed by charging up to 1.0 V.
3. Discharge 1500 mA h g^{-1} followed by charging up to 1.0 V.
4. Discharge 2000 mA h g^{-1} followed by charging up to 1.0 V.

   Steps 1-4 constituted the pre-cycling treatment (formation cycle), all done at C/20.
5. Discharge down to 0.05 V followed by charge up to 1.0 V for 25 or 55 cycles at 1 C.

1 C is defined as the current density required to completely discharge the cell in one hour, given a theoretical capacity of 3600 mA h g^{-1} active material. The active material for each cell was determined by subtracting the Cu current collector mass from the total electrode mass, then multiplying with the Si fraction of the active material (73.18%). In total, 30 cells were tested; 3-4 cells from each of the electrolyte compositions. 2 cells of the same electrolyte composition were tested in parallel; each undergoing 200 cycles while the final 1-2 underwent 10 cycles (in

parallel when 2 cells of the same composition were desired). By following this testing schedule, the cells ended cycling after charging to 1.0 V, and were then removed in order to be disassembled and investigated post-mortem. The 10-times cycled cell underwent the same test regime as described for the cells that underwent 200 cycles, but the cells were stopped after 10 cycles when they had reached 1.0 V after charging.

3.4 Post mortem characterization

3.4.1 Coin cell disassembly

After cycling, the cells were disassembled inside the glovebox using a coin cell disassembling tool (Hohsen Corp.). Immediately after opening, the silicon electrode was dipped three times in dimethyl carbonate (Sigma Aldrich, anhydrous, 99%) in order to remove any remaining lithium salts and solvents. After drying in vacuum in the glovebox antechamber for 30-45 minutes, the anodes were taken out and inspected using FTIR, XPS and FIB/SEM/EDX.

3.4.2 FTIR

To characterize the composition of the SEI, a Bruker Vertex 80v ATR-FTIR was used with a diamond crystal. It was vital for the post-mortem characterization that the anodes avoided any contact with air, as this may lead to a range of unwanted reactions, altering the SEI composition. Therefore, the setup shown in figure 3.4.1 was used during FTIR investigations:

i The FTIR plate with the diamond crystal (small square) was properly cleaned with isopropanol, before it was brough into the glovebox.

ii The anode was placed face-down onto the diamond crystal of the FTIR sample plate.

iii A small piece of aluminum foil was placed on top of the anode, and a piece of contact paper was used to seal the anode and Al-foil in place, making sure no air would reach the anode.

iv As an insurance, another layer of Al-foil and contact paper was placed on top of the contact paper seal, and the plate was removed from the glovebox.

During measurements, proper contact between the samples and the diamond crystal was assured by applying pressure with the module piston. In order to obtain spectra that reflected the SEI composition, the spectrum of an uncycled, pristine electrode, was subtracted from the spectrum of the cycled electrode. This way, the changes observed with FTIR reflected deviations in interfacial chemistry during cycling. In order to better identify the peaks present, a standard baseline correction, described in the Bruker software,[81] was applied on the FTIR spectra. A scan range from 400-4000 cm^{-1} was used, with a resolution of 2 cm^{-1}.

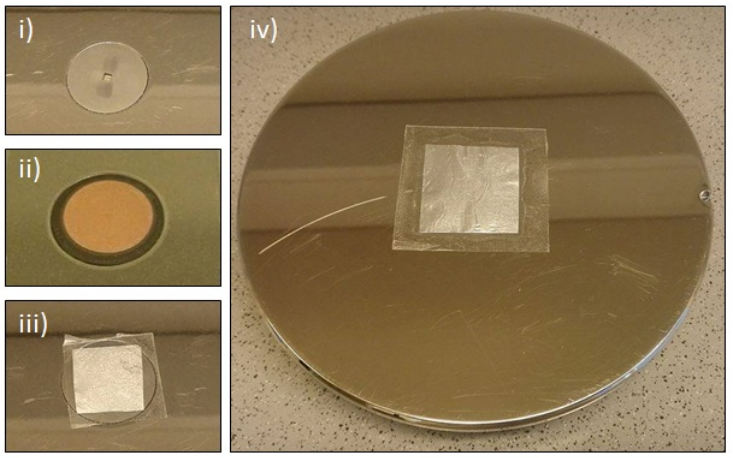

Figure 3.4.1: Setup used to avoid air contact during FTIR analysis. Steps i) to iv) are explained above.

3.4.3 XPS

For the XPS measurements, a Kratos Analytical Axis Ultra DLD XPS was used. The XPS uses an aluminum monochromatic X-ray source operating at 100 W. For each sample, three survey scans with pass energy 160 eV and resolution 0.5 eV from 1200-0 eV were performed in order to identify the elements present on the anode. Next, each core peak of interest underwent 20 narrow scans at pass energy 20 eV with resolution 0.1 eV in order to get high resolution data. The measurements were done at $\sim$1 $\times 10^{-9}$ Torr, with an acceleration voltage of 15 kV with a 10 mA beam current.
The XPS is equipped with a sample transporter holder that contains a small closeable chamber with a moveable sample stage inside (shown in figure 3.4.2). In order to keep the cycled anodes in an inert atmosphere, the XPS transporter holder was brought into the glovebox with the small chamber opened. Inside the glovebox, the anode was assembled onto a Cu sample stub by using some ultra-high vacuum (UHV) compatible carbon tape. The stub was then fastened in the sample holder of the closeable chamber (figure 3.4.2 iii)), which was retracted into the XPS transporter holder before the chamber was closed. This way, the anode was kept in an argon atmosphere. For the XPS measurements, the sample holder was connected to one of the XPS antechambers. This chamber was then flushed with argon, so that it matched the $\sim$2 mbar argon over-pressure found in the glovebox, and consequencely, in the XPS transfer holder. When this was done, the small chamber of the XPS transfer holder was opened, such that the anode sample could be transferred into the antechamber. Afterwards, the antechamber was evacuated to UHV, in order to introduce the sample into the measurement chamber.
For the XPS data-fitting, the software Casa XPS was used. In order to obtain comparable results to literature, the XPS spectra had to be charged corrected by using

adventitious carbon in the C 1s spectrum as a reference. The peak for adventitious carbon was shifted from its measured value to the value of 285.0 eV (typically this shift corresponded to 2-3 eV). Afterwards, both the core-peak spectra and survey spectra were shifted a corresponding amount. The underlying assumption for the calculation of atomic chemical composition in CasaXPS is that the number of electrons recorded is proportional to the number of atoms in a given state. The program uses an element library that contains all relevant spectral information, including relative sensitivity factors for the different core-peaks, to calculate atomic percentages. Deconvolution of the peaks was done by using the "quantify" tool which allows the creation of regions of interest and the addition of components. The background was set to a U2 Tougaard background for both the survey scans and the core-peak scans.

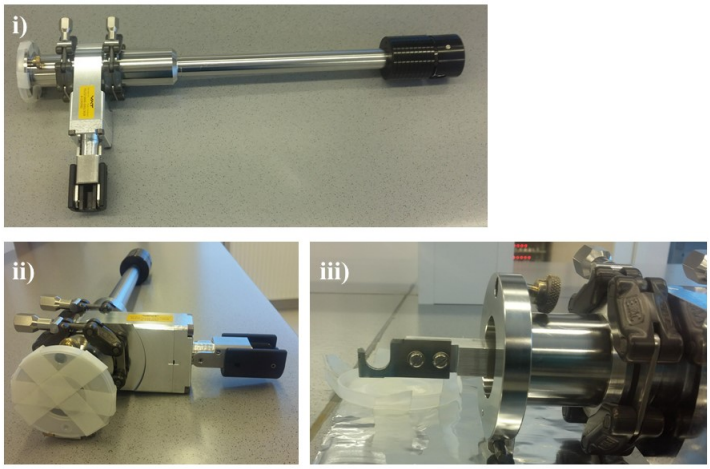

Figure 3.4.2: XPS transporter holder and its features. i) shows the entire holder, including the chamber opening/closing lever (underneath yellow sticker) and movable handle (right side) ii) shows the plastic cap protecting the opening of the inner chamber, while iii) shows the closeable chamber in an open configuration, with the sample stage pushed out.

3.4.4 FIB

In order to investigate the cross-sectional composition of the anodes, a FEI Helios NanoLab DualBeam FIB was used. The dual beam FIB is equipped with both an electron beam and an ion beam (Ga^+). The ion beam is primarily used to do sputtering and deposition of material, as well as imaging. In order to obtain the cross sections, the "regular cross section" sputtering function of the FIB was chosen, and a volume of 20×17×4 µm (length, width, depth) was sputtered. It should be noted that a 4 µm depth refers to the expected depth for sputtering of Si. The sputtering ratio of the electrode to Si was roughly 5, implying that the

cross sections were roughly 20 µm deep. After the "regular cross section" was made, two steps using the "cleaning cross section" function were performed. This time, volumes of 20×2×4 µm and 20×1×4 µm were sputtered. For the "regular cross section", the ion source had an acceleration voltage of 30 kV and a high current of 9.3 nA. The "cleaning cross section" was performed at 30 kV with 2.1 nA and 0.28 nA, respectively. The sputtering was performed at a tilt of 52° (as this is the angle of the ion source to the sample stage), in order to obtain a perpendicular sputtering. In order to investigate the cross sections, the electron beam was used. Here, an acceleration voltage of 2 kV and an emission current of 86 pA, with a working distance of 4.1 mm was used. After obtaining cross sections in the anodes, the samples were transferred to the APREO SEM for SEM and EDX analysis. In order to minimize the air contact of the silicon anodes, they were transferred from the glovebox to the FIB in air tight, argon filled containers. However, in order to mount the samples into the FIB, they had to be taken out, which lead to unavoidable air exposure. Extra care was taken during transport so that the samples would not suffer from transportation-induced damages.

3.4.5 SEM and EDX

SEM was done using an FEI APREO Scanning Electron Microscope (SEM). In addition to having an electron beam for imaging, the APREO SEM has the possibility of inspecting multiple samples at once, as well as being equipped with a high-precision EDX detector (Oxford Xmax 80 mm^2, attached to the SEM). The working distance was set to 4 mm, the acceleration voltage to 2 kV and emission current to 50 pA for morphology and cross section investigations. For EDX analysis, the working distance was set to 10 mm, acceleration voltage to 5 kV and emission current to 0.8 nA. The transportation of the anodes from the FIB into the SEM lead to unavoidable air contact for about 5 minutes.

Chapter 4

Results

4.1 The effect of electrolyte concentration on solution structure and electrolyte properties

4.1.1 Visual inspection of the electrolytes

After mixing, the different electrolytes showed some variations in both appearance and wettability. Firstly, the viscosity increased with increasing salt concentration. The 3 M LiFSI electrolyte was still quite thin bodied, but the 5 M LiFSI electrolyte was highly viscous. When applying the electrolytes on the anode and separator, it was observed that the wettability reduced with increasing salt concentration. The 5 M solution spread out poorly, especially on the Celgard separators. However, by waiting 24 h before cycling the half cells, the electrolyte got the time to wet the surfaces better.
The most curious wettability effect was observed for the electrodes containing THFIPB. The addition of the anion receptor apparently hindered proper wetting of the electrolyte onto the anode. Instead of either spreading out or lying in droplets on the electrode surface, the solution did something in between; it spread out in some places but seemed to fizz somewhat, creating parts on the anode with droplet-like shapes in between the well-wetted parts. After leaving the electrolyte for a couple of days, its color turned slightly yellow-brown, and the fizzing effect stopped. However, the half-cell performances were the same regardless of using the electrolyte right after preparation or after it had settled for a few days. The yellow-brown color may come from thermal decomposition of the lithium salt as the anion receptor binds to it, creating gas (like HF) in the process.[82]

4.1.2 Characterization of electrolytes by FTIR

By stacking the FTIR plots of three different electrolyte compositions (EC:DEC, 1 M LiFSI in EC:DEC and 5 M LiFSI in EC:DEC), as seen in figure 4.1.1, differences between peak values and intensities can be observed.

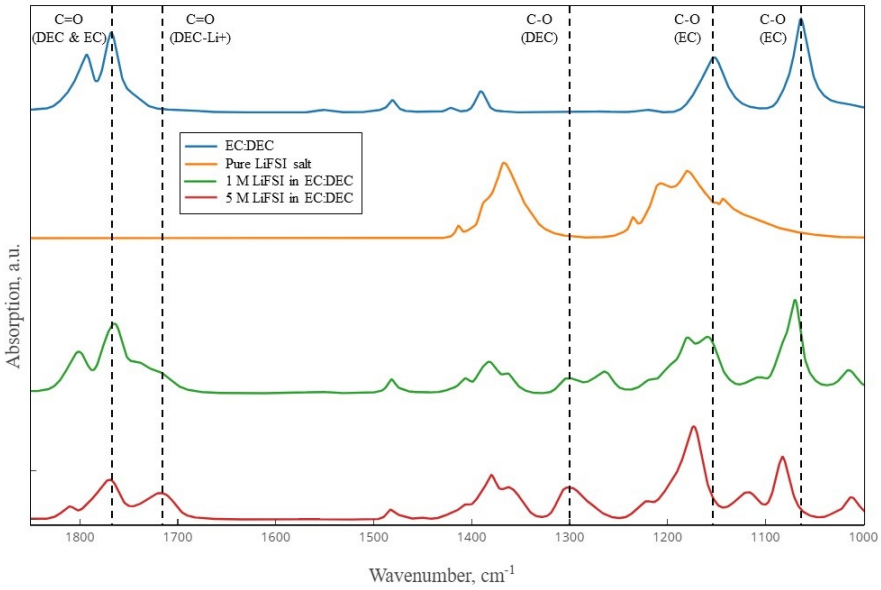

Figure 4.1.1: FTIR plots of three different electrolyte compositions; EC:DEC (blue), 1 M LiFSI in EC:DEC (green) and 5 M LiFSI in EC:DEC (red). The FTIR spectrum for pure LiFSI salt is also included (orange).

As is evident from figure 4.1.1, the increasing LiFSI concentration generally lead to a blueshift of the chemical bonds present. The dotted lines indicate the C-O and C=O bonds found in EC and DEC. Changes in the intensity or position of these peaks, often indicate changes in the chemical composition of the surrounding medium of these sensitive groups. From figure 4.1.1, it is seen that the EC:DEC solution had absorption peaks found at 1793, 1767, 1152 and 1063 cm^{-1}, along with minor peaks at 1481 and 1390 cm^{-1}. When 1 M LiFSI was added, the major peaks shifted to 1801, 1764, 1159 and 1069 cm^{-1}. For the 5 M concentration, the same peaks shifted to 1810, 1769, 1173 and 1083 cm^{-1}. The two LiFSI-containing electrolytes also got new absorption peaks at 1301 and 1720-1740 cm^{-1} for 1 M, and 1303 and 1718 cm^{-1} for 5 M LiFSI, respectively.

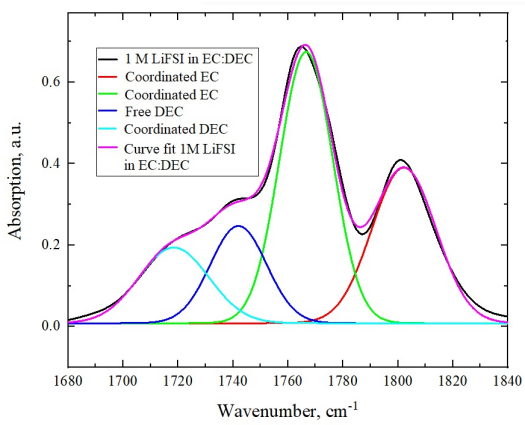

Figure 4.1.2: FTIR of carbonyl group in 1 M LiFSI in EC:DEC electrolyte.

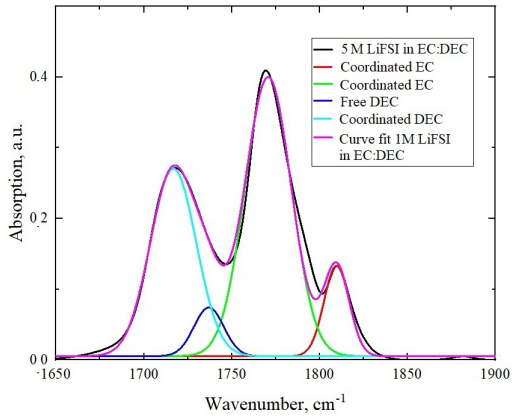

Figure 4.1.3: FTIR of carbonyl group in 5 M LiFSI in EC:DEC electrolyte.

Figures 4.1.2 and 4.1.3 show the carbonyl group present in the 1 M and 5 M LiFSI electrolytes. The curve fits for the uncoordinated and coordinated C=O-group present in DEC (at 1718 and 1742 cm^{-1}) were used to obtain a solvation number N for the electrolytes by equation (2.8). The spectra were fitted in OriginLab, and the areas under the coordinated and uncoordinated C=O peaks were obtained through Gaussian curve fits. The solvation number for the 1 M solution was calculated to be 4.06, while the solvation number for the 5 M electrolyte was calculated to 1.48. The coordinated C=O group of EC contains two peaks, but no peaks for free C=O in EC were found. Therefore, the coordination number using relative areas for coordinated and uncoordinated EC could not be obtained.

4.2 Effect of LiFSI concentration on cell performance and SEI formation

4.2.1 The effect of LiFSI concentration on cell capacity

The charge capacity versus the cycle number of the half cells of 1, 2, 3 and 5 M LiFSI in EC:DEC is given in figure 4.2.1. Additionally, the Coulombic efficiency (CE) is plotted on the right y-axis. For each composition, 2-3 cells were made and tested. The cycle data show the average (avg) capacity obtained for cells of the same composition. As error bars make it harder to see the trends, the same plots, with standard deviations, are given in figures A.2 and A.4 in the Appendix.
Generally, all the cells experienced a similar behaviour in terms of capacity. After the four formation cycles at C/20, ending at 2000 $\mathrm{mA\,h\,g^{-1}}$, the cells dropped to a capacity of about 1200 $\mathrm{mA\,h\,g^{-1}}$ during the first cycle at 1 C. Thereafter, the capacity for all cells dropped until cycle 150-160, where the capacity stabilized at about 100-120 $\mathrm{mA\,h\,g^{-1}}$. The data show that the half cells containing 1 M LiFSI experienced a severe capacity drop to 650 $\mathrm{mA\,h\,g^{-1}}$ at cycle 15, from where they gradually increased and reached a plateau at about 850 $\mathrm{mA\,h\,g^{-1}}$ from cycle 22 to around cycle 50. Then, the capacity dropped approximately linearly until cycle 160, where it stabilized at about 75 $\mathrm{mA\,h\,g^{-1}}$. The 2 M LiFSI containing half cells underwent a similar drop in capacity, but stabilized at about 920 $\mathrm{mA\,h\,g^{-1}}$ from cycle 14-25, where they experienced a similar linear drop in capacity as the 1 M LiFSI cells, stabilizing at about 100 $\mathrm{mA\,h\,g^{-1}}$ after 160 cycles. Overall, the linear drop from cycle 25 to 160 was not as steep as for 1 M, meaning that the 2M cells produced a higher capacity between cycles 50-150 than the 1 M LiFSI cells. The half cells containing 3 M LiFSI dropped to a capacity of about 1050 $\mathrm{mA\,h\,g^{-1}}$ from cycles 15-30, before they too decreased rapidly in capacity until cycle 140, where the capacity stabilized at about 120 $\mathrm{mA\,h\,g^{-1}}$. Finally, the cells containing 5 M LiFSI dropped rather continuously until cycle 120, where their capacity also stabilized at a level of about 120 $\mathrm{mA\,h\,g^{-1}}$.
In general, the CE for the cells deviated somewhat the first 10 cycles, before turning highly similar for all electrolytes until cycle 100. After 100 cycles, the half cells with highly concentrated electrolytes (3, 5 M) exhibited a more stable CE than the cells with more dilute electrolytes (1-2 M). The correlation between the CE and the SEI formation is discussed in section 5.2.1.
Based on the cell performance given in figure 4.2.1, the 3 M electrolyte was chosen as the optimal salt concentration, and was used in combination with the additives FEC and THFIPB, the results of which are presented in section 4.3.1.
Figure 4.2.2 shows the charge capacity of the 10-times cycled cells prior to the FTIR characterization, presented in figure 4.2.4.

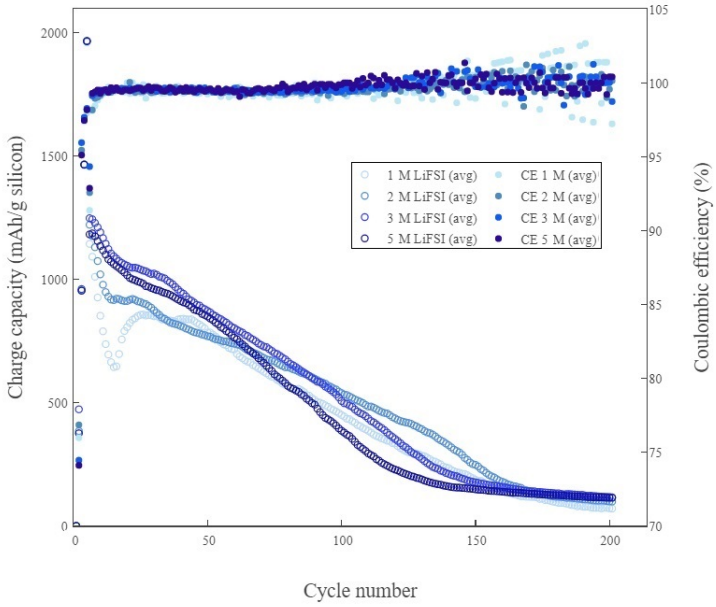

Figure 4.2.1: Effect of Li-salt concentration on charge capacity and Coulombic efficiency (CE).

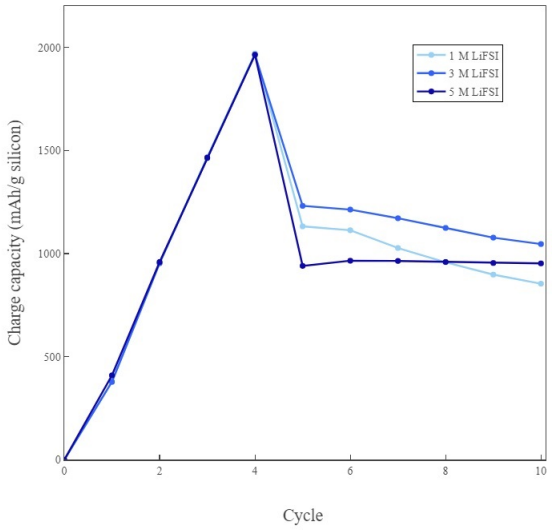

Figure 4.2.2: Charge capacity of the 10-times cycled cells that were subsequently investigated by FTIR.

4.2.2 Characterization of SEI layers by FTIR

In order to depict the SEI composition without the underlying original anode structure, the spectrum of the pure silicon anode (figure 4.2.3) was subtracted from the obtained spectra, resulting in the plots depicted in figure 4.2.4 and 4.2.5. Figure 4.2.4 shows the FTIR spectra of the anodes after being cycled 10 times with electrolytes of increasing LiFSI concentrations. Even though the original spectra were sampled from 400-4000 cm^{-1}, the resulting SEI-depicting spectra are plotted from 1800-600 cm^{-1}. The reason for excluding the wavenumbers outside this range, is that the spectra did not contain any useful information outside this interval (the absorption was either very low or contained too much noise).
The three spectra of increasing LiFSI concentration are quite alike, but some differences are apparent. Regarding the similarities, all of the spectra exhibit absorption peaks at about 1775, 1600, 1445, 1375, 1315, 1175, 1080, 990, 820, 715 and 565 cm^{-1}. The peaks do, however, show different intensities, pointing to different levels of the components associated with them. By increasing the LiFSI concentration, a new, more prominent peak arises at 1040 cm^{-1}, in addition to the emergence of a new peak at 900 cm^{-1}. Furthermore, the peaks at about 1775, 1600 and 1315 cm^{-1} get far less intense at higher salt concentrations.

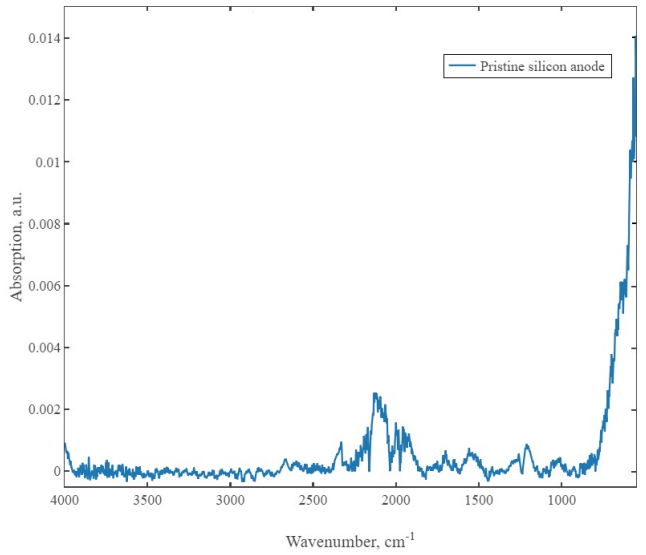

Figure 4.2.3: FTIR spectrum of the pristine silicon anode.

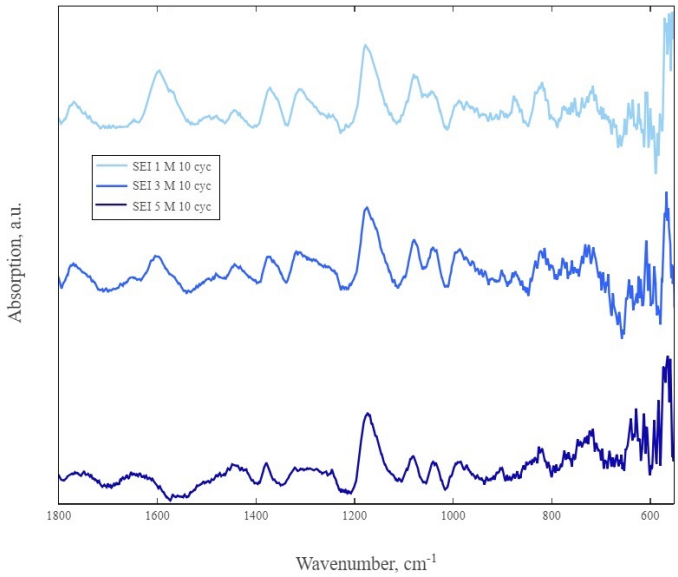

Figure 4.2.4: FTIR plots of the SEI layers formed on the silicon anodes during 10 cycles with differently concentrated electrolytes.

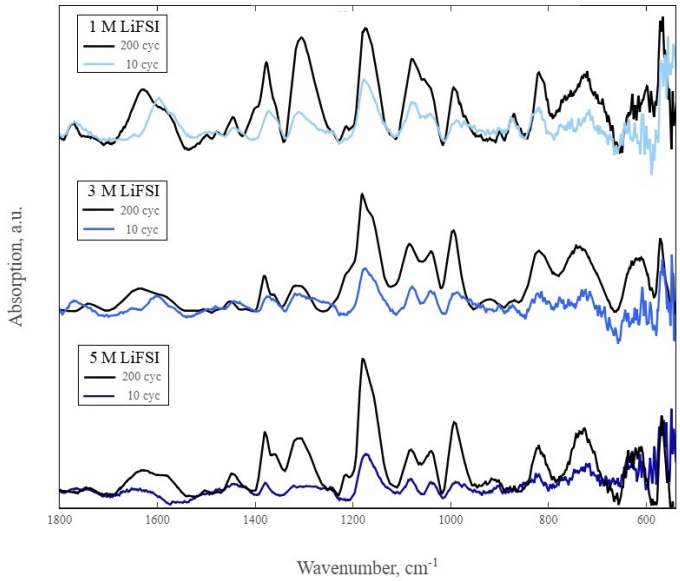

Figure 4.2.5: Comparison between FTIR plots of the SEI layers formed on the silicon anodes during 10 (color) and 200 (black) cycles with differently concentrated electrolytes.

Figure 4.2.5 shows the FTIR spectra of the SEI layers present on the anodes after both 10 and 200 cycles. The SEI signature is much stronger for 200 cycles, indicating that the SEI layer has grown thicker from cycle 10 to 200. Most of the peaks are still present. The biggest changes include a peak shift from 1600 cm^{-1} to 1650 cm^{-1} and the emergence of a strong peak at around 1000 cm^{-1} for all the spectra, while the peaks at 1375, 1315 and 1080 cm^{-1} are stronger for the 1 M sample.

4.2.3 Characterization of SEI layers by XPS

Figure 4.2.6 shows the survey scans performed on the silicon anodes cycled with 1 M (a) and 3 M LiFSI (b). Table 4.2.1 shows the atomic percentages of the different elements present in the two SEI layers, as obtained by CasaXPS.

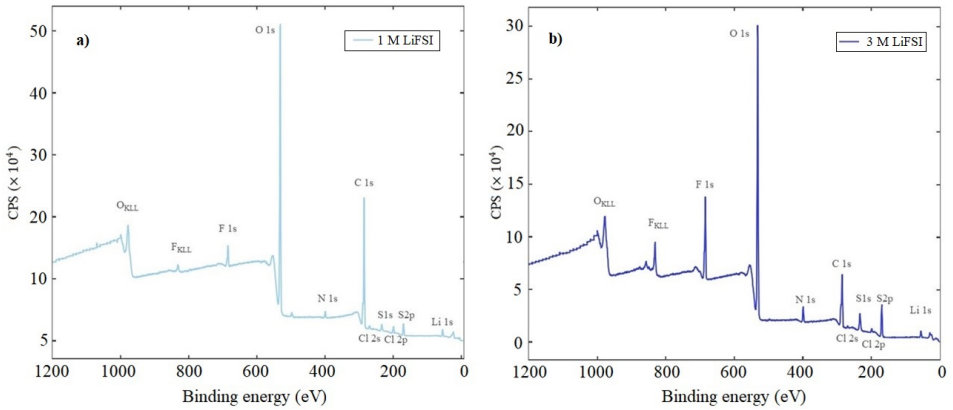

Figure 4.2.6: XPS survey scans of a 10–times cycled anode in 1 M (a) and 3 M LiFSI (b).

Table 4.2.1: Atomic percentages obtained by analyzing the survey spectra of the anodes cycled in 1 M and 3 M LiFSI. The figures do not add up to 100%, as there is Li, Cl and Na present as well.

Peak	**Atomic %, 1 M LiFSI**	**Atomic %, 3 M LiFSI**
C 1s	55.86	35.09
O 1s	36.00	43.02
F 1s	1.85	7.47
S 2p	3.36	10.18
N 1s	1.45	3.53

Table 4.2.1 indicates that the SEI layer formed on the anode cycled in 3 M LiFSI is much less carbonaceous than the anode cycled in 1 M LiFSI. Additionally, the elements corresponding to the LiFSI salt are present at a higher percentage in the SEI of the 3 M LiFSI-based electrolyte.

Figure 4.2.7 shows the core level peaks of C 1s and O 1s for the anode cycled with 1 M LiFSI. By using CasaXPS, the peaks have been deconvoluted to show the presence of several carbon and oxygen species. Additionally, the relative composition of each chemical species may be estimated by the area underneath the peaks. The relative areas are included in figure 4.2.7. The C 1s spectrum in figure 4.2.7 fits well with the presence of five different carbonaceous compounds, present at 285 (C-C and C-H bonds), 286.5 (C-OH and C-O-C bonds), 287.8 (C=O bonds), 288.9 (O-C=O bonds) and 289.9 eV (CO_3 bonds). The O 1s peak also fits well with the inclusion of five peaks, namely at 531.8 (C-OH and C-O-C bonds), 532.5 (CO_3 bonds), 531 (C=O bonds), 531.2 (O-C=O bonds) and 533.7 eV (the S=O bond in LiFSI).

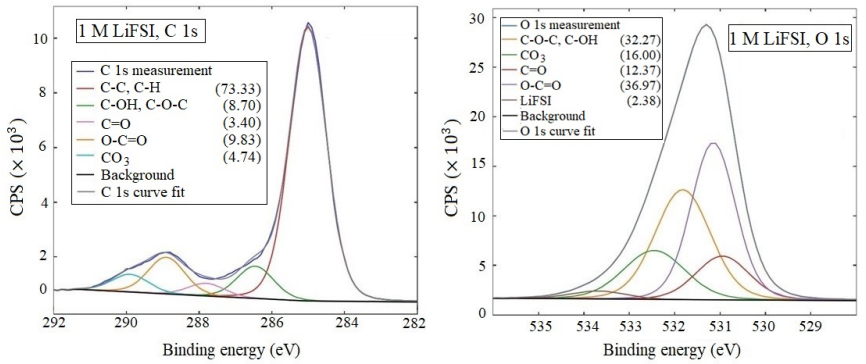

Figure 4.2.7: XPS scans of the C 1s and O 1s core peaks of the anode cycled 10 times in the 1M LiFSI electrolyte. The parentheses represent the relative area (in percent) of the peak.

The F 1s and Cl 2p spectra are shown in figure 4.2.8. The curves are deconvoluted to contain two peaks each. F 1s contains LiF at 685 eV and LiFSI at 687.8 eV, while Cl 2p contains the Cl $2p_{3/2}$ and Cl $2p_{1/2}$ at 198.6 and 200.2 eV, respectively. The presence of Cl indicates that the salt is not of high enough purity to avoid corroding the Al current collector in a full cell configuration.
Lastly, figure 4.2.9 shows the S 2p and N 1s spectra found in the SEI layer of the anode cycled in 1 M LiFSI. The S 2p and N 1s peaks consist of the same products, namely an undefined LiFSI salt degradation product at 169 and 398.7 eV, for S 2p and N 1s, respectively, LiFSI salt at 170.2 and 399.4 eV, and an X-ray degradation product related to salt decomposition at 167 and 400.4 eV, respectively.

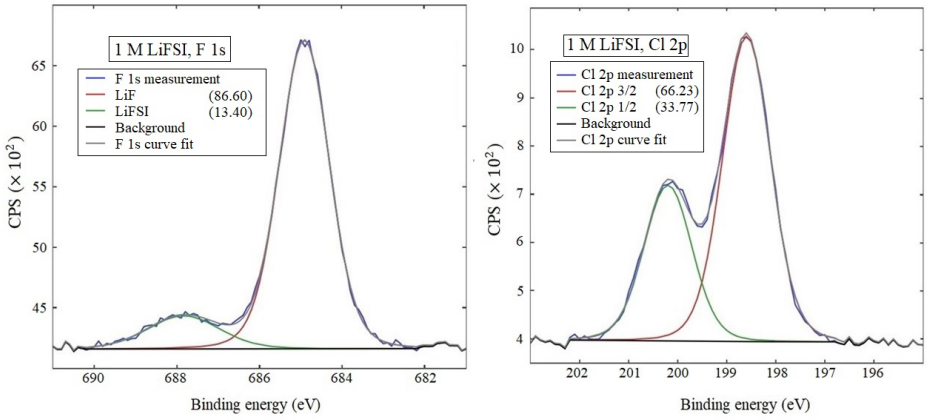

Figure 4.2.8: XPS scans of the F 1s and Cl 2p core peaks of the anode cycled 10 times in the 1 M LiFSI electrolyte. The parentheses represent the relative area (in percent) of the peak.

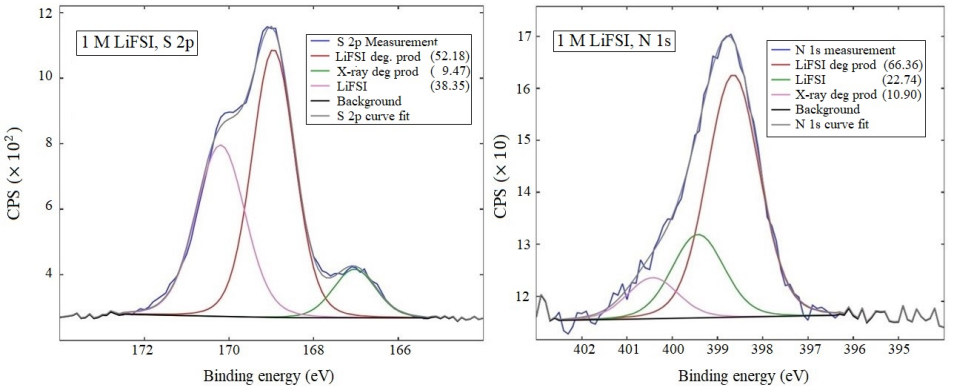

Figure 4.2.9: XPS scans of the S 2p and N 1s core peaks of the anode cycled 10 times in the 1 M LiFSI electrolyte. The parentheses represent the relative area (in percent) of the peak.

The anode cycled in 3 M LiFSI contains similar peaks as the core peaks of the anode that was cycled in 1 M LiFSI, as evident from figures 4.2.10 - 4.2.12. The core peaks for the 3 M sample are deconvoluted to show the same peaks as for the C 1s, O 1s, F 1s, N1s, S 2p and Cl 2p core peaks of the 1 M LiFSI sample.

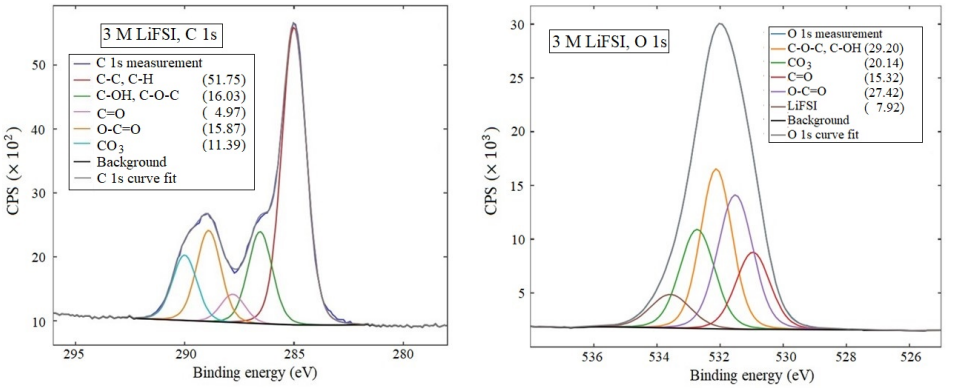

Figure 4.2.10: XPS scans of the C 1s and O 1s core peaks of the anode cycled 10 times in the 3 M LiFSI electrolyte for 10 cycles. The parentheses represent the relative area (in percent) of the peak.

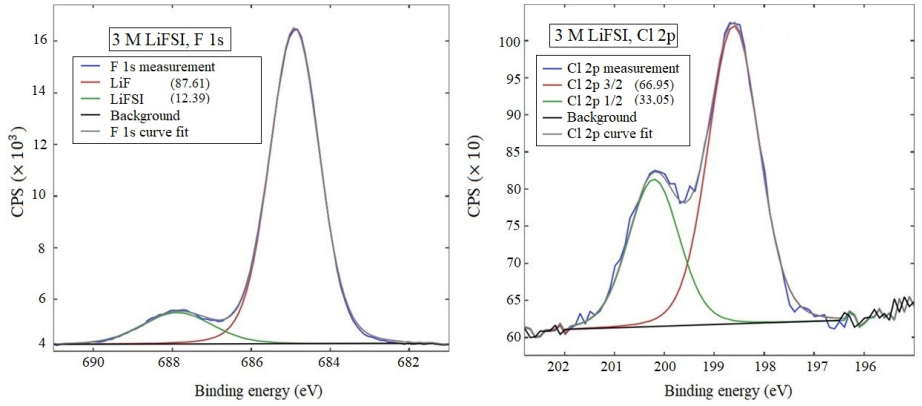

Figure 4.2.11: XPS scans of the F 1s and Cl 2p core peaks of the anode cycled 10 times in the 3 M LiFSI electrolyte for 10 cycles. The parentheses represent the relative area (in percent) of the peak.

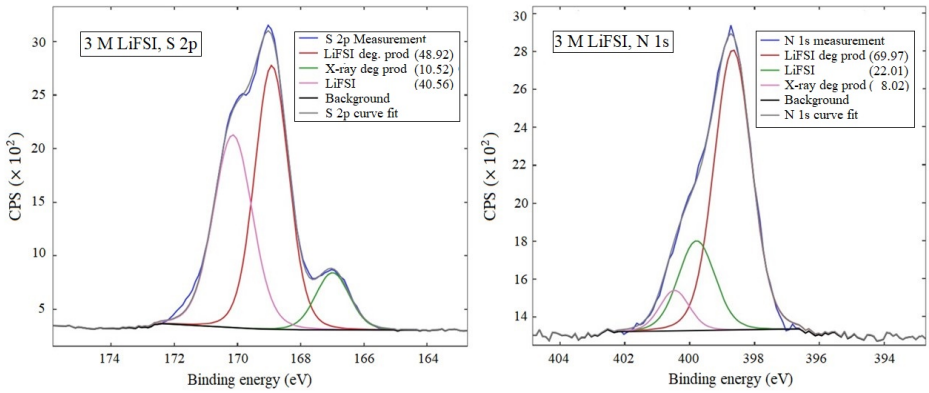

Figure 4.2.12: XPS scans of the S 2p and N 1s core peaks of the anode cycled 10 times in the 3 M LiFSI electrolyte for 10 cycles. The parentheses represent the relative area (in percent) of the peak.

4.2.4 Characterization of anode surfaces and SEI layers by SEM and EDX

Figure 4.2.13 shows the overall morphology of the pristine Si anode (in a and b), as well as a close-up image of the material (c) and a FIB cross-section (d). The material seemed to be highly uniform and porous. From figure 4.2.13 c) it can be seen that the silicon was present in micro-meter large chunks, while the carbon black was dispersed nicely in sizes ranging from tens to hundreds of nanometers. The cross-section image shows the porosity downwards in the anode. The thickness of the anode was found to be 12.8 ± 0.1 µm (the arrow stops at the dendritic copper foil).

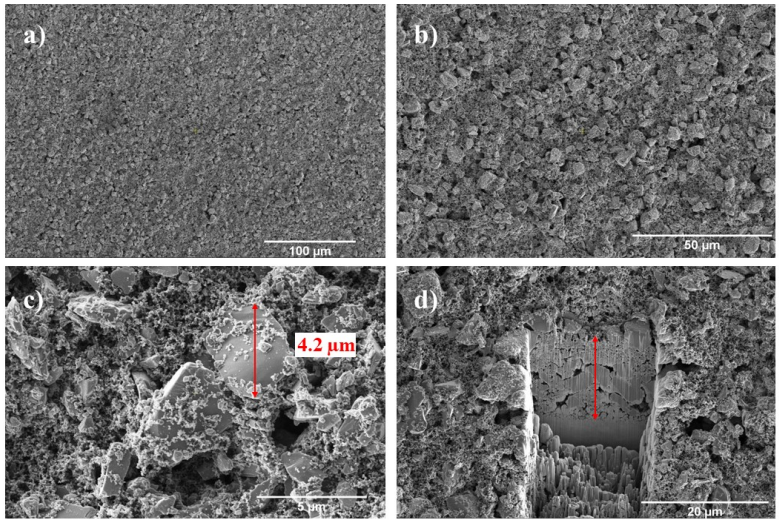

Figure 4.2.13: SEM images of the overall morphology of the pristine Si anode (a and b). The material consisted of micron-sized silicon chunks, dispersed with carbon black particulates (c). d) shows a cross section obtained by using FIB.

Figure 4.2.14 shows the EDX spectrum obtained from the surface of the pristine Si anode, indicating a strong presence of Si and C.

After 10 cycles, the surface morphology was highly similar regardless of which concentration was used. Therefore, only images of the 3 M sample are included. Figure 4.2.15 a) and b) give a general overview of the surface. It still appeared porous, with well-defined silicon particles and carbon black (c). The particles had aggregated a little more, making larger lumps of material stick together, separated by thin cracks. The carbon black was more "smeared out", indicating that a layer had formed on the anodes.

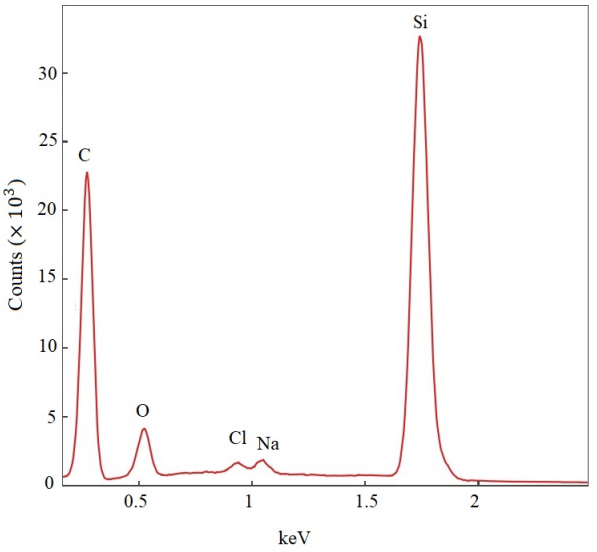

Figure 4.2.14: EDX data reflecting the surface composition of the pristine Si anode.

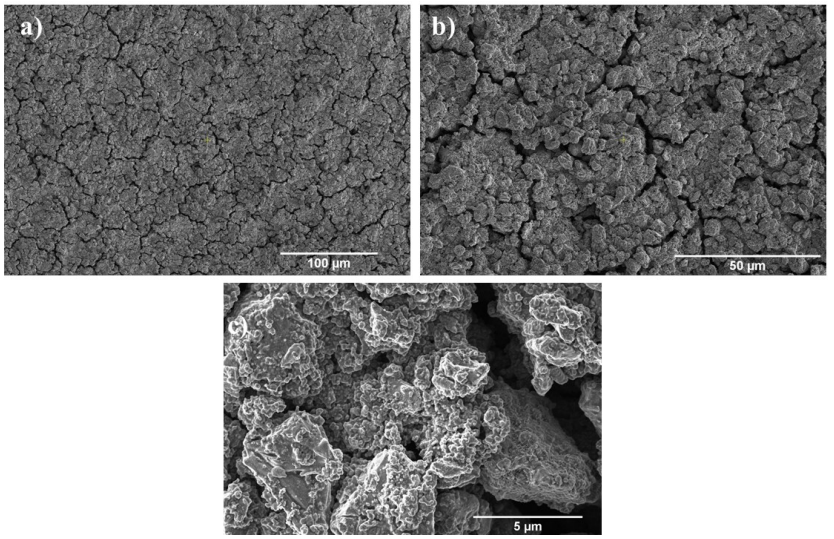

Figure 4.2.15: Example images of the anode morphology after 10 cycles for 3 M LiFSI. The morphology was highly similar regardless of LiFSI concentration, and consisted of more agglomerated particles and areas, separated by small cracks as visible in (a) and (b). c) represents a typical close-up image of the anode.

After 10 cycles, the cross-sections presented in figure 4.2.16, showed that the anode still was highly porous, with little difference between the varying electrolytes. The thickness of the anodes varied slightly, being measured to 13.1, 19.6 and 17.1 $\pm$ 0.1 µm for 1, 3 and 5 M LiFSI, respectively.
From figure 4.2.17, the surface composition of the anodes that underwent 10 cycles is seen. These results indicate a stronger C, O, F and S presence on the surface than for the pristine anode.

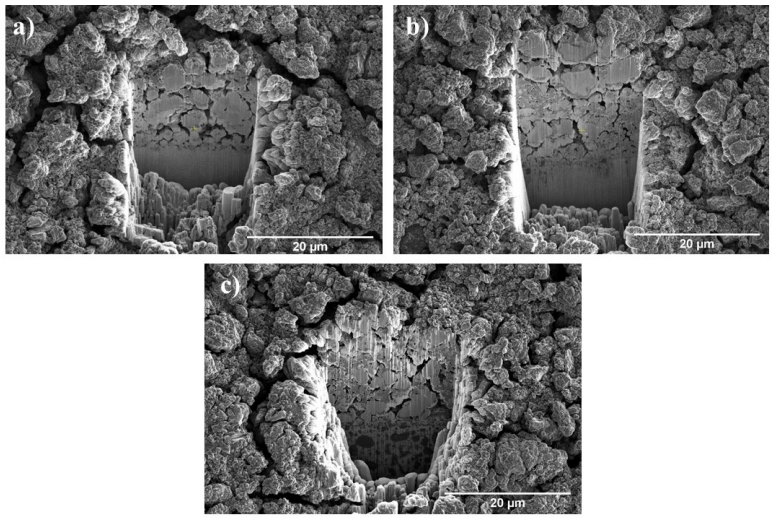

Figure 4.2.16: Cross-sections of the 1, 3 and 5 M LiFSI samples (a-c, respectively).

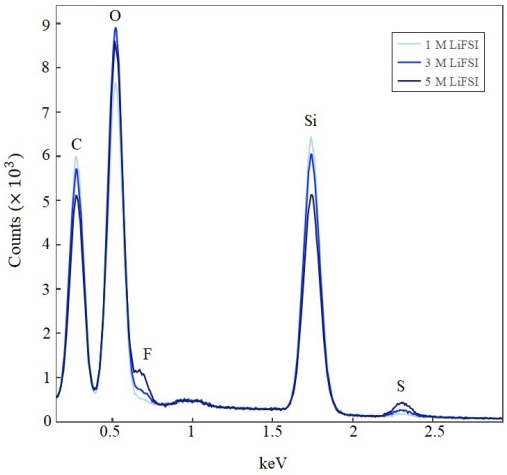

Figure 4.2.17: EDX data reflecting the surface composition of the anode, including the SEI, of the 1 M, 3 M and 5 M samples.

After 200 cycles, the 3 M sample was investigated. The results are presented in figure 4.2.18. The anode surface consisted of large particulates separated by narrow cracks (a), but also dense areas of a thick film-like structure, separated by large cracks (b and c). The obtained cross section is given in d), and was measured to be 22.5 ± 0.1 µm.

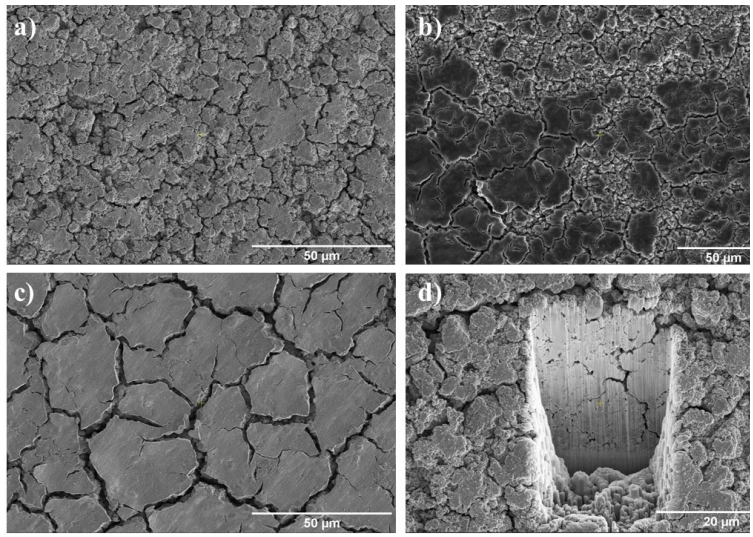

Figure 4.2.18: Surface morphology (a-c) and cross-section (d) on the 3 M anode after 200 cycles. Image b) is taken with 10 keV, to better see the flake-like films.

The EDX map scan of the 200-times cycled anode surface in figure 4.2.18 b) is given in figure 4.2.19. The flakes seem to consist of much F, while the surface is generally covered in O and C.

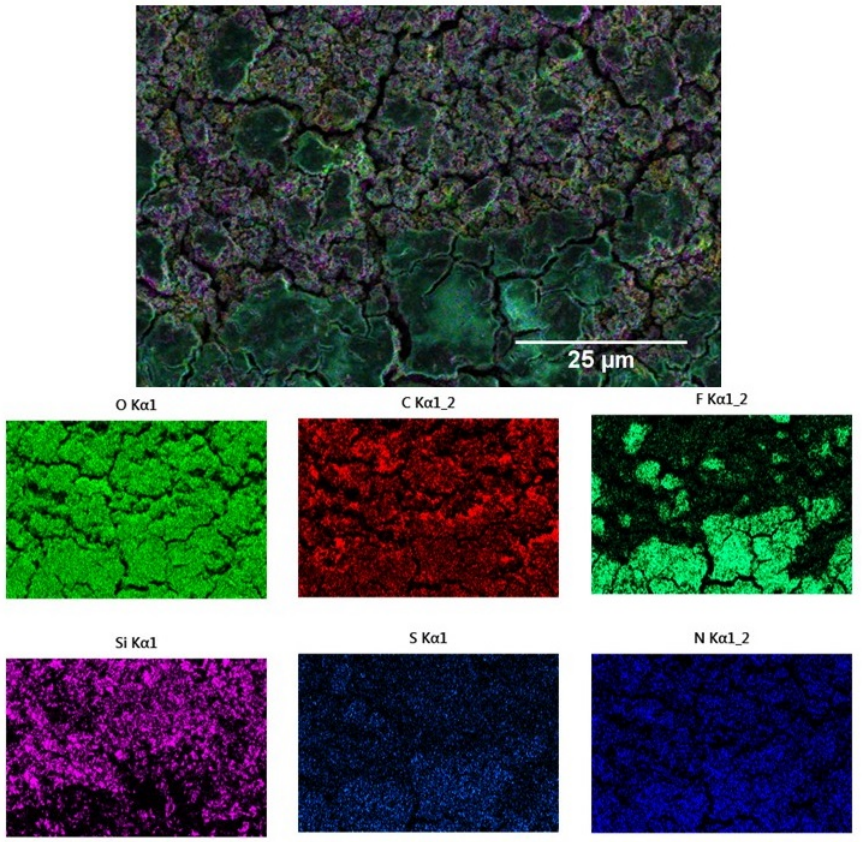

Figure 4.2.19: EDX map scan of figure 4.2.18 b). The differently colored images represent signals from the various elements measured on the anode surface, while the top image combines all the elemental signals into one image.

4.3 Effect of additives on cell performance and SEI formation

4.3.1 The effect of additives on cell capacity

Because the 3 M LiFSI concentration yielded the half cells with the highest capacity, this concentration was selected for further improvements by additives. Figure 4.3.1 shows the average charge capacities obtained when combining 3 M LiFSI in EC:DEC with increasing concentrations of THFIPB, as well as with 5 wt% FEC, and finally 10 wt% FEC + 2 wt% THFIPB. The latter composition is referred to as the "mix" electrolyte in later sections. Additionally, the Coulombic efficiency (CE) is plotted on the right y-axis. The pure salt electrolyte containing 3 M LiFSI is plotted as a reference. Again, the plots including standard deviation of the cells are given in figures A.3 and A.4 in the Appendix.

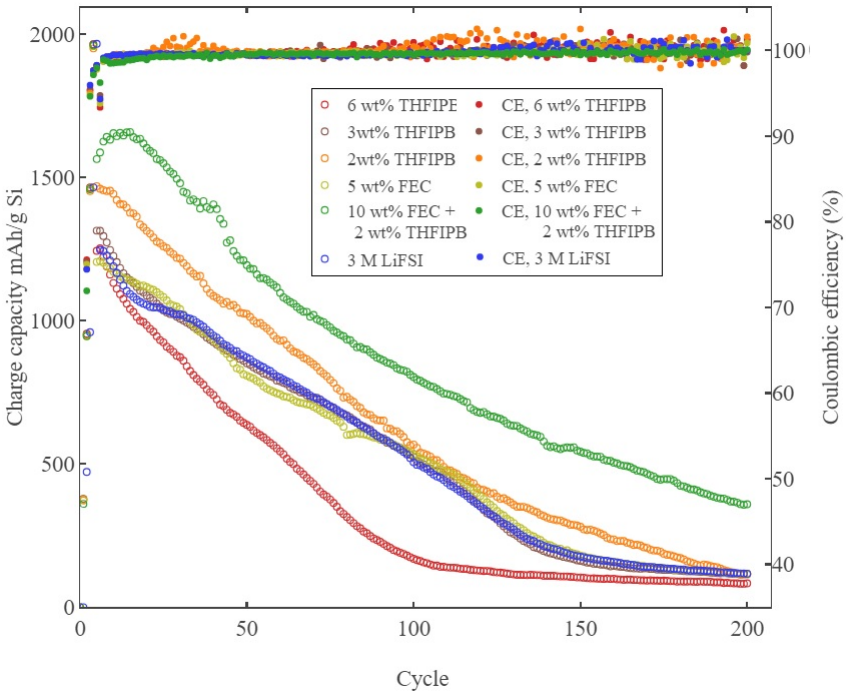

Figure 4.3.1: Charge capacity and Coulombic efficiency (CE) of the cells containing additives, as well as the 3 M LiFSI in EC:DEC electrolyte reference.

Of all the candidates, only two additive compositions significantly improved the capacity of the half cells. 2 wt% THFIPB lost less capacity than the 3 M LiFSI cells when going from the formation cycles at C/20 to the cycling at 1 C. However, the capacity dropped linearly from the first cycle to the 200th cycle, starting at 1470

$mA\,h\,g^{-1}$ and ending at 115 $mA\,h\,g^{-1}$. By adding 10 wt% FEC to this solution, a different behaviour was observed; after dropping to about 1560 $mA\,h\,g^{-1}$ during the first cycle at 1 C, the capacity increased to about 1660 $mA\,h\,g^{-1}$ for cycle 15, before it dropped quite linearly (but less steeply than for the other electrolyte compositions) to end at about 360 $mA\,h\,g^{-1}$ after 200 cycles.
The CE for the "mix" electrolyte had the lowest value during the first pre-cycle step, only 72%, which was 2-3% lower than for the other compositions. However, after reaching the first cycle at 1 C, the CE for the "mix" electrolyte was 3-4% higher than for the rest. It also exhibited a highly stable CE after cycle 15, when compared to the others. Generally, the CE for the additives was less spread out than for the pure LiFSI electrolytes, especially after cycle 100. Small deviations from 100% occured, with the 2 wt% THFIPB-containing half cells fluctuating the most.

The capacity of the 10-times cycled cells that were investigated by FTIR, is shown in figure 4.3.2.

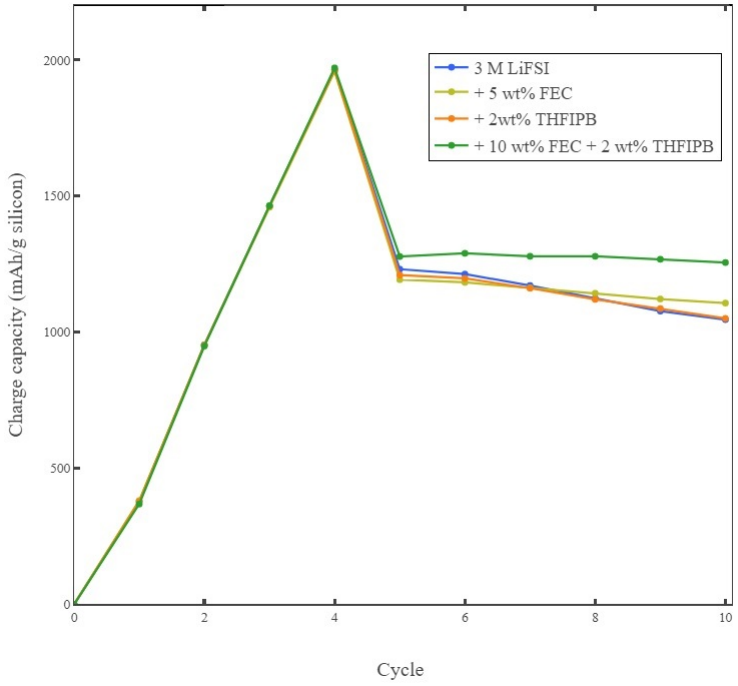

Figure 4.3.2: Charge capacity plots of the 10-times cycled cells containing 3 M LiFSI and additives, that underwent FTIR investigations.

4.3.2 Characterization of SEI layers by FTIR

The FTIR plots shown in figure 4.3.3 have again been subtracted by the signal obtained from the pristine silicon anode (figure 4.2.3) in order to only investigate the SEI layer. To best understand the FTIR plot of SEI formed on the anode cycled in the mix-electrolyte, both the anode from the 5 wt% FEC and the 2 wt% THFIPB electrolytes were investigated by FTIR as well. The FTIR spectra of the samples cycled in the additive-containing electrolytes, contain mostly the same peaks as the FTIR spectra of the anodes cycled in 3 M LiFSI. Still, small differences are notable: the peaks at 1445, 1250-1320, 1040 and 990 cm^{-1} are not present or less prominent in the FTIR spectra of the SEI layers formed during cycling in salt and additives. The differences between these latter spectra are even smaller, with the FTIR spectrum from the anode with the mixed electrolyte looking slightly more noisy.

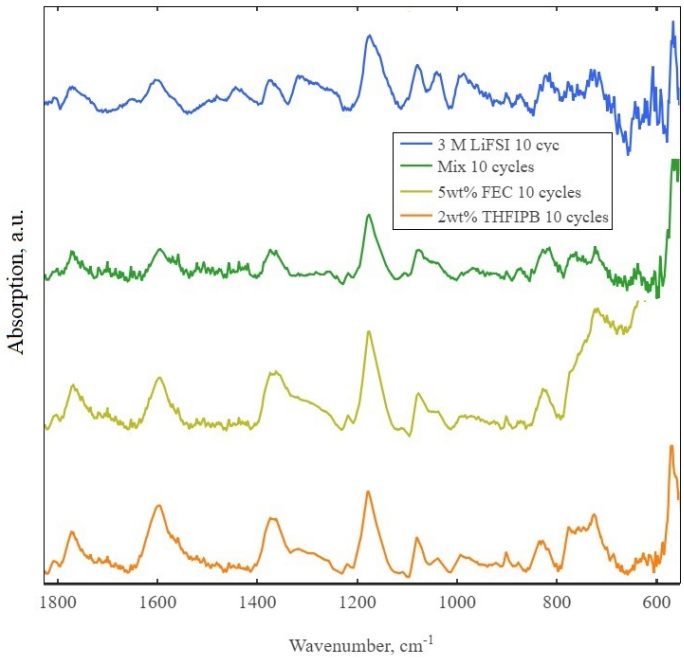

Figure 4.3.3: FTIR plots reflecting the SEI layers formed on the anodes in 3 M LiFSI and in presence of different additives during 10 cycles.

After 200 cycles, the FTIR signatures became much more intense, indicating a thicker SEI layer. As seen in figure, 4.3.4, there are some more noticeable changes between the anodes. The SEI formed on the anode with the mixed electrolyte has a more distinct peak than the others at 722 cm^{-1}, the peak at 995 cm^{-1} is not present, while peaks at 1300, 1380, 1600 and 1650 cm^{-1} are weaker than for the other spectra.

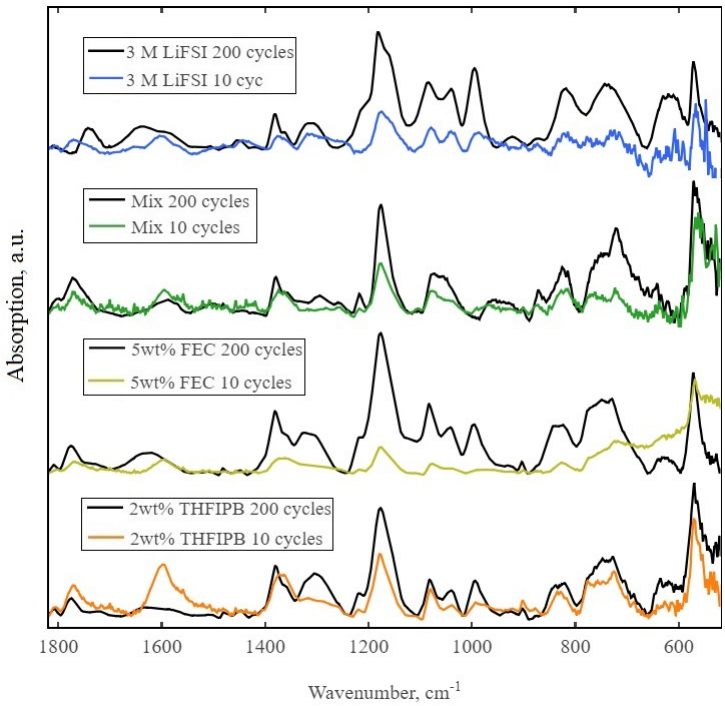

Figure 4.3.4: FTIR plots reflecting the SEI layers formed on the anodes in the presence of 3 M LiFSI and different additives during 10 (colors) and 200 cycles (black).

4.3.3 Characterization of SEI layers by XPS

The survey scan performed on the anode from the mixed electrolyte solution is presented in figure 4.3.5 (green plot) together with the survey spectra of the previously presented 1 M and 3 M samples. It is seen that the F 1s spectrum is similar to that of the 3 M sample, both being much stronger than the corresponding peak in the 1 M spectrum. However, the C 1s spectrum is stronger than the one for the 3 M sample, approaching that of the 1 M sample. Also, the peaks for the elements present in the salt (N, S and O) are close to the intensity of the 1 M sample.

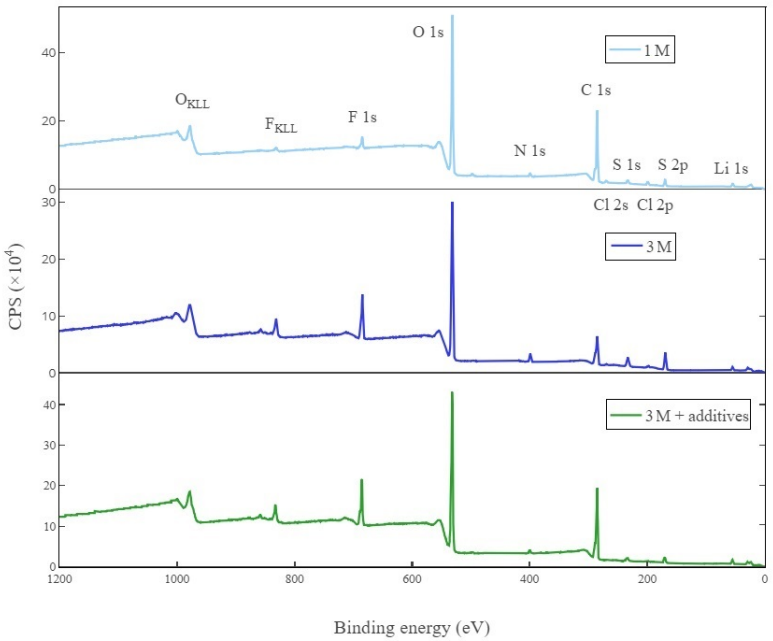

Figure 4.3.5: XPS survey scans of the anodes cycled 10 times in the 1 M LiFSI, 3 M LiFSI and "mix" electrolytes.

Table 4.3.1 shows the atomic percentages of the elements present in the SEI layer formed on the anode in the mixed electrolyte. The carbon levels were close to those of the 1 M sample. This was also the case for the oxygen, sulphur and nitrogen levels. The fluorine level was much higher than for the 1 M sample, and closer to the 3 M sample. Lastly, the survey spectrum revealed a minor silicon signature, better seen in figure 4.3.6. This signature was not evident in any of the two other samples that underwent XPS. The amount of silicon is, however, very low, and only ascribed to 0.49% of the total atomic percentage.

Table 4.3.1: Atomic percentages obtained through the survey spectrum of the anode cycled in 3 M LiFSI + 2 wt% THFIPB + 10 wt% FEC. The figures do not add up to 100%, as there is Li, Cl and Na present as well.

Peak	**Atomic %**
C 1s	53.88
O 1s	34.45
F 1s	6.35
S 2p	3.14
N 1s	1.41
Si 2p	0.49

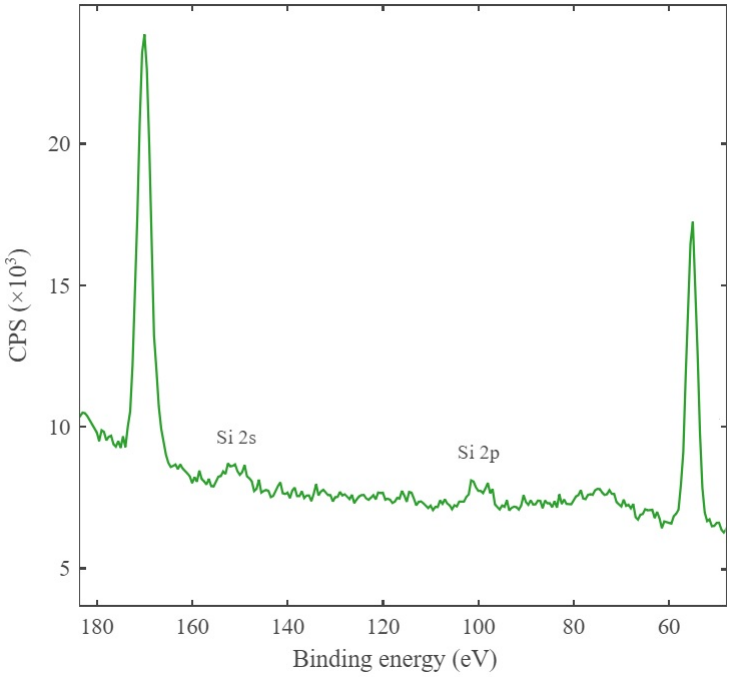

Figure 4.3.6: Enlarged part of the survey spectrum for the "mix" sample that underwent 10 cycles, showing the traces of the Si 2s and Si 2p peaks.

The C 1s and O 1s core peaks for the anode cycled in the mixed electrolyte are given in figure 4.3.7. Again, the relative areas for the different carbon and oxygen components are included. The C 1s spectrum in figure 4.3.7 fits, like the 1 M and 3 M LiFSI samples, well with the presence of five different carbonaceous compounds, present at 285 (C-C and C-H bonds), 286.4 (C-OH and C-O-C bonds), 287.6 (C=O bonds), 288.8 (O-C=O bonds) and 289.9 eV (CO_3 bonds). The O 1s peak also fits well with the inclusion of five peaks, namely at 531.7 (C-OH and C-O-C bonds), 532.5 (CO_3 bonds), 531.1 (C=O and O-C=O bonds) and 533.8 eV (the S=O bond in LiFSI).

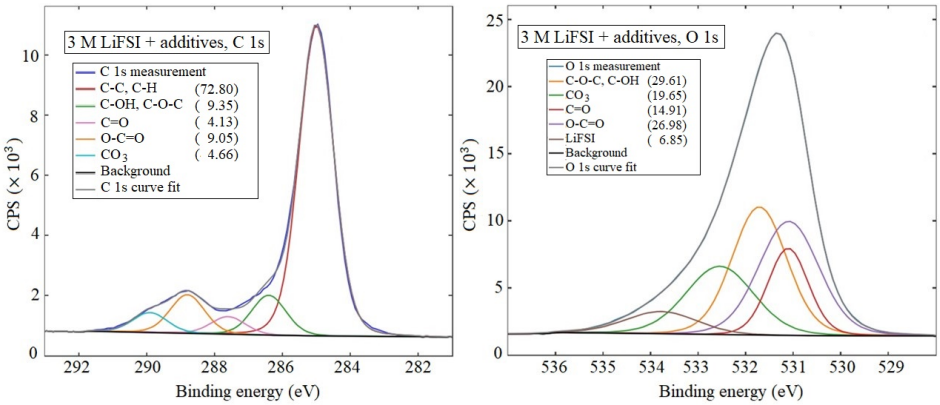

Figure 4.3.7: XPS scans of the C 1s and O 1s core peaks of the anode cycled in the mixed electrolyte for 10 cycles. The parentheses represent the relative area (in percent) of the peak.

The F 1s and Cl 2p spectra are shown in figure 4.3.8. The curves are again deconvoluted to contain two peaks each. F 1s contains LiF at 685.4 eV and LiFSI at 688.3 eV, while Cl 2p contains the Cl $2p_{3/2}$ and Cl $2p_{1/2}$ at 198.6 and 200.2 eV, respectively. The chlorine peak was, however, much weaker for this sample than for the 1 M and 3 M anodes.
Lastly, figure 4.3.9 shows the S 2p and N 1s spectra found in the SEI layer of the anode cycled in the mixed electrolyte. The S 2p and N 1s peaks consist of the same products, namely an undefined LiFSI salt degradation product at 168.7 and 398.6 eV, for S 2p and N 1s, respectively, LiFSI salt at 170.0 and 399.9 eV, and an X-ray degradation product related to salt decomposition at 167.0 and 400.8 eV, respectively. As for the Cl 2p peak, the N 1s and S 2p peaks were very weak, and the S 2p peak had a much lower S $2p_{3/2}$ contribution than in the 1 M and 3 M samples.

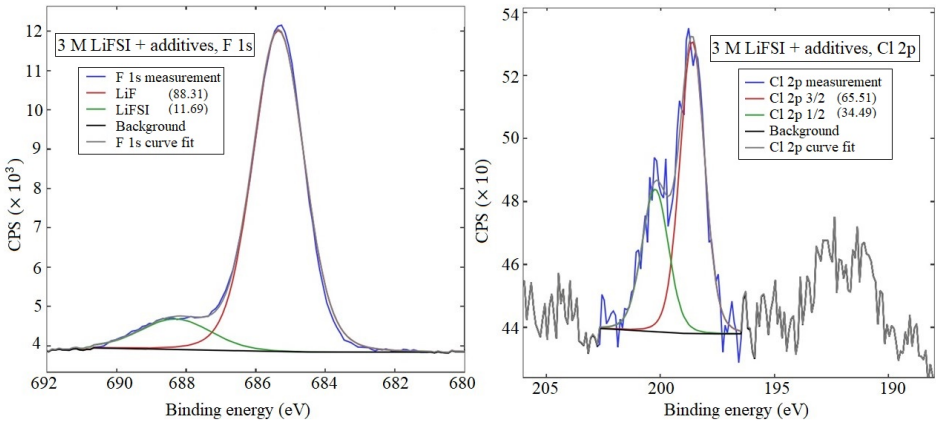

Figure 4.3.8: XPS scans of the F 1s and Cl 2p core peaks of the anode cycled in the mixed electrolyte for 10 cycles.The parentheses represent the relative area (in percent) of the peak.

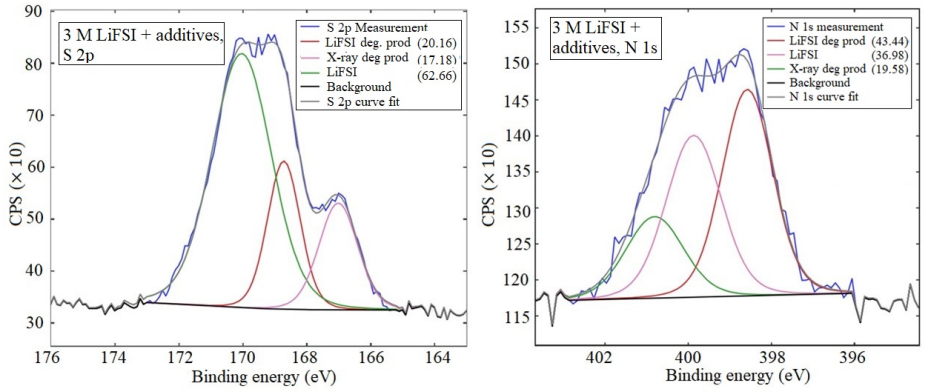

Figure 4.3.9: XPS scans of the S 2p and N 1s core peaks of the anode cycled in the mixed electrolyte for 10 cycles. The parentheses represent the relative area (in percent) of the peak.

4.3.4 Characterization of anode surface and SEI layers by SEM and EDX

Because the cells with the "mix" electrolyte performed the best, anodes from this composition were investigated by SEM and underwent EDX map scans as well. The morphology of the 10-times cycled anode, seen in figure 4.3.10 a), was highly similar to that of the anodes cycled in 1-5 M LiFSI. The cross section made with FIB is presented in figure 4.3.10 b). Its thickness was measured to be 16.1 ± 0.1 µm. In the cross-section image, a large silicon particle shows at the very top. Figure 4.3.11 exhibits a close-up of the particle, as well as a map-scan, which indicated that a carbon- and oxygen-rich layer had formed around the silicon particle. The layer is measured to around 450 nm.

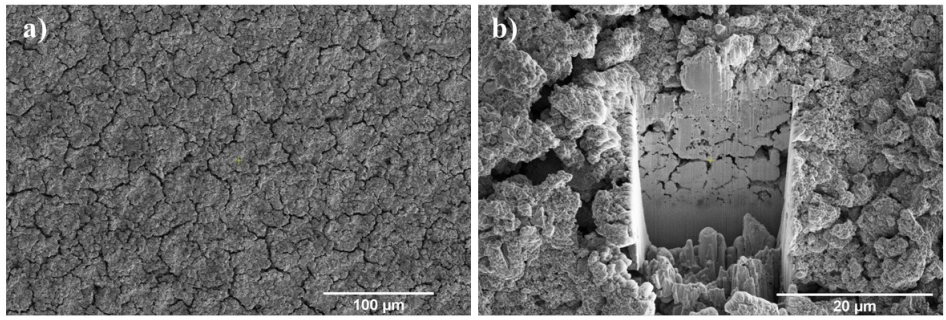

Figure 4.3.10: Morphology and cross-section of the "mix" anode after 10 cycles.

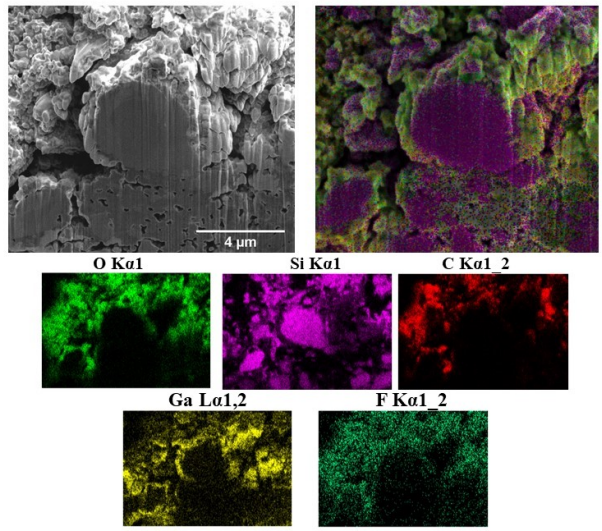

Figure 4.3.11: SEM and EDX map scan of an SEI-covered silicon particle, found at the very top of the cross section of the "mix" sample after 10 cycles.

The EDX spectra obtained for the surfaces of the anodes cycled in electrolytes consisting of 3 M LiFSI with additives, as well as the reference spectrum for the 3 M sample, are shown in figure 4.3.12 .

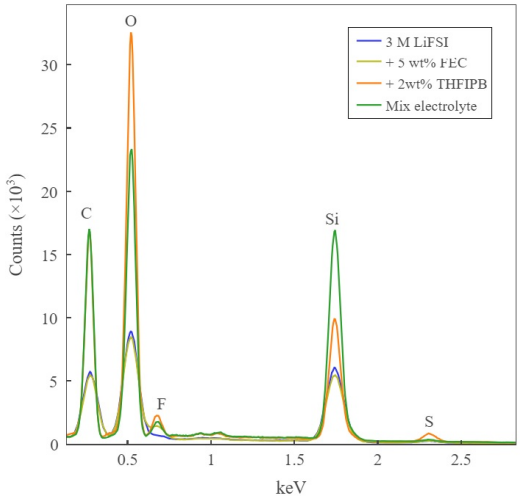

Figure 4.3.12: EDX data reflecting the morphological composition of the anode, including the SEI, of the 3 M LiFSI, 3 M LiFSI + 5 wt% FEC or 2 wt% THFIPB, and "mix" samples.

After 200 cycles, the cross section looked more compact (figure 4.3.13), and was 20.9 ± 0.1 µm thick. As observed from the map-scan, the FIB sputtered down to the Cu foil. The inner parts of the anode consisted of Si, while the outermost layer mostly consisted of O, C and F.
The surface of the 200-times cycled anode mainly contained three different structures: dense particles separated by cracks (upper left of figure 4.3.14 a), thick films making large flakes separated by thicker cracks (lower right of figure 4.3.14 a), and particles that formed on top of the anode (figure 4.3.14 b). From the EDX map-spectrum in figure 4.3.15 it seems that the flakes largely consist of F, while O and C are the most abundant species. The particles formed on top contain carbon and oxygen.

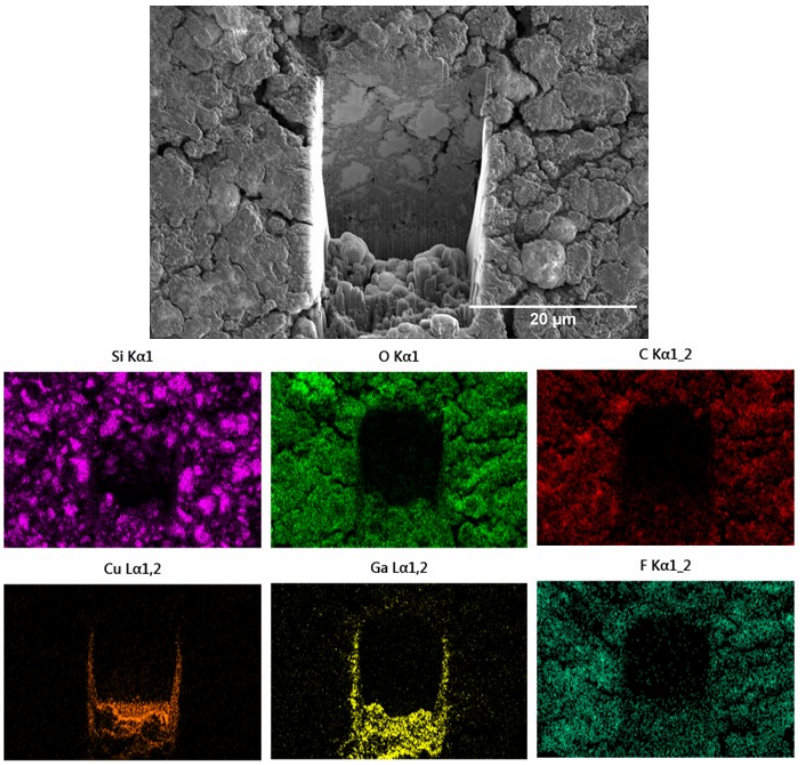

Figure 4.3.13: Cross-section of the "mix" sample after 200 cycles, with its respective EDX map signature.

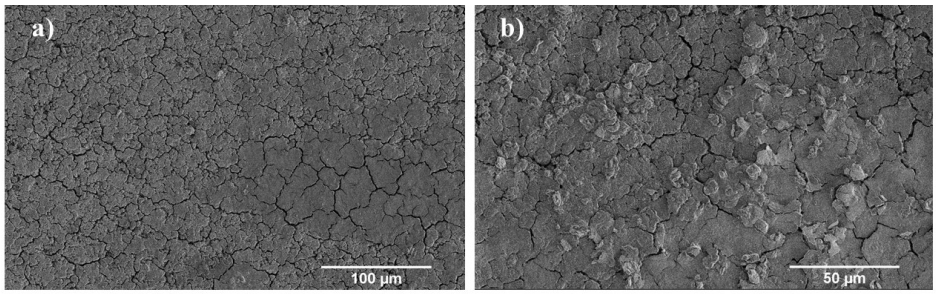

Figure 4.3.14: SEM images showing the general morphology of the "mix" sample, cycled 200 times. a) shows the general morphology of the anode surface, while b) shows C-O containing particles that formed some places on the "mix" sample surface.

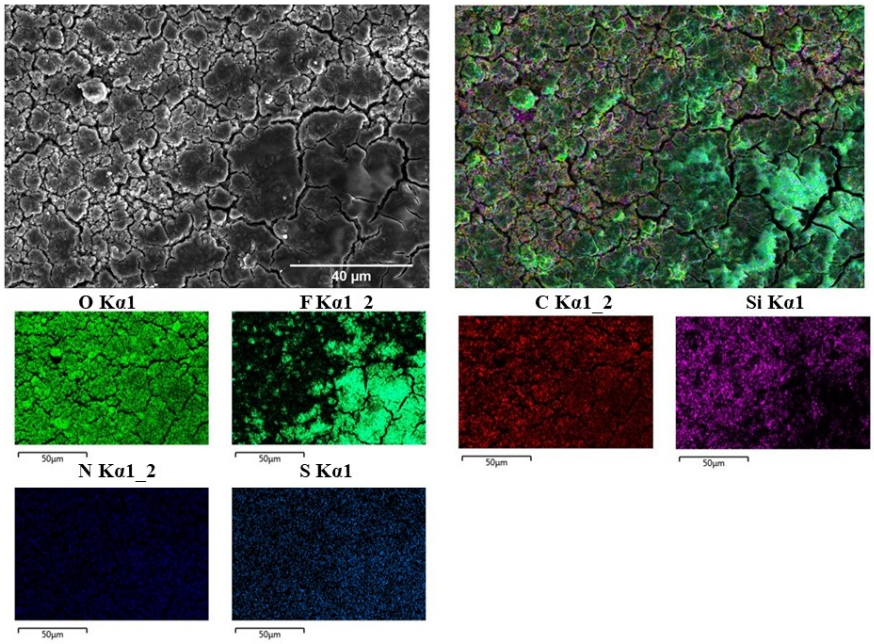

Figure 4.3.15: EDX map spectrum of the 200-times cycled "mix" anode surface.

Chapter 5

Discussion

5.1 Characterization of electrolytes by FTIR

The electrolyte solution structure undergoes changes when the LiFSI concentration is increased, according to the findings presented in section 4.1.2. Originally, the C=O bond present in both EC and DEC exhibits absorption at 1767 cm^{-1},[83,84] but the peak shifts to 1769 cm^{-1} for 5 M LiFSI in EC:DEC, indicating a change in the chemical environment. Second of all, the C-O bond for EC, prominent at 1157 and 1063 cm^{-1} for EC:DEC,[83–85] undergoes a large blueshift for 1 M LiFSI in EC:DEC, and an even larger one for 5 M LiFSI, again indicating changes in the chemical environment. In addition, two new peaks are evident for LiFSI in EC:DEC; both at 1300 and 1720 cm^{-1}. They indicate that the C-O and C=O bonds in DEC are being coordinated with Li^+,[83] and it is apparent also here that the peak becomes more intense with increasing concentration, indicating that more Li^+ coordinates to DEC. The C-O peak for EC found at 1157 cm^{-1} represents the amount of free EC found in solution,[83] and it drops with increasing LiFSI concentration. For 5 M, this C-O peak is situated at 1173 cm^{-1}, but it also overlaps with the S-O vibrational bonding in LiFSI,[86] which may explain why the peak is so intense. Based on these data, it is evident that the solution structure changes according to the findings summarized by Zheng et al. and Yamada and Yamada.[50,51]

The curve-fitted spectra of the carbonyl groups present in 1 M and 5 M LiFSI in EC:DEC, presented in figures 4.1.2 and 4.1.3, pose some in-depth results regarding the solution structure. The peak at 1742 cm^{-1}, synonymous with free DEC,[83] is much stronger for the dilute electrolyte than for the highly concentrated one. Correspondingly, the peak attributed to coordinated DEC at about 1720 cm^{-1} is much less intense for the 1 M electrolyte than for the concentrated electrolyte. This difference in peak intensity already indicates that the solution structure undergoes a radical change when moving from low to high salt concentration. The change in relative areas also leads to different solvation numbers, according to equation (2.8). The higher solvation number for 1 M LiFSI (4.06) than for 5 M LiFSI (1.48) reflects that there are more solvent molecules per Li^+ cation present in the dilute

electrolyte. In fact, at 1 M concentration, a solvation number of 4 is consistent with the generally accepted tetra-coordinated Li cation solvated by four carbonate solvents with an uncoordinated salt anion.[56] The decrease in solvation number for the highly concentrated electrolyte is also consistent with a higher level of CIPs and AGGs in the electrolyte.[56] These results are consistent with the work presented by Seo et. al,[56] as presented in section 2.5.2.

5.2 The effect of electrolyte concentration on cell performance and SEI formation

5.2.1 The effect of electrolyte concentration on cell capacity

The cycle data in figure 4.2.1, show that the capacity of all the half cells, independent of salt concentration, dropped severely after about 50 cycles. It seems that the SEI has grown so much here, that the behaviour of all the electrolytes is independent of salt concentration. At the same time, there are some significant differences during the first 50 cycles. It seems that increasing the Li-salt concentration is positive up to 3 M. For 5 M, however, the electrolyte became too viscous, with too low ionic conductivity and poor wetting capability, indicating that a too high amount of LiFSI has a negative impact on the cell performance. At 3 M, on the other hand, the solution was still thin enough to wet properly, and the surplus of Li^+ available seems to have a positive effect. The high C-rate had a negative impact on the capacity retention achieved for the half cells. At high currents, the cut-off voltages are reached at an earlier stage due to increased polarization. By using a lower C-rate, the capacity retention would therefore be higher.
The CE is comparable for all electrolytes, even though the highly concentrated electrolytes had a slightly lower CE during the first formation step. Here, the CE was between 74-76% for all electrolyte compositions, suggesting that much lithium is lost to the formation of the SEI layer during the first cycle. The fact that the higher concentrated electrolytes had the lowest CE during the first cycle, may indicate that the change in solution structure slightly altered the SEI formation mechanism to include more salt reduction. The change in the SEI formation mechanism is in line with the findings of Zheng et al.[50] and Nie et al.,[48] as presented in section 2.5.3. In addition, the CE for all cells dropped from around 98% after the last formation step, to 91-94% in the first cycle at 1 C, indicating that much Li^+ is lost to SEI formation here as well. Interestingly, the CE for the first cycle at 1 C was higher for the highly concentrated electrolytes ($\sim$94%), which arguably indicates that the SEI passivates the anode better. However, when the cells reached cycle 15-20, the capacity dropped earlier for the highly concentrated electrolytes. It therefore seems that the SEI formed at high salt concentrations initially passivates the anode better, but that it is less stable during cycling, which leads to poor capacity retention. The SEI composition will be investigated further in the upcoming sections. From about cycle 100, the CE is spread out much more for all the cells, but the cells containing 1 M LiFSI had the largest spread in CE. This may indicate that the Li-salt starts to decompose and takes part in the SEI

formation at a higher degree than before. Another effect observed after about cycle 100, is that the CE reaches levels over 100% during some of the cycles. This may indicate that some of the lithium got trapped in the silicon and/or SEI, and became available with cycling. This behaviour is typically seen in poor electrodes. Another explanation can be that the battery tester used is not sufficiently precise. All in all, it seems that increasing the salt concentration is beneficial up to 3 M, after which the positive effects of more LiFSI diminish. A probable explanation for the increased capacity is that Li^+ is coordinated to less solvent molecules, as found in section 4.1.2 and discussed in the previous section. The lower solvation number will reduce the activation energy for Li^+ desolvation, thus enhancing capacity, as proposed by Xu, von Cresce and Lee.[57] Yet, too high concentration leads to an electrolyte with too high viscosity, too low conductivity, and poor wetting properties, resulting in a capacity drop. The enhanced performance might also indicate that the higher concentrated electrolytes have an increased reductive stability, and therefore form a thinner SEI layer compared to the 1 M solution. The poor capacity retention at high concentration, however, questions the latter statement. The SEI formation and characteristics will be further investigated in the upcoming sections.

5.2.2 Characterization of SEI layers by FTIR

The FTIR spectra of the 10-times cycled anodes, seen in figure 4.2.4, show that the different electrolyte compositions gave rise to quite similar SEI compositions. All the samples contain $ROCO_2Li$, as evidenced by responses from bonds at 1600 (C=O asymmetric stretching), 1445 (CH_2 bending), 1370 (CH_2 bending), 1310-1320 (C=O symmetric stretching), 1080 (C-O stretching) and 820 cm^{-1}(CO_3 bending).[30,87] Additionally, LEDC corresponds to these wavenumbers as well,[30] and is likely present. The most abundant species seems to be $ROCO_2Li$, as LEDC has its C=O asymmetric stretching peak at about 1650, and not at 1600 cm^{-1}, as is the case for $ROCO_2Li$.[30] Peaks at about 1770 and 1175 cm^{-1} correspond to polycarbonates resulting from EC decomposition.[88] The main inorganic part of the SEI layers seems to come from the LiFSI salt itself, or from a LiFSI decomposition product. Peaks corresponding to LiFSI are found at about 1173-1178, 1371-1378 cm^{-1} (SO_2 symmetric out-of-phase stretching), and about 565 cm^{-1} (asymmetric bending motion of SO_2), as well as smaller peaks at 903 (SNS asymmetric stretching) and 820 cm^{-1} (SF stretching).[33]
Even though the aforementioned peaks are present in all SEI layers, the peaks differ in intensity for the various salt concentrations. First of all, the SEI on the electrode from 1 M LiFSI has more prominent peaks at 1600 and 1310 cm^{-1}, indicating more $ROCO_2Li$ and LEDC than in the SEI formed in higher salt concentrations. Additionally, the peak situated at 1770 cm^{-1} decreases in relative intensity with increasing concentration, suggesting that less EC is decomposed to polycarbonates as the salt concentration of the electrolyte is increased.[89] The other peak corresponding to polymeric decomposition of EC (at about 1175 cm^{-1}[89]), however, does not seem to decrease with increasing salt concentration. This may be explained by the fact that this peak also corresponds to the LiFSI salt itself. This is equally the case for the 1370-peak, which increases versus the 1310 peak for the 5 M LiFSI

SEI. This increase is possibly explained by additional LiFSI salt being present, as well as the CH_2 bending of $ROCO_2Li$. The notion that there is more LiFSI or LiFSI related decomposition products in the SEI of the anodes cycled in higher concentrated electrolytes, is further strengthened by the fact that both 3 M and 5 M SEI layers exhibit a stronger peak at around 900 cm^{-1}, attributed to the S-N-S bonding. Another difference that seems to occur, is that the peak at around 873 cm^{-1}, corresponding to the CO_3^{-2} bending motion of $LiCO_3$,[30] shrinks with increasing concentration. In addition, the double peak at 1080-1040 cm^{-1} becomes more prominent with increasing LiFSI concentration. This may be caused by less ROLi in the structure, which typically exhibits its C-O stretching motion at 1050-1060 cm^{-1},[30] splitting the 1080-1040 peak into two peaks.
The SEI signature of the 3 M and 5 M samples reveal only minor differences. The most clear difference seems to be that the peaks corresponding to LEDC and $ROCO_2Li$ are relatively less intense for the 5 M sample, and typically less distinct. This may indicate that there are less organic species in the SEI at higher concentrations of LiFSI. Also, the peak at about 1770 cm^{-1} is less distinct for the 5 M SEI, suggesting that less EC is degraded. Lastly, it seems that the peaks corresponding to the LiFSI salt or LiFSI decomposition products are slightly stronger for the 5 M SEI than the 3 M SEI.
These results support the proposition of Zheng et al.[50] and Nie et al.,[48] that dilute electrolytes produce more organic SEI layers, while concentrated electrolytes typically include inorganic species like lithium salt decomposition products, as well as LiF.
Figure 4.2.5 shows the FTIR spectra of the anodes with increasing salt concentration after 200 cycles (black plots). It is apparent that the SEI signature is much stronger after 200 cycles than it is after 10, indicating a thicker SEI layer. In addition, the peak previously located at about 1600 cm^{-1} shifted for all SEI layers to around 1630 cm^{-1}, indicating that the main carbonate species has shifted from $ROCO_2Li$ to LEDC. Another difference is the emerging of three new peaks at about 990 cm^{-1} (C-O stretching in ROLi[30]), 620 cm^{-1} (Li-O stretching in ROLi) and at 740 cm^{-1}. The 740-peak may arise due to increased presence of LiFSI salt, which according to literature should have a peak at 760 cm^{-1}.[33] As the peaks for the lithium salt are more prominent, it seems that cycling the cells for 200 times leads to decomposition and entrapment of the lithium salt onto/into the SEI. Other than that, it seems that the relative SEI composition is highly similar for the samples of the same chemistry, regardless of being cycled 10 or 200 times, except that the thickness increases.

5.2.3 Characterization of SEI layers by XPS

From the survey scans of the 10-times cycled anodes cycled in 1 M and 3 M LiFSI, a couple of things stand out. Firstly, the silicon signal is absent in both spectra, indicating that the silicon anode was completely covered by the SEI layer. To back up the fact that the SEI was thick already after 10 cycles, neither of the C 1s core peaks (figure 4.2.7 and 4.2.10, respectively) show any sign of a carbon black peak, typically evident at 284 eV.[32] As carbon black is only found in the anode

material and not the SEI, it is evident that the SEI covered the entire anode. Secondly, the elemental analysis done on the survey scans in CasaXPS, seen in table 4.2.1, shows that the relative atomic percentage of carbon is much higher in the 1 M LiFSI sample than in the 3 M LiFSI sample. Furthermore, the 3 M anode contains more oxygen, fluorine, sulphur and nitrogen. This corresponds well with the notion that higher concentrated electrolytes have an SEI layer composed of more inorganic components and less carbonaceous species. Lastly, it seems that both samples contain impurities: chlorine is present in both samples, and is likely a result of impurities in the LiFSI-salt, as it is a by-product formed during the synthesis process of LiFSI.[10] Additionally, the 1 M LiFSI sample contains trace amounts of sodium. Sodium impurities may arise in many of the fabrication processes, by cross contamination, or due to careless handling. Therefore, it is not surprising to only find Na in one of the SEI layers.

The core peak scans confirm the general results observed in the survey scans, but additionally provide some more in-depth results. In the following paragraphs, the core peak scans for the SEI of the 1 M and 3 M samples will be discussed separately, before they are compared.

Figure 4.2.7 shows the C 1s and O 1s core peaks for the SEI formed on the anode cycled in 1 M LiFSI. The C 1s spectrum fits well with the presence of five carbonaceous species, namely adventitious carbon and other polymeric species present in the SEI at 285 eV,[30] alcohols and ethers (C-OH and C-O-C bonds) like polyethylene oxide (PEO) at about 286.5 eV, carbonyls (C=O double bond) at 287.8 eV, esters and acids (O-C=O species) like $ROCO_2Li$, at 288.9 eV, and carbonates (CO_3^{2-}) like Li_2CO_3 at 289.9 eV.[30,32,90] The O 1s spectrum also fits well with the presence of five oxygen compounds. The C=O peak is situated at 531 eV, O-C=O at 531.2 eV, C-O-C and C-OH at 531.8, CO_3^{2-} at 532.4, while the S=O bond in LiFSI is situated at 533.6 eV.[90]

Figure 4.2.8 and figure 4.2.9 show the F 1s, Cl 2p, N 1s and S 2p core-peak levels. The F 1s spectrum is dominated by LiF at 685 eV, with a small contribution of LiFSI at 287.8 eV as well.[30,90] The S 2p spectrum fits well to the presence of three peaks. The main peak (S $2p_{3/2}$ at 169 eV) is attributed to an undefined LiFSI salt degradation product.[90] The LiFSI signature is detectable (S $2p_{1/2}$) at 170.2 eV, while the third and weakest component at 167 eV is another degradation product of the salt, but mainly resulted from the XPS analysis itself.[90] The N 1s peak has similar component characteristics as the S 2p peak, with the main peak at 398.7 eV, attributed to an undefined salt degradation product, the LiFSI signature peak at 399.4 eV, and another salt degradation product due to X-ray exposure at 400.4 eV.[90]

The anode cycled in 3 M LiFSI is highly similar to the the one cycled in 1 M. The C 1s spectrum includes the same peaks at the same binding energy values, although some are shifted by ± 0.1 eV. The O 1s sprectrum is slightly more shifted, with the peaks generally being 0.3 eV higher (except the S=O bond in LiFSI, which is only shifted up by 0.1 eV). Additionally, the LiFSI signature in the N 1s spectrum is shifted up by 0.4 eV.

The shape of the C 1s peak is different for 1 M and 3 M, and apparently re-

veals a surprising result; the SEI formed during cycling in 1 M LiFSI contains less carbon-oxygen species, and far more pure carbonaceous species than the SEI formed during cycling in 3 M LiFSI. The C-O species are typically attributed to EC decomposition, so the fact that the 3 M sample contains relatively more of these species goes against the concept that a higher salt concentration should cause less decomposition of EC. There is, however, a reasonable explanation for this apparent contradiction: different amounts of adventitious carbon. Adventitious carbon is a thin layer of a variety of relatively short chained, perhaps polymeric hydrocarbon species, that form upon even slight contact with air.[91] The peak for adventitious carbon, at 284.8-285 eV, will always be present in XPS spectra.[92] Even though the glovebox only contains trace amounts of air (< 0.1 ppm), prolonged exposure to the glovebox atmosphere will cause gradual build-up of adventitious carbon, which grows as a function of time.[93,94] Unfortunately, the 1 M and 3 M samples were stored in the glovebox for very different times after disassembly. The 3 M sample spent three nights in the glovebox after disassembly, before it was prepared in the XPS transporter stage and brought to the XPS. The 1 M sample, on the other hand, lay in the glovebox for about one month before XPS measurements were done. The reason for the long time between disassembly and XPS measurements was unforeseen heavy booking of the instrument, causing the investigations of the 1 M (and "mix") sample(s) to be given a lower priority. Also, the effect of adventitious carbon and its growth was not known to the author at the time. Otherwise, the anodes would have spent similar time in the glovebox between disassembly and XPS measurements. The fact that the anodes contain different amounts of adventitious carbon will also affect the atomic percentages obtained in the survey scans presented in table 4.2.1. Therefore, the difference in carbon content was probably not as large as the $\sim$20% reported. The FTIR measurements (that were performed on another group of 10-times cycled cells right after disassembly), however, suggest that the higher concentrated sample does contain less carbonaceous species, so it would be expected that the 3 M sample does contain less C and more LiFSI components.

Examining the core-peaks of F, N and S for both samples, shows that the signals of these compounds are stronger for the 3 M sample than for 1 M. Comparing intensities like this between different XPS measurements does generally not give completely reliable answers, but the fact that the core peaks for the 1 M sample contain more noise (less smooth curves), along with the lower atomic percentages of these elements, indicates that there were less salt and salt degradation products present in the 1 M SEI. Furthermore, the LiF/LiFSI ratio for the 3 M sample is 7.1 (versus 6.4 for 1 M LiFSI), so it seems that higher salt concentration also leads to more LiF in the SEI layer, as proposed by Nie et al.[48] and Zheng et al.[50] Still, these findings may be affected by the fact that the layer of adventitious carbon on the 3 M sample is thinner than that of the 1 M sample, which again will lead to uncertainties regarding the peak intensities and atomic percentages. Also, the difference in the LiF/LiFSI ratio is not big enough to definately conclude that higher salt concentrations promote LiF formation, as the XPS peaks are fitted to Gaussian curves that will be prone to errors. Based on the FTIR data as well, however,

it seems fair to say that the XPS data confirm that increased salt concentration leads to a less carbonaceous SEI layer, with higher levels of inorganic compounds present.
Relating these findings to the difference in capacity retention behaviour during the first 50 cycles, as seen in figure 4.2.1, suggests that highly concentrated electrolytes promote more inorganic SEI layers, that do not sufficiently passivate the Si anode. This results in an unstable SEI, that gradually consumes Li^+, leaving the capacity to drop more and more linearly with increased concentration. For dilute electrolytes, on the other hand, much EC is reduced during the first 10 cycles, after which the capacity increases and is constant until cycle 50. After 50 cycles, it seems that the SEI has grown too thick, and too much Li^+ is lost for proper capacity retention.

5.2.4 Characterization of the anode surfaces and SEI layers by SEM and EDX

The morphology investigations in figure 4.2.15 and 4.2.16, reveal that some of the porosity in the anode was lost during the first 10 cycles. The thickness measurements performed on the cross-section in figure 4.2.16 reveal that the thickness increased with cycling. It is not clear whether the salt concentration increase leads to overall thicker anodes or not, even though the thickness of the 1 M anode was 4-6 µm below that of 3 and 5 M. This result may be due to local differences in the anode thickness to begin with.
Upon close investigation, the cross-sections reveal a slight difference in color of the silicon particles making up the anode; they are darker grey towards the edges and light gray towards the center. This is true for all cross-sections investigated in this project, and especially evident in figure 4.2.16 b). The entire particle is still silicon, but the reason for the color change may be that the inner part of the silicon still is crystalline and has not been lithiated, while the edges have turned amorphous upon lithiation. If this is in fact the case, much of the active silicon material is not utilized during cycling, which limits the capacity. In fact, most of the silicon in the anode becomes dead weight, not contributing to cell performance at all. This seems understandable, as the half cells were only discharged to a maximum of 2000 $mA\,h\,g^{-1}$, far off its theoretical specific capacity. For the cycling parameters used, smaller Si particles would result in less dead weight. Thereore, testing finer silicon particles ($\sim$1 µm) would be interesting.
The increase of electrolyte concentration does not reveal any obvious differences in morphology; all anode surfaces look like those presented in figure 4.2.15. During the 10 cycles, the anodes underwent some changes with regard to particle size, especially with respect to the carbon black, which is not as clear anymore (figure 4.2.15 c). The partial disappearance of carbon black indicates the presence of an SEI layer.
The difference between the EDX spectra for the surface of the pristine silicon anode and the surface of the anodes after 10 cycles in figures 4.2.14 and 4.2.17, is striking. The silicon signal drops with respect to all the other elements, indicating that an

SEI layer has formed on top of the pristine anode, weakening its signal strength. Additionally, the Cl and Na impurities are far less prominent after cycling, also reflecting the fact that an SEI layer has formed. The relative ratios of Si/C seem to be approximately constant for all compositions. This may be explained by the fact that the anodes have been exposed to unavoidable air contact during transportation into the FIB and SEM. This is also the case for the oxygen levels; they do not reflect the SEI composition of the cell during operation. In addition, the 5 kV acceleration voltage is not low enough for the EDX to only be surface sensitive, obvious by the fact that silicon has a strong presence. Therefore, a large part of the carbon peak is ascribed to carbon-black. The Si/F and Si/S ratios decrease with increasing LiFSI concentration. The decrease of LiFSI elements is in line with both the XPS and FTIR results, suggesting that increased salt concentration gives a more inorganic SEI layer.
After 200 cycles, the anode surface is entirely different. The general morphology shows that the material underwent severe changes, leading to large agglomerates, flake-like films and large cracks. Also, the thickness of the anode grew by around 3 µm, possibly due to Li^+ entrapment in the silicon (leading to volume expansion), and SEI formation. Furthermore, the porosity of the cross-section is gone, and is replaced by large, dense silicon particles. This effect will put serious limitations on both the ionic and electrical conductivity. The additional film-like layers seen in figures 4.2.18 b) and c), will shut of other parts of the anode in a similar fashion. Not all anodes were investigated after 200 cycles, but the cycle data suggest that all of them met a similar fate with regard to the morphology of the anode. By performing a map-scan, the flake-like dense films on the surface of the anode are found to largely consist of F, most likely LiF. However, the signal from S (and N, if examined closely) show a similar distribution as F, indicating that the flakes also may consist of LiFSI, or a LiFSI degradation product. It is further apparent that the silicon is covered by a quite thick SEI layer after 200 cycles, as the silicon spectrum is weaker than O, F and C.

5.3 The effect of additives on cell performance and SEI formation

5.3.1 The effect of additives on cell capacity

The charge capacity plots shown in figure 4.3.1 provide some interesting information about the additives in combination with 3 M LiFSI in EC:DEC. The addition of THFIPB at 6 wt% significantly reduced the capacity during cycling, most likely caused by too strong binding to the FSI^- anion, decomposing the salt, as seen from equation (2.15). As the weight percentage of THFIPB was lowered, the capacity was retained better, with 3 wt% THFIPB performing similarly as the electrolyte without the additive. By reducing the weight percentage to 2%, there was a significant increase in the capacity of the cells, which indicates that the anion receptor succeeded in reducing the attraction between the lithium cation and the salt anion, thus enhancing the ionic conductivity of the electrolyte.
The addition of 5 wt% FEC does not seem to have a significant effect on the half cells. A doubling to 10 wt% FEC in combination with 2 wt% THFIPB, however, boosted the capacity even further than only the THFIPB managed, resulting in the cells with the highest capacity. The reason that FEC has to be added in high concentrations, may be that the solution structure and inner Helmholtz layer is dominated by the salt anions, preventing the reduction of FEC. When the FEC concentration is increased, the solution structure is altered, such that FEC may decompose on the Si anode.
The CE data for the cells provide a few surprising results. The CE for the electrolyte containing only 2 wt% THFIPB fluctuated the most, reaching over 100% between cycle 20-45 and again from cycle 70-150, after which it frequently was above 100% as well. This may be due to potentiostat errors, but may also indicate a sub-optimal electrode. The other additives typically exhibited a stable CE to about cycle 100, after which the CE fluctuated more. This may be because the anode morphology is severely altered after 100 cycles at 1 C, forming large cracks that can trap Li^+ and promote SEI formation as well. The CE of the "mix" samples, however, was very stable after the first 15 cycles, indicating that a stable SEI layer had formed, which can explain the higher capacity during cycling. Interestingly, the CE for the "mix" samples was lower during the formation cycles at C/20 (for instance 72% for the very first pre-cycle step versus 74.5-75% for the others) and the first 15 cycles at 1 C, except for the first cycle at 1 C. Here, it exhibited a CE of 96.2%, far above the 93-94% of the other half cells. This CE behaviour suggests that more Li^+ is lost to SEI formation during the first cycles, and may be due to the earlier reduction of FEC than EC onto the anode. The FEC-derived SEI seems to grow slightly more than for the other samples, but after cycle 15, the CE stabilizes until cycle 200. The lower CE might be caused by FEC reduction, which forms a more stable SEI layer than EC/salt reduction does on the other anodes.
From the cycle data, it seems that the additives can have a positive effect on cell performance, but only in appropriate concentrations; otherwise the capacity might suffer compared to cells without the additives.

5.3.2 Characterization of SEI layers by FTIR

From figure 4.3.3 it can be seen that the additives did not severely alter the SEI composition during 10 cycles, as the SEI signatures largely look the same. Again, it seems that $ROCO_2Li$ is the main component in the SEI, with corresponding peaks at 1595-1600 (C=O asymmetric stretching), 1440 (weak CH_2 bending), 1250-1330 (C=O symmetric stretching), 1079 (C-O stretching) and around 830 cm^{-1} (CO_3 bending). Additionally, there are other polymeric species from EC decomposition present in all SEI layers, as evident from the peaks at 1770 cm^{-1} and 1175-1180 cm^{-1}. As for the 3 M LiFSI SEI, LiFSI salt is also present, with peaks at 1177-1180, 1362-1376 cm^{-1} (SO_2 symmetric out-of-phase stretching), 566-570 cm^{-1} (asymmetric bending motion of SO_2), 900-902 cm^{-1} (SNS asymmetric stretching) and 820-825 cm^{-1} (SF stretching). The disappearance of the peak at 1440 cm^{-1} seems odd, as this corresponds to CH_2 bending in both $ROCO_2Li$ and LEDC, which have all of the other corresponding peaks present. However, when enlarging the 1440-area, a small peak is visible in the FTIR spectra. It is, however, weaker in the SEI for anodes cycled with additives than without. An explanation for the weak 1445-peak is that there is more Li_2CO_3 present in the pure salt samples, as Li_2CO_3 exhibits its C-O stretching motion at 1445 cm^{-1}.[30] The presence of Li_2CO_3 is further confirmed by the presence of a peak at about 875 cm^{-1} for the 3 M LiFSI sample, corresponding to the CO_3^{2-} bending motion in Li_2CO_3.[30]
The FTIR spectra for the samples containing 2wt% THFIPB and 5wt% FEC are highly similar, and offer no real clues as to why THFIPB addition achieved higher cell capacity than 5 wt% FEC. Equation 2.14 postulates that the anion receptor may bind to the FSI^- anion to keep FSI^- from degrading. If this protection were the case, less intense salt signatures would be expected for the SEI formed in the THFIPB-containing electrolyte. However, this is not clear from its spectrum. From this data, it seems that the AR binds to the FSI^- anion to promote Li^+ diffusion, but that it does not hinder the salt from degrading and becoming part of the SEI layer during cycling.
The addition of 5 wt% FEC had no effect on the performance of the half cells. the FTIR spectrum of the 5 wt% FEC sample indicates that the presence of the additive did not lead to any major changes in the SEI. The addition of both 2 wt% THFIPB and 10 wt% FEC, on the other hand, seems to give lower intensity in the peaks situated at 1770, 1600 and 1375 cm^{-1}, as the peaks are smaller and contain more noise than for the other spectra. Additionally, this "mix" sample lacks the long ridge between 1250-1330 cm^{-1}, which should correspond to less $ROCO_2Li$ in the SEI layer. The decrease in peak intensity at 1770 cm^{-1} may indicate that less EC is being reduced to polymeric species. Instead, the peak might represent polymeric decomposition products due to the reduction of VC, according to reaction scheme 1 in figure 2.5.5. The less intense 1600-peak further points to less EC-decomposition, while the lower 1375-peak suggests less salt degradation. This indicates that FEC, at sufficient concentration with regards to the 3 M salt concentration, reduces onto the Si anode to form a protective SEI layer that keeps the LiFSI salt from degrading as easily. This can explain the improved cycleability with respect to the cells containing only 2 wt% THFIPB. This suggestion is

not unambiguous from the collected data, as not all the peaks that correspond to EC-decomposition and LiFSI salt get less intense. FTIR is, however, a challenging technique with the possibility of many overlapping peaks, which makes it challenging to draw firm conlcusions.
After 200 cycles, the FTIR spectra are still highly similar with and without additives, as seen in figure 4.3.4. Again, the spectra are much more intense, indicating thicker SEI layers on all anodes. The biggest difference is that the "mix" sample lacks strong peaks at 1040 and 615 cm^{-1}, suggesting that less Li_2O and ROLi is formed here.[30] Other than that, the composition of the SEI seems to be similar for all the samples, suggesting that all FEC has been consumed, and that EC reduction has dominated the SEI formation and composition thereafter.

5.3.3 Characterization of SEI layers by XPS

The addition of both 2 wt% THFIPB and 10 wt% FEC, lead to an XPS spectrum that resembled the one measured on the 1 M LiFSI anode, as can be seen from figure 4.3.5 and table 4.3.1. The dominating element is once again carbon, and there is less O, S and N in the SEI. However, there is more F present in the SEI for the anode with the "mix" electrolyte than for 1 M LiFSI, containing 6.35 atomic % F versus 1.85 atomic % F. The atomic percentages further confirm the suggestions based on the FTIR data, namely that FEC forms a protective SEI layer consisting of both carbonaceous species and LiF (as evidenced by the high C and F atomic %). This again seems to decrease the salt degradation. Based on these data, it seems that reaction scheme 2 in figure 2.5.5, proposed by Nakai, Kubota Kita and Kawashima[70] is plausible. Another interesting observation, is that a very weak Si signature is observed in the survey spectrum (enlarged in figure 4.3.6), indicating that the SEI is thinner with the mixed electrolyte composition than for the others. The aforementioned results are reflected in the measured core-peaks. The C 1s spectrum in figure 4.3.7 suggests that adventitious carbon (285 eV) still is the dominant carbonaceous species, and is present in approximately the same amount as in the SEI of the anode with 1 M LiFSI. The "mix" sample was also kept in the glovebox about one month between disassembly and XPS measurements, backing up the hypothesis that the adventitious carbon had longer time to form and dominate the outermost layer of the SEI on the "mix" and 1 M samples. This will again affect the atomic percentages, but it still seems highly reasonable that FEC forms a protective initial SEI layer, preventing salt decomposition and promoting LiF formation.
Like before, the C 1s spectrum includes the same components as observed in the two previous XPS-investiagted SEI layers, with alcohols and ethers (C-OH and C-O-C bonds) at 286.4 eV, carbonyls (C=O double bond) at 287.6 eV, esters and acids (O-C=O species) at 288.8 eV, and carbonates (CO_3^{2-}) at 289.9 eV. The O 1s peak also consists of the same oxygen species as the SEI layers on the 1 M and 3 M LiFSI anodes, and the two most dominant species seem to be O-C=O and C-O-C. The F 1s, Cl 2p, N 1s and S 2p spectra in figures 4.3.8 and 4.3.9 are also similar to the two previously XPS-investigated SEI layers, but the spectra of the three latter components are weaker. The F1s spectrum is dominated by LiF, with the

LiF/LiFSI ratio being 7.7; the highest for all the samples. The higher level of LiF found on the "mix" sample suggests that Nakai, Kubota, Kita and Kawashima,[70] as well as Jaumann et al.[12] are right when claiming that FEC produces more LiF. Furthermore, it may be argued that LiF is beneficial for cell performance, as suggested by Schroder et al.,[72] as the "mix" electrolyte-containing half cells outperformed those with only AR. However, the cell performance may also be better due to the initial SEI layer formed by FEC, preventing salt decomposition, which renders LiF as a by-product as suggested by Etacheri et al.[69] and Jaumann et al.[71] Therefore, it is still ambiguous whether LiF is positive or not in the SEI of silicon anodes.
The Cl 2p spectrum includes a trace element between 191 and 193 eV, which is attributed to Boron. Boron is only present in the AR THFIPB, and the fact that there is so little of it in the SEI, indicates that it binds to the FSI^- anion to promote Li^+ conduction, and that it does not take part in the SEI formation reactions. Also, as the amount of LiF is so high, it seems that THFIPB is not a strong enough AR to dissolve LiF, as proposed by Qin et al.[13]
The N 1s and S 2p spectra are weaker than for the 1 M and 3 M LiFSI samples. The S 2p peak, for example, still consists of three peaks, but the undefined salt degradation product is weaker than the LiFSI salt signature this time. For N 1s, the LiFSI signature is not stronger than the undefined salt degradation product, but the signal is relatively stronger compared to the LiFSI peak when compared to the XPS spectra of the anodes without additives. This may again imply that the salt is not degraded to the same extent as before, due to the protective role of FEC.
All in all, the XPS analysis has showed that the "mix" electrolyte promotes a thinner SEI, as evidenced by the emergence of the weak silicon peaks. It seems that FEC forms an initial protective SEI that keeps the salts and EC from degrading as easily, evidenced by a lower content of O, S, N and Cl with respect to the 3 M sample. Additionally, FEC promotes LiF formation. It is, however, not clear whether LiF promotes cell performance and reversibility or if the FEC-derived polycarbonate layer is responsible for this.

5.3.4 Characterization of anode surfaces and SEI layers by SEM and EDX

The morphology of the 10-times cycled "mix" anode (figure 4.3.10) is highly similar to the cycled samples without additives. Again, the particles have merged somewhat, creating larger agglomerates divided by small cracks. The cross-section is also comparable to those of the anodes cycled without additives. The close-up of the cross section, presented in figure 4.3.11, shows where the SEI layer has grown on the particle, and that the center is pure silicon. Again, when investigated closely, the silicon particle is seen to consist of different grey-tones, possibly attributed to crystalline and amorphous silicon. The SEI layer was measured to be 450 nm, which is very thick for only 10 cycles. A probable cause for the apparently thick SEI, is that the anodes have been in contact with air, leading to changes in the SEI

layer, which likely increases the thickness of the SEI layer observed. Therefore, an inert technique for performing FIB, SEM and EDX is desired in order to find out how the SEI layer actually looks when the half cell is in operation.
The EDX spectra presented in figure 4.3.12, show that the addition of 5 wt% FEC increases the amount of F versus Si, while the relative C, O and S levels are similar to those found in the 3 M sample. This result suggests that LiF is formed, but that it does not have a positive effect with regards to cell performance (which is not significantly improved by the additive), as suggested by Etacheri et al.[69] and Jaumann et al.[71] The "mix" electrolyte has a higher Si/F intensity ratio (meaning less LiF) than the sample with only 5 wt% FEC, which further promotes the idea that LiF does not necessarily have a positive effect on cell performance. The ratio between Si/S for the "mix" sample is only half of the ratio of the 3 M sample, which suggests that more salt is protected by the FEC-formed SEI, thus preserving the salt. Surprisingly, the spectrum of the 2 wt% THFIPB-containing sample has the lowest Si/C and Si/O ratios, indicating that large amounts of SEI has been formed on this anode. The reason for the substantial SEI layer may be that the electrolyte had been unused for too long before preparing the 2 wt% THFIPB-containing sample, such that the effect of the AR is lower.
After 200 cycles, the FIB cross-section reveals that the anode is almost 5 µm thicker than after 10 cycles. Figure 4.3.13 shows that the anode is now made up of dense silicon. Again, there are differences in grey-tones observed for the silicon particles in the cross section image, possibly reflecting the crystalline and amorphous phase of the silicon. The large amount of Ga observed comes from sputtering of Ga-ions during FIB, showing the intrusion of the technique. The morphology of the 200-times cycled "mix" anode, as seen in figures 4.3.14 and 4.3.15, resembles that of the 3 M anode, with large flakes and dense particles. In addition, large C-O agglomerates were found at different locations on the anode, as seen in figure 4.3.14 b). These particles were not found on the 3 M sample, and the reason for their presence is not clear. By performing an EDX map-scan, as seen in figure 4.3.15, it was found that the flake-like dense films on the surface of the anode largely consist of F, most likely LiF, as the S and N maps do not show a similar distribution as F. This is different than for the 3 M LiFSI sample, where N and S had a similar distribution as F. This discrepancy again suggests the protective role of FEC, hindering LiFSI decomposition. It is also seen that the Si is covered by a thick SEI, as the silicon spectrum is weaker than O, F and C.

Chapter 6

Conclusions

In this project, the effect of concentrated electrolytes and selected additives on the performance of Si anode lithium-ion half cells has been investigated. FTIR investigations of the electrolytes revealed that the solution structure changed from being dominated by solvent separated ion pairs at dilute salt concentration, to being dominated by contact-ion pairs and aggregates at high salt concentration. Based on the FTIR investigations of the electrolytes, the solvation number for the dilute and concentrated electrolytes was calculated to be 4.06 and 1.48, respectively. The lower solvation number at high concentration indicates that less solvent molecules coordinate to the Li^+ cations at high salt concentration. Electrochemical testing showed that increasing the electrolyte concentration resulted in half cells with higher capacity, especially for the first 50 cycles. The half cells containing 3 M LiFSI in EC:DEC provided the highest capacities, averaging around 1050 $mA\,h\,g^{-1}$ from cycles 15-30, before they decreased rapidly in capacity until cycle 140, where the capacity stabilized at about 120 $mA\,h\,g^{-1}$. Post-mortem investigations using FTIR, XPS, SEM and EDX on the cycled anodes, all concluded that the dilute electrolytes formed a highly carbonaceous SEI layer with few inorganic components. The concentrated electrolytes, on the other hand, formed SEI layers that consisted of more inorganic components, like LiF, LiFSI and LiFSI degradation products. In the latter SEI layers, the higher level of inorganic compounds is explained by the difference in the solution structure for dilute and concentrated electrolytes. Even though the overall capacity generally was increased at higher concentration, it is ambiguous to say that the reason for this can be ascribed to the more inorganic SEI. Instead, it seems likely that the concentrated electrolytes require less energy for Li^+ desolvation, as the Li^+ cations are coordinated to less solvent molecules, according to the calculated solvation numbers. The lower energy loss leads to lower internal resistance, and higher cell performance. The capacity retention during the first 15 cycles is higher for highly concentrated electrolytes, but lower after about 30 cycles. This behaviour suggests that an SEI dominated by inorganic components is not sufficiently stable. Therefore, the incorporation of additives in highly concentrated electrolytes seems vital.
The addition of THFIPB to the 3 M LiFSI electrolyte confirmed its bilateral na-

ture; in low concentrations (2 wt%), the anion receptor bonded moderately to the salt anions, increasing Li^+ conduction, which improved cell capacity. At too high concentrations (6 wt%), it bonded too strongly to the anion, decomposing it, and decreasing the cell capacity. Post-mortem investigations gave no indications that THFIPB takes part in the SEI formation mechanism. The addition of 10 wt% FEC and 2 wt% THFIPB to the 3 M LiFSI electrolyte resulted in the highest performing half cells. These cells reached capacities of about 1660 $mA\,h\,g^{-1}$ at cycle 15, before they dropped quite linearly (but less steeply than for the other electrolyte compositions) to about 360 $mA\,h\,g^{-1}$ after 200 cycles. The lower CE during the formation cycles indicated that FEC reduced early onto the Si anode, passivating it. Post-mortem investigations concluded that the SEI was carbonaceous, but also included much LiF. It seems that the addition of FEC better passivated the Si (by forming more flexible polycarbonates than by EC reduction), and incorporated more LiF in the SEI for better Li^+ diffusion. Additionally, less salt elements were found in the SEI, further confirming the passivating effect of FEC, while also suggesting that LiFSI salt and its degradation products in the SEI do not improve the SEI characteristics.

Increasing the LiFSI concentration in EC:DEC electrolytes seems to have a positive effect on cell capacity, even though the capacity retention is reduced. To overcome this issue, more research should be conducted on the effect of different additives in order to promote a stable SEI that better passivates the anode surface. Furthermore, full cell testing is crucial, as both LiFSI and FEC reportedly have a negative impact on the Al current collector and the cathode, respectively.

The findings and insights provided by this project can hopefully contribute to the ongoing research field of Si anodes for LIBs. Research done on concentrated electrolytes is still scarce, but this work provides encouraging results that may aid in the development of both higher performing and safer Si anode LIBs.

Chapter 7

Further work

As concentrated electrolytes deliver higher capacities, they hold much promise for further development and optimization. The notion that dilute electrolytes present the best electrolyte properties due to the maximiation of ion conductivity is not correct, but it is unclear if the increased cost of highly concentrated electrolytes will be more profitable in the long run. Still, the positive results obtained in this project encourage further research on the topic. Specifically, the issue regarding capacity retention must be addressed. Further research on finding optimal additives seems the obvious way to go, as combinations of for instance FEC, VC, and THFIPB could achieve a more stable SEI and higher capacity retention. As a C-rate of 1 was used in this project, it would be interesting to investigate the cell performance at lower C-rates to see if even larger differences between the various electrolyte concentrations are observed.
In any case, full cell configuration must be investigated, as LiFSI and FEC reportedly have negative impacts on the Al current collector and cathode, respectively. In a full cell configuration, the addition of small amounts of $LiPF_6$ could be of interest, as $LiPF_6$ produces HF. Small amounts of HF are proposed to have a positive effect on full cell configurations, as HF promotes the formation of a protective layer on the Al current collector.[95] The addition of $LiPF_6$ may therefore contribute to overcoming the Cl impurity issue of LiFSI. Full cell testing should also be done at a range of temperatures, as the thermal stability of LiFSI is still discussed.
Finer Si particles could be tested as anode material, as the core of the Si particles still seemed to be crystalline. However, the size-reduction of the Si particles should not be too drastic, as the increasing surface area/volume ratio will promote more SEI formation.
With regard to post-mortem spectroscopic techniques, the fact that XPS can be done inert is positive, and more efforts should be put into optimizing this technique for SEI investigations. The anodes from the disassembled half cells should spend equal amounts of time in the glovebox after disassembly and before XPS measurements, to get more comparable results. Finally, NTNU Nanolab have purchased a vacuum-sealed box that can be brought into their FIB-SEM and be opened once inside. This will keep the samples inert, and will provide great progress in under-

standing how the surface morphology and SEI actually look during inert operation in the half cells. A combination of FIB, SEM and EDX can then be used to try to image the SEI and directly measure its thickness.

Bibliography

[1] L. Lu, X. Han, J. Li, J. Hua, and M. Ouyang. A review on the key issues for lithium-ion battery management in electric vehicles. *Journal of power sources*, 226:272–288, 2013.

[2] V. Etacheri, R. Marom, R. Elazari, G. Salitra, and D. Aurbach. Challenges in the development of advanced li-ion batteries: a review. *Energy & Environmental Science*, 4(9):3243–3262, 2011.

[3] J.B. Goodenough and K.S. Park. The li-ion rechargeable battery: a perspective. *Journal of the American Chemical Society*, 135(4):1167–1176, 2013.

[4] H.K. Liu, Z.P. Guo, J.Z. Wang, and K. Konstantinov. Si-based anode materials for lithium rechargeable batteries. *Journal of Materials Chemistry*, 20(45):10055–10057, 2010.

[5] X. Su, Q. Wu, J. Li, X. Xiao, A. Lott, W. Lu, B.W. Sheldon, and J. Wu. Silicon-based nanomaterials for lithium-ion batteries: a review. *Advanced Energy Materials*, 4(1), 2014.

[6] M.H. Park, M. G. Kim, J. Joo, K. Kim, J. Kim, S. Ahn, Y. Cui, and J. Cho. Silicon nanotube battery anodes. *Nano letters*, 9(11):3844–3847, 2009.

[7] J.R. Szczech and S. Jin. Nanostructured silicon for high capacity lithium battery anodes. *Energy & Environmental Science*, 4(1):56–72, 2011.

[8] B. Philippe, R. Dedryvere, M. Gorgoi, H. Rensmo, D. Gonbeau, and K. Edstrom. Role of the lipf6 salt for the long-term stability of silicon electrodes in li-ion batteries–a photoelectron spectroscopy study. *Chemistry of Materials*, 25(3):394–404, 2013.

[9] Y. Yu, L. Gu, C. Zhu, S. Tsukimoto, P.A. van Aken, and J. Maier. Reversible storage of lithium in silver-coated three-dimensional macroporous silicon. *Advanced Materials*, 22(20):2247–2250, 2010.

[10] H.B. Han, S.S. Zhou, D.J Zhang, S.W Feng, L.F. Li, K. Liu, W.F Feng, J. Nie, H. Li, X.J. Huang, et al. Lithium bis (fluorosulfonyl) imide (lifsi) as conducting salt for nonaqueous liquid electrolytes for lithium-ion batteries: Physicochemical

and electrochemical properties. *Journal of Power Sources*, 196(7):3623–3632, 2011.

[11] M. Nie, D.P. Abraham, Y. Chen, A. Bose, and B.L. Lucht. Silicon solid electrolyte interphase (sei) of lithium ion battery characterized by microscopy and spectroscopy. *The Journal of Physical Chemistry C*, 117(26):13403–13412, 2013.

[12] T. Jaumann, J. Balach, U. Langklotz, V. Sauchuk, M. Fritsch, A. Michaelis, V. Teltevskij, D. Mikhailova, S. Oswald, M. Klose, et al. Lifetime vs. rate capability: Understanding the role of fec and vc in high-energy li-ion batteries with nano-silicon anodes. *Energy Storage Materials*, 6:26–35, 2017.

[13] Y. Qin, Z. Chen, H.S. Lee, X.Q. Yang, and K. Amine. Effect of anion receptor additives on electrochemical performance of lithium-ion batteries. *The Journal of Physical Chemistry C*, 114(35):15202–15206, 2010.

[14] M. Park, X. Zhang, M. Chung, G.B. Less, and A.M Sastry. A review of conduction phenomena in li-ion batteries. *Journal of Power Sources*, 195(24):7904–7929, 2010.

[15] S.E. Sloop, J.K. Pugh, S. Wang, J.B. Kerr, and K. Kinoshita. Chemical reactivity of pf 5 and lipf6 in ethylene carbonate/dimethyl carbonate solutions. *Electrochemical and Solid-State Letters*, 4(4):A42–A44, 2001.

[16] G.B. Han, J.N. Lee, J.W Choi, and J.K. Park. Tris (pentafluorophenyl) borane as an electrolyte additive for high performance silicon thin film electrodes in lithium ion batteries. *Electrochimica Acta*, 56(24):8997–9003, 2011.

[17] X. Sun, H.S. Lee, X.Q. Yang, and J. McBreen. Using a boron-based anion receptor additive to improve the thermal stability of lipf6-based electrolyte for lithium batteries. *Electrochemical and solid-state letters*, 5(11):A248–A251, 2002.

[18] N.G. Nair, M. Blanco, W. West, F.C. Weise, S. Greenbaum, and V.P. Reddy. Fluorinated boroxin-based anion receptors for lithium ion batteries: fluoride anion binding, ab initio calculations, and ionic conductivity studies. *The Journal of Physical Chemistry A*, 113(20):5918–5926, 2009.

[19] C. Julien, A. Mauger, A. Vijh, and K. Zaghib. Lithium batteries. In *Lithium Batteries*, pages 29–68. Springer, 2016.

[20] M. Osiak, H. Geaney, E. Armstrong, and C. O'Dwyer. Structuring materials for lithium-ion batteries: advancements in nanomaterial structure, composition, and defined assembly on cell performance. *Journal of Materials Chemistry A*, 2(25):9433–9460, 2014.

[21] S. Goriparti, E. Miele, F. De Angelis, E. Di Fabrizio, R.P Zaccaria, and C. Capiglia. Review on recent progress of nanostructured anode materials for li-ion batteries. *Journal of Power Sources*, 257:421–443, 2014.

[22] M. Yoshio, T. Tsumura, and N. Dimov. Electrochemical behaviors of silicon based anode material. *Journal of Power Sources*, 146(1):10–14, 2005.

[23] File:Battery Potential vs. Capacity depending on materials.gif. `https://commons.wikimedia.org/wiki/File:Battery_Potential_vs._Capacity_depending_on_materials.gif`. Accessed: June 16th, 2018.

[24] Attribution-ShareAlike 3.0 Unported (CC BY-SA 3.0). `https://creativecommons.org/licenses/by-sa/3.0/deed.en`. Accessed: June 16th, 2018.

[25] W.R. Bennett. Considerations for estimating electrode performance in li-ion cells. In *Energytech, 2012 IEEE*, pages 1–5. IEEE, 2012.

[26] K. Xu. Electrolytes: Overview. 5:51–70, 01 2009.

[27] K. Xu. Nonaqueous liquid electrolytes for lithium-based rechargeable batteries. *Chemical reviews*, 104(10):4303–4418, 2004.

[28] G.M. Veith, M. Doucet, R.L. Sacci, B. Vacaliuc, J.K Baldwin, and J.F. Browning. Determination of the solid electrolyte interphase structure grown on a silicon electrode using a fluoroethylene carbonate additive. *Scientific reports*, 7(1):6326, 2017.

[29] M. Gauthier, T.J. Carney, A. Grimaud, L. Giordano, N. Pour, H.H Chang, D.P. Fenning, S.F. Lux, O. Paschos, C. Bauer, et al. Electrode-electrolyte interface in li-ion batteries: current understanding and new insights. *The journal of physical chemistry letters*, 6(22):4653–4672, 2015.

[30] P. Verma, P. Maire, and P. Novák. A review of the features and analyses of the solid electrolyte interphase in li-ion batteries. *Electrochimica Acta*, 55(22):6332–6341, 2010.

[31] S.F. Lux, I.T. Lucas, E. Pollak, S. Passerini, M. Winter, and R. Kostecki. The mechanism of hf formation in lipf 6 based organic carbonate electrolytes. *Electrochemistry Communications*, 14(1):47–50, 2012.

[32] B. Philippe, R. Dedryvere, M. Gorgoi, H. Rensmo, D. Gonbeau, and K. Edstrom. Improved performances of nanosilicon electrodes using the salt lifsi: a photoelectron spectroscopy study. *Journal of the American Chemical Society*, 135(26):9829–9842, 2013.

[33] M. Kerner, N. Plylahan, J. Scheers, and P. Johansson. Thermal stability and decomposition of lithium bis (fluorosulfonyl) imide (lifsi) salts. *RSC Advances*, 6(28):23327–23334, 2016.

[34] M. Nie and B.L. Lucht. Role of lithium salt on solid electrolyte interface (sei) formation and structure in lithium ion batteries. *Journal of The Electrochemical Society*, 161(6):A1001–A1006, 2014.

[35] M.N. Obrovac and L. Christensen. Structural changes in silicon anodes during lithium insertion/extraction. *Electrochemical and Solid-State Letters*, 7(5):A93–A96, 2004.

[36] B. Key, R. Bhattacharyya, M. Morcrette, V. Seznec, J.M. Tarascon, and C.P. Grey. Real-time nmr investigations of structural changes in silicon electrodes for lithium-ion batteries. *Journal of the American Chemical Society*, 131(26):9239–9249, 2009.

[37] M.T. McDowell, S.W. Lee, W.D. Nix, and Y. Cui. 25th anniversary article: Understanding the lithiation of silicon and other alloying anodes for lithium-ion batteries. *Advanced Materials*, 25(36):4966–4985, 2013.

[38] K. Ogata, E. Salager, C.J. Kerr, A.E. Fraser, C. Ducati, A.J. Morris, S. Hofmann, and C.P Grey. Revealing lithium–silicide phase transformations in nano-structured silicon-based lithium ion batteries via in situ nmr spectroscopy. *Nature communications*, 5:3217, 2014.

[39] Y. Zhang, Y. Li, Z. Wang, and K. Zhao. Lithiation of SiO_2 in li-ion batteries: in situ transmission electron microscopy experiments and theoretical studies. *Nano letters*, 14(12):7161–7170, 2014.

[40] A.M. Andersson, M. Herstedt, A.G. Bishop, and K. Edström. The influence of lithium salt on the interfacial reactions controlling the thermal stability of graphite anodes. *Electrochimica Acta*, 47(12):1885–1898, 2002.

[41] H. Wu, G. Chan, J.W. Choi, I. Ryu, Y. Yao, M.T. McDowell, S.W. Lee, A. Jackson, Y. Yang, L. Hu, et al. Stable cycling of double-walled silicon nanotube battery anodes through solid-electrolyte interphase control. *Nature nanotechnology*, 7(5):310–315, 2012.

[42] H. Li, X. Huang, L. Chen, G. Zhou, Z. Zhang, D. Yu, Y.J. Mo, and N. Pei. The crystal structural evolution of nano-si anode caused by lithium insertion and extraction at room temperature. *Solid State Ionics*, 135(1-4):181–191, 2000.

[43] N. Dimov, S. Kugino, and M. Yoshio. Carbon-coated silicon as anode material for lithium ion batteries: advantages and limitations. *Electrochimica Acta*, 48(11):1579–1587, 2003.

[44] N. Liu, H. Wu, M.T. McDowell, Y. Yao, C. Wang, and Y. Cui. A yolk-shell design for stabilized and scalable li-ion battery alloy anodes. *Nano letters*, 12(6):3315–3321, 2012.

[45] N. Liu, Z. Lu, J. Zhao, M.T. McDowell, H.W. Lee, W. Zhao, and Y. Cui. A pomegranate-inspired nanoscale design for large-volume-change lithium battery anodes. *Nature nanotechnology*, 9(3):187, 2014.

[46] N.S. Choi, K.H. Yew, W.U. Choi, and S.S. Kim. Enhanced electrochemical properties of a si-based anode using an electrochemically active polyamide imide binder. *Journal of Power Sources*, 177(2):590–594, 2008.

[47] A. Magasinski, B. Zdyrko, I. Kovalenko, B. Hertzberg, R. Burtovyy, C.F. Huebner, T.F. Fuller, I. Luzinov, and G. Yushin. Toward efficient binders for li-ion battery si-based anodes: polyacrylic acid. *ACS Applied Materials & Interfaces*, 2(11):3004–3010, 2010.

[48] M. Nie, D.P Abraham, D.M. Seo, Y. Chen, A. Bose, and B.L. Lucht. Role of solution structure in solid electrolyte interphase formation on graphite with lipf6 in propylene carbonate. *The Journal of Physical Chemistry C*, 117(48):25381–25389, 2013.

[49] D.M. Seo, S. Reininger, M. Kutcher, K. Redmond, W.B. Euler, and B.L. Lucht. Role of mixed solvation and ion pairing in the solution structure of lithium ion battery electrolytes. *The Journal of Physical Chemistry C*, 119(25):14038–14046, 2015.

[50] J. Zheng, J.A. Lochala, A. Kwok, Z. D. Deng, and J. Xiao. Research progress towards understanding the unique interfaces between concentrated electrolytes and electrodes for energy storage applications. *Advanced Science*, 2017.

[51] Y. Yamada and A. Yamada. Superconcentrated electrolytes for lithium batteries. *Journal of The Electrochemical Society*, 162(14):A2406–A2423, 2015.

[52] J. Qian, W. A Henderson, W. Xu, P. Bhattacharya, M. Engelhard, O. Borodin, and J.G. Zhang. High rate and stable cycling of lithium metal anode. *Nature communications*, 6:6362, 2015.

[53] Y. Yamada, M. Yaegashi, T. Abe, and A. Yamada. A superconcentrated ether electrolyte for fast-charging li-ion batteries. *Chemical Communications*, 49(95):11194–11196, 2013.

[54] Y. Yamada, K. Furukawa, K. Sodeyama, K. Kikuchi, M. Yaegashi, Y. Tateyama, and A. Yamada. Unusual stability of acetonitrile-based superconcentrated electrolytes for fast-charging lithium-ion batteries. *Journal of the American Chemical Society*, 136(13):5039–5046, 2014.

[55] D.W. McOwen, D.M. Seo, O. Borodin, J. Vatamanu, P.D. Boyle, and W.A. Henderson. Concentrated electrolytes: decrypting electrolyte properties and reassessing al corrosion mechanisms. *Energy & Environmental Science*, 7(1):416–426, 2014.

[56] D.M. Seo, S. Reininger, M. Kutcher, K. Redmond, W.B. Euler, and B.L. Lucht. Role of mixed solvation and ion pairing in the solution structure of lithium ion battery electrolytes. *The Journal of Physical Chemistry C*, 119(25):14038–14046, 2015.

[57] K. Xu, A. von Cresce, and U. Lee. Differentiating contributions to ion transfer barrier from interphasial resistance and li+ desolvation at electrolyte/graphite interface. *Langmuir*, 26(13):11538–11543, 2010.

[58] K. Xu. Electrolytes and interphases in li-ion batteries and beyond. *Chemical reviews*, 114(23):11503–11618, 2014.

[59] Y. Yamada, C.H. Chiang, K. Sodeyama, J. Wang, Y. Tateyama, and A. Yamada. Corrosion prevention mechanism of aluminum metal in superconcentrated electrolytes. *ChemElectroChem*, 2(11):1687–1694, 2015.

[60] D. Lv, P. Yan, Y. Shao, Q. Li, S. Ferrara, H. Pan, G.L. Graff, B. Polzin, C. Wang, J. Zhang, et al. High performance li-ion sulfur batteries enabled by intercalation chemistry. *Chemical Communications*, 51(70):13454–13457, 2015.

[61] H. Kim, F. Wu, J.T. Lee, N. Nitta, H.T. Lin, M Oschatz, W.I. Cho, S. Kaskel, O. Borodin, and G. Yushin. In situ formation of protective coatings on sulfur cathodes in lithium batteries with lifsi-based organic electrolytes. *Advanced Energy Materials*, 5(6), 2015.

[62] B. Liu, W. Xu, P. Yan, X. Sun, M.E. Bowden, J. Read, J. Qian, D. Mei, C.M. Wang, and J.G. Zhang. Enhanced cycling stability of rechargeable li–o2 batteries using high-concentration electrolytes. *Advanced Functional Materials*, 26(4):605–613, 2016.

[63] R. Cao, K. Mishra, X. Li, J. Qian, M.H. Engelhard, M.E. Bowden, K.S. Han, K.T. Mueller, W.A. Henderson, and J.G. Zhang. Enabling room temperature sodium metal batteries. *Nano Energy*, 30:825–830, 2016.

[64] Liumin Suo, Oleg Borodin, Tao Gao, Marco Olguin, Janet Ho, Xiulin Fan, Chao Luo, Chunsheng Wang, and Kang Xu. water-in-salt electrolyte enables high-voltage aqueous lithium-ion chemistries. *Science*, 350(6263):938–943, 2015.

[65] L. Suo, O. Borodin, W. Sun, X. Fan, C. Yang, F. Wang, T. Gao, Z. Ma, M. Schroeder, A. von Cresce, et al. Advanced high-voltage aqueous lithium-ion battery enabled by water-in-bisalt electrolyte. *Angewandte Chemie International Edition*, 55(25):7136–7141, 2016.

[66] D.M. Piper, T. Evans, K. Leung, T. Watkins, J. Olson, S.C. Kim, S.S. Han, V. Bhat, K.H. Oh, D.A. Buttry, et al. Stable silicon-ionic liquid interface for next-generation lithium-ion batteries. *Nature communications*, 6:6230, 2015.

[67] A. Budi, A. Basile, G. Opletal, A.F. Hollenkamp, A.S. Best, R.J. Rees, A.I. Bhatt, A.P. OMullane, and S.P. Russo. Study of the initial stage of solid electrolyte interphase formation upon chemical reaction of lithium metal and n-methyl-n-propyl-pyrrolidinium-bis (fluorosulfonyl) imide. *The Journal of Physical Chemistry C*, 116(37):19789–19797, 2012.

[68] G.M. Veith, M. Doucet, R.L. Sacci, B. Vacaliuc, J.K Baldwin, and J.F. Browning. Determination of the solid electrolyte interphase structure grown on a silicon electrode using a fluoroethylene carbonate additive. *Scientific reports*, 7(1):6326, 2017.

[69] V. Etacheri, O. Haik, Y. Goffer, G.A. Roberts, I.C. Stefan, R. Fasching, and D. Aurbach. Effect of fluoroethylene carbonate (fec) on the performance and surface chemistry of si-nanowire li-ion battery anodes. *Langmuir*, 28(1):965–976, 2011.

[70] H. Nakai, T. Kubota, A. Kita, and A. Kawashima. Investigation of the solid electrolyte interphase formed by fluoroethylene carbonate on si electrodes. *Journal of The Electrochemical Society*, 158(7):A798–A801, 2011.

[71] T. Jaumann, J. Balach, M. Klose, S. Oswald, U. Langklotz, A. Michaelis, J. Eckert, and L. Giebeler. Sei-component formation on sub 5 nm sized silicon nanoparticles in li-ion batteries: the role of electrode preparation, fec addition and binders. *Physical Chemistry Chemical Physics*, 17(38):24956–24967, 2015.

[72] K. Schroder, J. Alvarado, T.A. Yersak, J. Li, N. Dudney, L.J. Webb, Y.S. Meng, and K.J. Stevenson. The effect of fluoroethylene carbonate as an additive on the solid electrolyte interphase on silicon lithium-ion electrodes. *Chemistry of Materials*, 27(16):5531–5542, 2015.

[73] S.E. Trask, K.Z. Pupek, J.A. Gilbert, M. Klett, B.J. Polzin, A.N. Jansen, and D.P. Abraham. Performance of full cells containing carbonate-based lifsi electrolytes and silicon-graphite negative electrodes. *Journal of The Electrochemical Society*, 163(3):A345–A350, 2016.

[74] Z. Chen and K. Amine. Computational estimates of fluoride affinity of boron-based anion receptors. *Journal of The Electrochemical Society*, 156(8):A672–A676, 2009.

[75] V.P. Reddy, M. Blanco, and R. Bugga. Boron-based anion receptors in lithium-ion and metal-air batteries. *Journal of Power Sources*, 247:813–820, 2014.

[76] Z. Chen and K Amine. Tris (pentafluorophenyl) borane as an additive to improve the power capabilities of lithium-ion batteries. *Journal of The Electrochemical Society*, 153(6):A1221–A1225, 2006.

[77] A. von Wald Cresce, M. Gobet, O. Borodin, J. Peng, S.M. Russell, E. Wikner, A. Fu, L. Hu, H.S. Lee, Z. Zhang, et al. Anion solvation in carbonate-based electrolytes. *The Journal of Physical Chemistry C*, 119(49):27255–27264, 2015.

[78] B.E. Nilssen, A.O. Tezel, and A.M. Svensson. The carbon-electrolyte interface at high cathodic voltages. *ECS Transactions*, 69(21):1–12, 2015.

[79] T. Fukutsuka, T. Nakagawa, Ko. Miyazaki, and T. Abe. Electrochemical properties of licopo4-thin film electrodes in lif-based electrolyte solution with anion receptors. *Journal of Power Sources*, 306:753–757, 2016.

[80] C.R. Birkl, E. McTurk, M.R. Roberts, P.G. Bruce, and D.A. Howey. A parametric open circuit voltage model for lithium ion batteries. *Journal of The Electrochemical Society*, 162(12):A2271–A2280, 2015.

[81] S. Wartewig. *IR and Raman spectroscopy: fundamental processing*. John Wiley & Sons, 2006.

[82] S.S. Zhang, K. Xu, and T.R. Jow. A thermal stabilizer for lipf6-based electrolytes of li-ion cells. *Electrochemical and solid-state letters*, 5(9):A206–A208, 2002.

[83] F. Shi, P.N. Ross, G.A. Somorjai, and K. Komvopoulos. The chemistry of electrolyte reduction on silicon electrodes revealed by in situ atr-ftir spectroscopy. *The Journal of Physical Chemistry C*, 121(27):14476–14483, 2017.

[84] B.M. Gatehouse, S.E. Livingstone, and R.S. Nyholm. 636. the infrared spectra of some simple and complex carbonates. *Journal of the Chemical Society (Resumed)*, pages 3137–3142, 1958.

[85] Y. Ikezawa and H. Nishi. In situ ftir study of the cu electrode/ethylene carbonate+ dimethyl carbonate solution interface. *Electrochimica Acta*, 53(10):3663–3669, 2008.

[86] J. Huang and A.F. Hollenkamp. Thermal behavior of ionic liquids containing the fsi anion and the li+ cation. *The Journal of Physical Chemistry C*, 114(49):21840–21847, 2010.

[87] D. Aurbach, K. Gamolsky, B. Markovsky, Y. Gofer, M. Schmidt, and U. Heider. On the use of vinylene carbonate (vc) as an additive to electrolyte solutions for li-ion batteries. *Electrochimica Acta*, 47(9):1423–1439, 2002.

[88] J. Yang, N. Solomatin, A. Kraytsberg, and Y. Ein-Eli. In-situ spectro–electrochemical insight revealing distinctive silicon anode solid electrolyte interphase formation in a lithium–ion battery. *ChemistrySelect*, 1(3):572–576, 2016.

[89] J. Yang, N. Solomatin, A. Kraytsberg, and Y. Ein-Eli. In-situ spectro–electrochemical insight revealing distinctive silicon anode solid electrolyte interphase formation in a lithium–ion battery. *ChemistrySelect*, 1(3):572–576, 2016.

[90] B. Philippe. *Insights in Li-ion Battery Interfaces through Photoelectron Spectroscopy Depth Profiling*. PhD thesis, Acta Universitatis Upsaliensis, 2013.

[91] H. Piao and N.S. Mcintyre. Adventitious carbon growth on aluminium and gold–aluminium alloy surfaces. *Surface and interface analysis*, 33(7):591–594, 2002.

[92] T.L. Barr and S. Seal. Nature of the use of adventitious carbon as a binding energy standard. *Journal of Vacuum Science & Technology A: Vacuum, Surfaces, and Films*, 13(3):1239–1246, 1995.

[93] G. Greczynski and L. Hultman. C 1s peak of adventitious carbon aligns to the vacuum level: Dire consequences for material's bonding assignment by photoelectron spectroscopy. *ChemPhysChem*, 18(12):1507–1512, 2017.

[94] F. Lindgren, C. Xu, J. Maibach, A.M. Andersson, M. Marcinek, L. Niedzicki, T. Gustafsson, F. Björefors, and K. Edström. A hard x-ray photoelectron spectroscopy study on the solid electrolyte interphase of a lithium 4, 5-dicyano-2-(trifluoromethyl) imidazolide based electrolyte for si-electrodes. *Journal of Power Sources*, 301:105–112, 2016.

[95] H.J. Gores, J. Barthel, S. Zugmann, D. Moosbauer, M. Amereller, R. Hartl, and A. Maurer. Liquid nonaqueous electrolytes. *Handbook of Battery Materials, Second Edition*, pages 525–626, 2011.

Appendix

Overview of the electrolyte testing scheme is given in figure A.1.

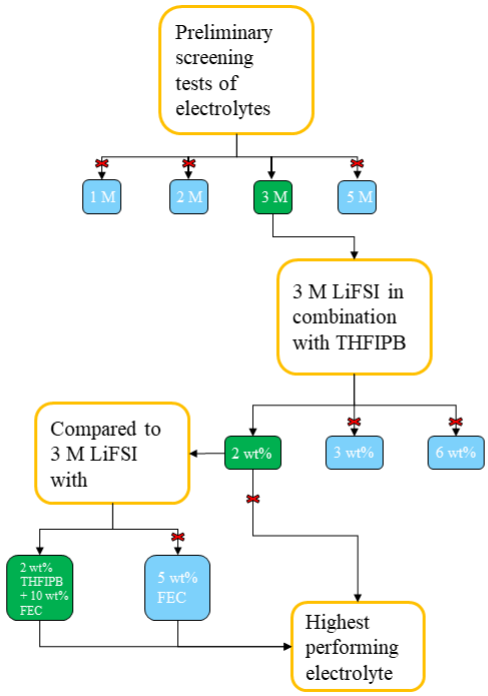

Figure A.1: Graphic overview of electrolyte testing scheme.

The cycle data including the standard deviations for all cells are shown in figures A.2 - A.4. There were made 2-3 cells for each electrolyte composition that underwent 200 cycles. Figure A.4 shows the capacity of the cells composed of 1 M LiFSI in EC:DEC, 3 M LiFSI in EC:DEC and 3 M LiFSI + 10 wt% FEC + 2 wt% THFIPB that were tested in FTIR and XPS.

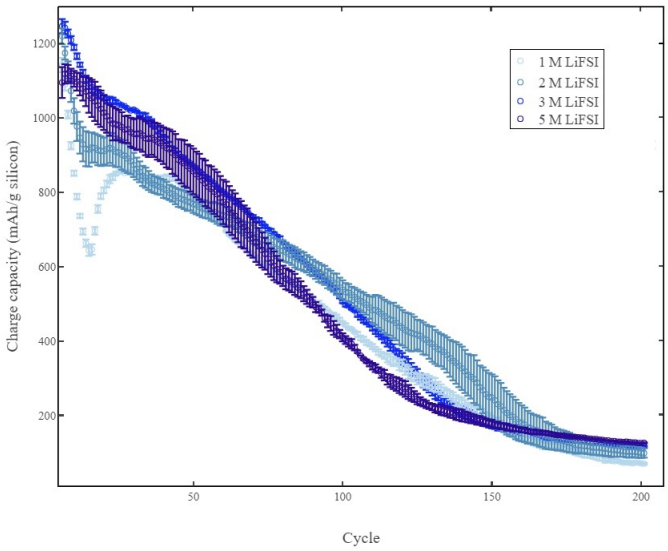

Figure A.2: The capacity for the 200-times cycled cells containing electrolytes without additives.

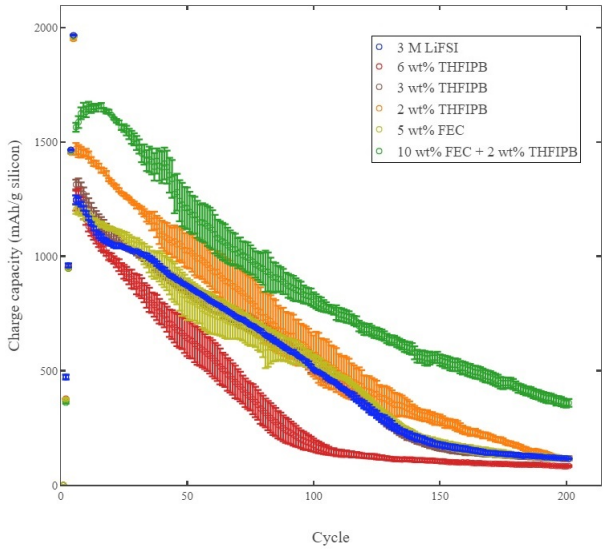

Figure A.3: The capacity for the 200-times cycled cells containing electrolytes with additives.

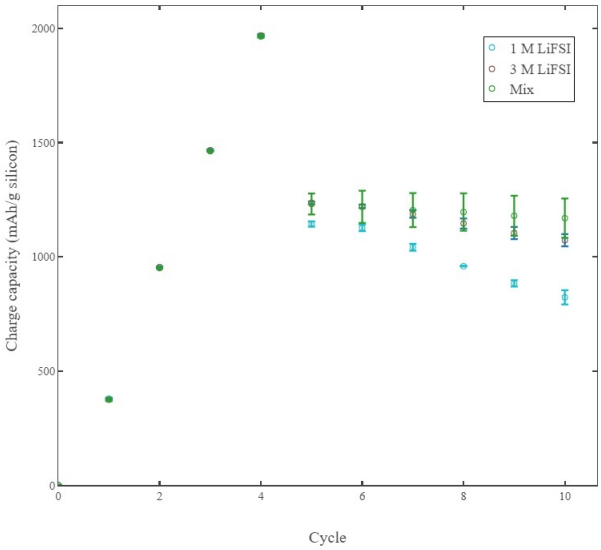

Figure A.4: The capacity of the 10-times cycled cells used for FTIR and XPS investigations.